Petroleum Geochemistry of the Daryanah Formation in the offshore well Al-NC 128, Cyrenaica Basin, NE Libya

By

Abobakar E. Algomati

Supervisor

Dr. Osama Shaltami

This Thesis was Submitted in Partial Fulfillment of the Requirements for Master's Degree of Science in Geology.

University of Benghazi
Faculty of Science
Department of Earth Science

Fall 2019

University of Benghazi **Faculty of Science**

Department of Earth Science

Petroleum Geochemistry of the Daryanah Formation in the offshore well Al-NC 128, Cyrenaica Basin, NE Libya

By

Abobakar E. Algomati

This Thesis was Successfully Defended and Approved on 4/12/2019

Supervisor

Assist. Prof. Osama Shaltami

Signature:……

Prof. Ahmed M. Muftah **(Internal Examiner)**

Signature:……

Assist. Prof. Rahel G. Rahel **(External Examiner)**

Signature:……

Dean of Faculty **Director of Graduate Studies and Training**

بِسْمِ اللَّـهِ الرَّحْمَـٰن الرَّحِيم

(إنَّ في خلْقِ السَّمواتِ والأرضِ واختلافِ اللَّيلِ والنَّهارِ
لآياتٍ
لأولي ا لألباب الَّذين يَذْكُرونَ الله قياماً وقعوداً وعلى
جُنوبهم ويتفَكَّرونَ في خلْقِ السَّمواتِ والأرضِ ربَّنا
ما خلَقْت
هذا باطلاً سبحانَك فَقِنَا عذابَ النَّار)

DEDICATION

I dedicated my work to people who have been my pillars of strength throughout my life, my parents, and my other family members.

ACKNOWLEDGMENT

I would like to express my sincere gratitude to my supervisor Dr. Osama Shaltami, for his help and advice in the preparation of this thesis.

I would also like to thank the Agip Company for giving all the data that used in the current study, and also I would love to give a special thanks to the laboratory of Chemostratigraphy and Organic Geochemistry (LGQM), State University of Rio de Janeiro (UERJ), Brazil, for preparing and analyzing samples.

Special thanks must go to all Staff Members of the Department of the Earth Sciences, Faculty of Science, Benghazi University, for their help during the academic years of my study at this department.

Abobakar E. Algomati

CONTENTS

TABLE OF CONTENTS

LIST OF FIGURES

LIST OF TABLES

CHAPTER TWO
ORGANIC PETROGRAPHY AND GEOCHEMISTRY OF SOURCE ROCK

CHAPTER THREE
RESERVOIR GEOCHEMISTRY

ABBREVIATIONS

TOC = total organic carbon (wt. %).

S_1 = amount of free hydrocarbons in sample (mg/g).

S_2 = amount of hydrocarbons generated through thermal cracking (mg/g) – provides the quantity of hydrocarbons that the rock has the potential to produce through digenesis.

S_3 = amount of CO_2 (mg of CO_2/g of rock) - reflects the amount of oxygen in the oxidation step.

T_{max} = the temperature at which maximum rate of generation of hydrocarbons occurs.

Hydrogen index: $HI = 100 * S_2 / TOC$

Oxygen index: $OI = 100 * S_3 / TOC$

Production index: $PI = S_1 / (S_1 + S_2)$

Semi-quantitative index: $GP = S_1 / S_2$

Ro = vitrinite reflectance (wt. %)

Pr/Ph = Pristane/Phytane

Carbon preference index: $CPI = 2(C_{23} + C_{25} + C_{27} + C_{29})/(C_{22} + 2[C_{24}+ C_{26} + C_{28}] + C_{30})$

Waxiness index: $WI = \Sigma(n\text{-}C_{21}\text{-}n\text{-}C_{31})/\Sigma(n\text{-}C_{15}\text{-}n\text{-}C_{20})$

TPP = tetracyclic polyprenoid

Petroleum Geochemistry of the Daryanah Formation in the offshore well Al-NC 128, Cyrenaica Basin, NE Libya.

By

Abobakar E. Algomati

Supervisor

Dr. Osama Shaltami

ABSTRACT

Petrographical and geochemical assessments of source rock (Darnah Shale) and reservoir (Darnah Limestone) in the offshore well Al-NC 128 in the Cyrenaica Basin were achieved in the present study. In the Darnah Shale, the biomarkers indicate the mixed inputs of aquatic plankton and terrigenous organic matter deposited under suboxic conditions. The kerogen is of types II/III and III. The source rock has a fair quality. The reservoir contains medium crude oil. This oil belongs to source rock of the Darnah Shale as proven by oil-source rock correlation. C1 is the main gas in the reservoir. Both crude oil and source rock are located in the immature window. The Darnah Reservoir has been charged with hydrocarbons in two different times. The middle shale can be considered a cap rock in the petroleum system of the Darnah Formation.

Keywords: Organic Petrography, Organic Geochemistry, Source Rock, Reservoir, Darnah Formation, Cyrenaica Basin, Libya.

CHAPTER ONE
INTRODUCTION

1.1. General

The Cyrenaica Basin is located in northeastern Libya (Fig. 1.1). The age of exposed rocks in the basin ranges from Late Cretaceous to Quaternary (e.g., Hallett and Clark-Lowes, 2016; Shaltami *et al.*, 2018, Figs. 1.2-4). The rocks of the rest of the geological ages (from Precambrian to Early Cretaceous) are found in the subsurface (Hallett and Clark-Lowes, 2016).

1.2. Regional Geology

The Al Jabal Al Akhdar is the largest part of the Cyrenaica Basin. It was developed at the southern margin of the Mediterranean geosynclines of the Tethys, on an attenuated continental crust of the north passive margin of the Afro-Arabian shield (El Hawat and Shelmani, 1993). The age of rocks in the Cyrenaica Basin ranges from Precambrian to Quaternary, but the exposed rocks range only from Cretaceous to Quaternary, while the rest of ages are found in the subsurface (e.g., El Hawat and Abdulsamad 2004; Hallett and Clark-Lowes, 2016, Fig. 1.2).

1.2.1. Regional Stratigraphic Setting

The Cyrenaica Basin largely covered by sediments belonging to a sequence ranging from Late Cretaceous to Quaternary (Fig. 1.4). The stratigraphic sequence can be described as following:

1.2.1.1. Late Cretaceous

Previous studies (e.g., Rohlich, 1974; El Hawat and Shelmani, 1993) suggested that the Al Jabal Al Akhdar was formed during the Late Cretaceous. This age is represented by six formations (Klen, 1974; Rohlich, 1974). According to Rohlich (1974) the Al Hilal and Al Athrun formations were deposited on the coast and these formations have equivalents in the inland (Qasr Al Abid, Al Baniyah, Al Majahir and Wadi Dukhan formations). Shaltami *et al.*, (2018) found that the $^{87}Sr/^{86}Sr$ data suggest an age of Late Cenomanian for the Qasr Al Abid Formation, Late Turonian-Late Coniacian for the Al Baniyah, Late Santonian for the Al Hilal Formation, Middle

Campanian for the Al Majahir Formation, Early Maastrichtian for the Al Athrun Formation and Late Maastrichtian for the Wadi Dukhan Formation. The new age of the Late Cretaceous formations refers to the similarity of deposition at the coast and inland.

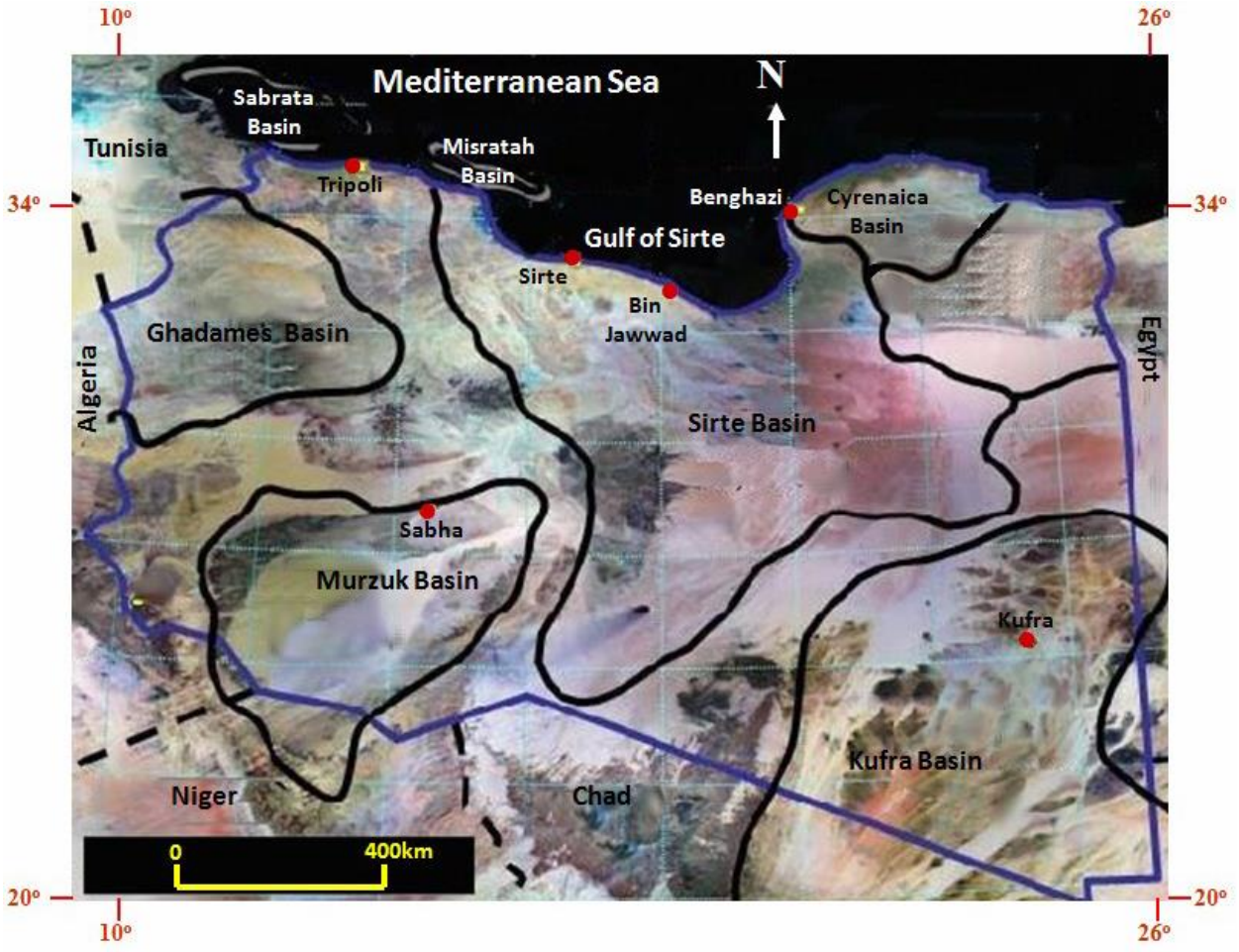

Fig. 1.1: Satellite image showing the sedimentary basins in Libya (after Shaltami, 2012).

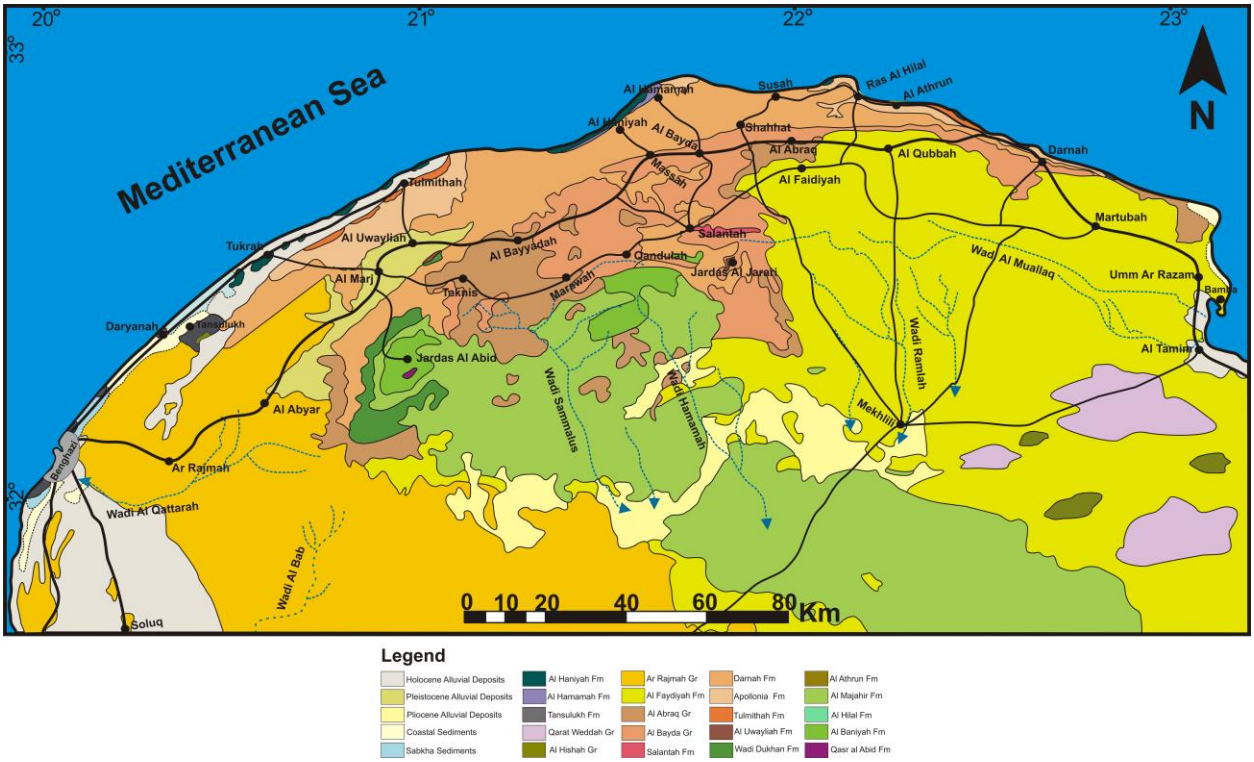

Fig. 1.2: Geological map of the Cyrenaica Basin (after Shaltami et al., 2018).

1.2.2.2. Paleocene

The Al Uwayliayah Formation is the only rock unit representing the Paleocene epoch in the Al Jabal Al Akhdar (Rohlich, 1974). Many authors (Rohlich, 1974; El Hawat and Shelmani, 1993; El Hawat and Abdulsamad, 2004) believed that the Middle Paleocene is completely absent. The $^{87}Sr/^{86}Sr$ data suggest an age of Middle Danian-Middle Thanetian for the Al Uwayliayah Formation, which indicate that the Middle Paleocene is present (Shaltami *et al.*, 2018).

1.2.1.3. Eocene

Pietersz (1968) divided the Eocene deposits in the Al Jabal Al Akhdar into the Apollonia, Darnah and Salantah (or Slonta) formations. The type localities of the three formations mentioned above are situated at the Susah village, Darnah city and Salantah village, respectively (Pietersz, 1968). It is very difficult to separate the Darnah Formation from the Salantah

Formation; consequently the former is incorporated within the Darnah Formation (Rohlich, 1974). It is now generally accepted that the Eocene deposits in the Al Jabal Al Akhdar are divided into two formations; a basal Apollonia Formation and an overlying Darnah Formation. It is dreadfully hard to determine the contact between these two formations, because in some areas in the Al Jabal Al Akhdar, the Apollonia Formation interfingers with the Darnah Formation (Rohlich, 1974; Hallett, 2002). Based on the fossil content, the probable depositional environment of the Apollonia Formation is the deep marine, whereas the Darnah Formation was definitely deposited in a shallow marine environment (Rohlich, 1974). Shaltami *et al.,* (2018) calculated the numeric age for the Eocene deposits in the Al Jabal Al Akhdar. This new age is as follows: 1) Early Ypresian and Late Ypresian-Early Lutetian for the lower and upper parts of the Apollonia Formation, respectively, and 2) Late Lutetian-Early Priabonian and Late Priabonian for the lower and upper parts of the Darnah Formation, respectively. Obviously, the Apollonia and Darnah formations are unquestionably separated by an unconformity, because the Middle Lutetian is missing. Furthermore, the Middle Priabonian is not present in the Darnah Formation; therefore it is necessary to separate the Darnah Formation from the Salantah Formation. Additionally, the Middle Ypresian is completely absent in the Apollonia Formation. Based on the new age and new type locality, they suggest a new name (Tulmithah Formation) for the lower part of the Apollonia Formation.

1.2.1.4. Oligocene

The Oligocene in Libya marks a period of regression in which the shoreline migrated northwards (Hallett, 2002). Significant outcrops of Oligocene rocks are present in the Jabal Al Akhdar. According to Rohlich (1974) these Oligocene rocks are divided into two formations namely; the Al Bayda Formation (Early Oligocene) and Al Abraq Formation (Late Oligocene). The name Al Bayda Formation was introduced by Rohlich (1974) and comprises two members; the Shahhat Marl Member and Algal Limestone Member. The lithological nature and paleontoloical content of the formation suggest a neritic, largely shallow marine environment (Rohlich, 1974). Shaltami *et al.,* (2017) found that the Sr isotope analysis of crystalline calcites from the two members gave an age of Early Rupelian for the Shahhat Marl Member, and Late Rupelian for the Algal Limestone Member. Moreover, the K-Ar age of the fine illites (<0.2μm)

from the Shahhat Marl Member was also defined at Early Rupelian. There is an obvious lack of the Middle Rupelian. Thus, they concluded that the sediments of the two members mentioned above are unquestionably separated by an unconformity. Accordingly, they changed the Al Bayda Formation to the Al Bayda Group, divided into Shahhat Formation (previously called Shahhat Marl Member) and Marawah Formation (formerly called Algal Limestone Member).

The name of the Al Abraq formation was established by Rohlich (1974) on the Al Abraq village. Shaltami *et al.,* (2018) found that the ages derived from strontium isotope analysis of crystalline calcites are Late Oligocene (Early Chattian and Late Chattian) for the Al Abraq Formation, which indicate that there is an unconformity surface, because the Middle Chattian is completely absent. Consequently, they changed the Al Abraq Formation to the Abraq Group. They divided this group into two formations: a basal Massah Formation and an overlying Qasr Al Balatah Formation.

1.2.1.5. Miocene

There were many local names that were used for the Miocene deposits in the Cyrenaica Basin, but now only seven formations have been recognized. These formations are Al Faidiyah, Benghazi, Al Sceleidima, Msus, Wadi Al Qattarah, Qarat Mariem and Al Jaghbub formations (Hallett, 2002). The proved depositional environment for the formations is the shallow marine (e.g., Klen, 1974; Francis and Issawi, 1977; Giammarino, 1984; El Hawat and Abdulsamad, 2004). The Al Faidiyah and Ar Rajmah formations were defined by Pietersz (1968) and Klen (1974), respectively. The last author used the name Benghazi Member for the lower part of the Ar Rajmah Formation, and Wadi Al Qattarah Member for the upper part. El Hawat and Abdulsamad (2004) changed the status of the Ar Rajmah Formation to the Ar Rajmah Group, divided into the Benghazi and Wadi Al Qattarah formations. The Al Sceleidima and Msus formations are also parts of the Ar Rajmah Group (Francis and Issawi, 1977). These formations were introduced by Francis and Issawi (1977) and Mazhar and Issawi (1977), respectively. Di Cesare *et al.,* (1963) identified the Al Jaghbub Formation in the Al Jaghbub oasis. Giammarino (1984) divided this formation into two members: a basal Wadi Al Hamim Member and an overlying Wadi Al Khali Member. The Qarat Mariem Formation is a transitional facies between

the Al Jaghbub and Msus formations (Swedan and Issawi, 1977). Shaltami *et al.,* (2018) calculated the absolute age for the Miocene deposits in the Cyrenaica Basin. They found that these deposits from oldest to youngest are as follows: Al Faidiyah Formation (Middle Aquitanian), Jardinah Formation (Early Burdigalian), Benghazi Formation (Late Burdigalian-Early Serravallian), Al Sceleidima Formation (Late Serravallian), Msus Formation (Middle Tortonian), Al Jaghbub Formation (Early Messinian), Wadi Al Qattarah Formation (Middle Messinian), Bu Mariam Formation (earliest Late Messinian) and Al Abyar Formation (latest Late Messinian). They also found that the unconformity between the Wadi Al Qattarah and Bu Mariam formations marks the beginning of the MSC event in the Cyrenaica Basin. Furthermore, they have re-formed the Ar Rajmah Group to include the Jardinah, Benghazi, Al Sceleidima, Msus, Al Jaghbub, Wadi Al Qattarah, Bu Mariam and Al Abyar formations.

1.2.1.6. Pliocene

Previous studies (e.g., Carmignani, 1984; El Hawatand Abdulsamad, 2004) showed that the Pliocene-Early Pleistocene sediments in the Cyrenaica Basin are represented by Qarat Weddah Formation, while Shaltami *et al.,* (2018) found that there are two formations in this age in the Cyrenaica Basin; a basal Al Hishah Formation and an overlying Qarat Weddah Formation. The Al Hishah Formation was introduced by Mijalkovic (1977) after Al Hishah village. Shaltami *et al.,* (2018) found that the isotope data gave ages of Early Zanclean and Late Zanclean for the Al Hishah Formation. Clearly there is an unconformity surface because the Middle Zanclean is not present (Shaltami *et al.,* 2018). Therefore, they changed the status of the Al Hishah Formation to the Al Hishah Group divided into the Umm Al Gharaniq and Uyun Ghuzayil formations (with names based on new type localities). The $\delta^{30}Si$ and trace element ratios indicated that the Umm Al Gharaniq and Uyun Ghuzayil formations were deposited in fluvial and shallow marine environments, respectively (Shaltami *et al.,* 2018). Unlike all previous studies, Shaltami *et al.,* (2018) found that the Pliocene deposits are present in the Al Jabal Al Akhdar represented by the Umm Al Gharaniq Formation. This formation represents the Zanclean flood that coincided with the end of the MSC event in the Cyrenaica Basin. There was also deposition of alluvial sediments (terra rossa soil, conglomerate and calcrete) during the Late Pliocene (Middle-Late Piacenzian) (Shaltami *et al.,* 2018).

1.2.1.7. Quaternary

The Qarat Weddah Formation was established by Di Cesare *et al.,* (1963) on the Qarat Weddah hill. The isotope data suggested two different ages (Middle-Late Piacenzian and Middle Gelasian) for the Qarat Weddah Formation (Shaltami *et al.,* 2018). The ages derived from isotope analysis indicate the complete absence of the Early Piacenzian and Early Gelasian, indicating the presence of two unconformity surfaces. The first surface separates the Al Hishah Group and Qarat Weddah Formation and the other separates the lower and upper parts of the Qarat Weddah Formation (Shaltami *et al.,* 2018). Thus, they concluded that the Qarat Weddah Formation must be changed to the Qarat Weddah Group which can be divided into the Qarat Al Asi and Wadi Al Maqar formations. The possible depositional environments for the Qarat Al Asi and Wadi Al Maqar formations are the shallow marine and fluvial environments, respectively (Shaltami *et al.,* 2018).

Klen (1974), Rohlich (1974) and Zert (1974) showed that there are two types of the Quaternary calcarenites in the Al Jabal Al Akhdar: marine and aeolian. Shaltami *et al.,* (2017) supported this assumption by the PAAS-normalized REE patterns. They used crystalline calcite to determine the age of the calcarenites. The $^{87}Sr/^{86}Sr$ ratio gave an age of Early-Late Calabrian for the marine calcarenite and Middle Ionian for the lower part of the aeolian calcarenite, while the $^{230}Th/^{238}U$ ratio suggested a Middle-Late Tarantian age for the upper part. Obviously, there are two unconformities because the Early Ionian and Late Ionian-Early Tarantian are not present. Based on the new age and new type localities they gave names for the calcarenites (Tansulukh Formation for the marine calcarenite, while they divided the aeolian calcarenite into two formations; a basal Al Hamamah Formation and an overlying Al Haniyah Formation). According to Shaltami *et al.,* (2018) the Early Pleistocene (Middle Gelasian) is the numeric age for the tufa and travertine in the Cyrenaica Basin. There are alluvial sediments belonging to the Late Pleistocene (Middle-Late Tarantian) (Shaltami *et al.,* 2018).

According to Shaltami *et al.,* (2018) the Early Holocene in the Cyrenaica Basin is represented by the sabkha deposits (Early-Middle Boreal) and alluvial sediments (Late Boreal).

They also added that the youngest deposits in the basin are the coastal sediments (Middle Holocene (Early-Late Atlantic).

1.3. Daryanah Formation

The Daryanah Formation was introduced by Duronio *et al.*, (1991) for subsurface sequences encountered in the Al-NC 120 and Al-NC 128 wells (Fig. 1.5). This formation contains large foraminifera, gastropods, echinoderms and pelecypods which indicate an Early Cretaceous age (Aptian-Albian, Hallett, 2002). The proved depositional environment of the Daryanah is the shallow marine (Hallett, 2002).

1.4. Objectives

The current work is a petrographical and geochemical study of the Daryanah Formation in the offshore well Al-NC 128 (Fig. 1.5). The specific objectives of this study are the following:

1) Conduct an organic petrographical and geochemical assessment of the Daryanah Shale (source rock) in the studied well. This assessment will give information about the maceral type, source rock quality, organic matter type, thermal maturity, organic matter origin, depositional environment and paleosalinity.
2) Geochemical evaluation of natural gas and crude oil of the Daryanah Limestone (reservoir) using petroleum inclusions.
3) Identification of the charging times.

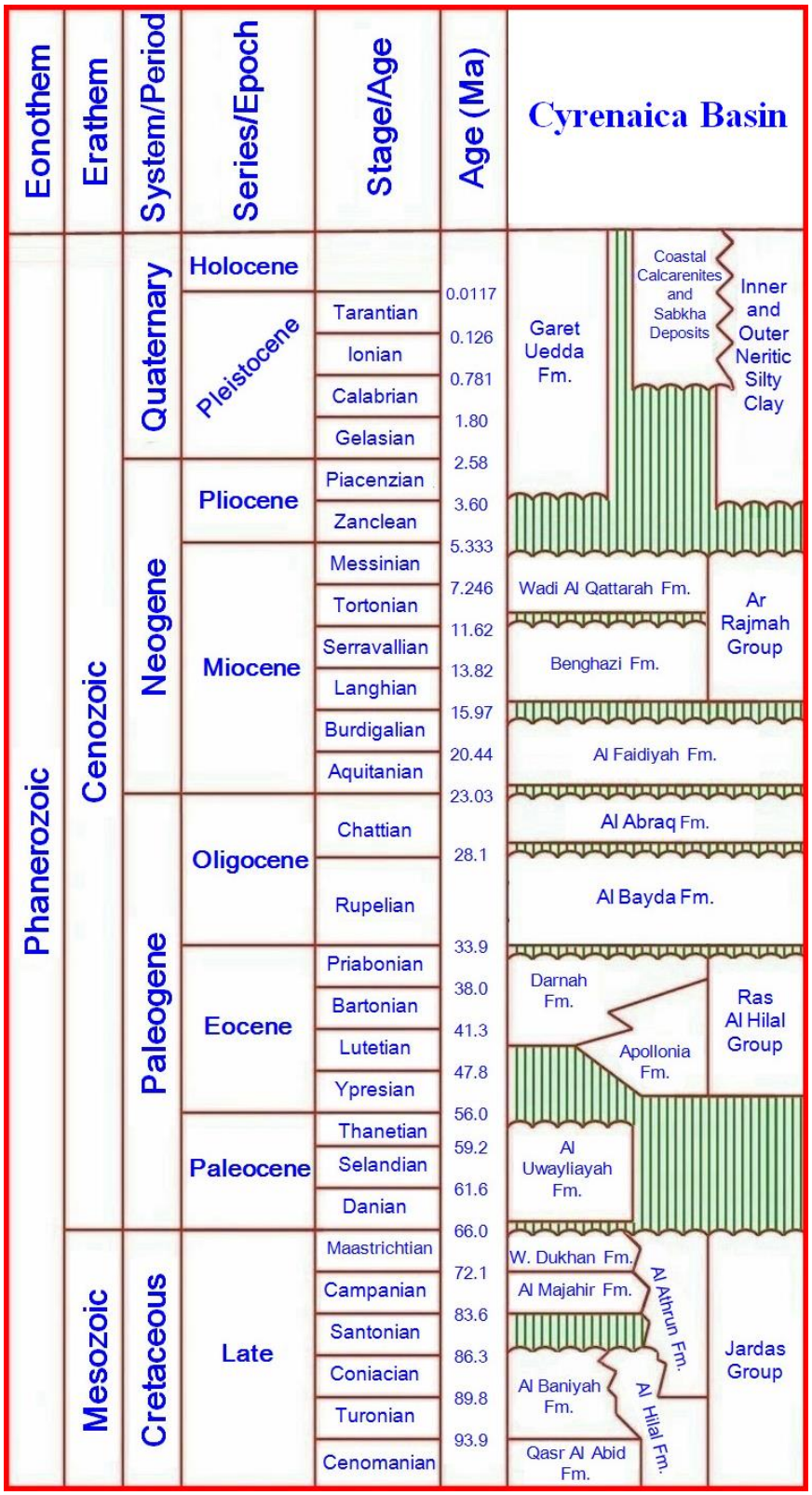

Fig. 1.3: Stratigraphic chart of the exposed rocks in the Cyrenaica Basin (after El Hawat and Abdulsamad, 2004).

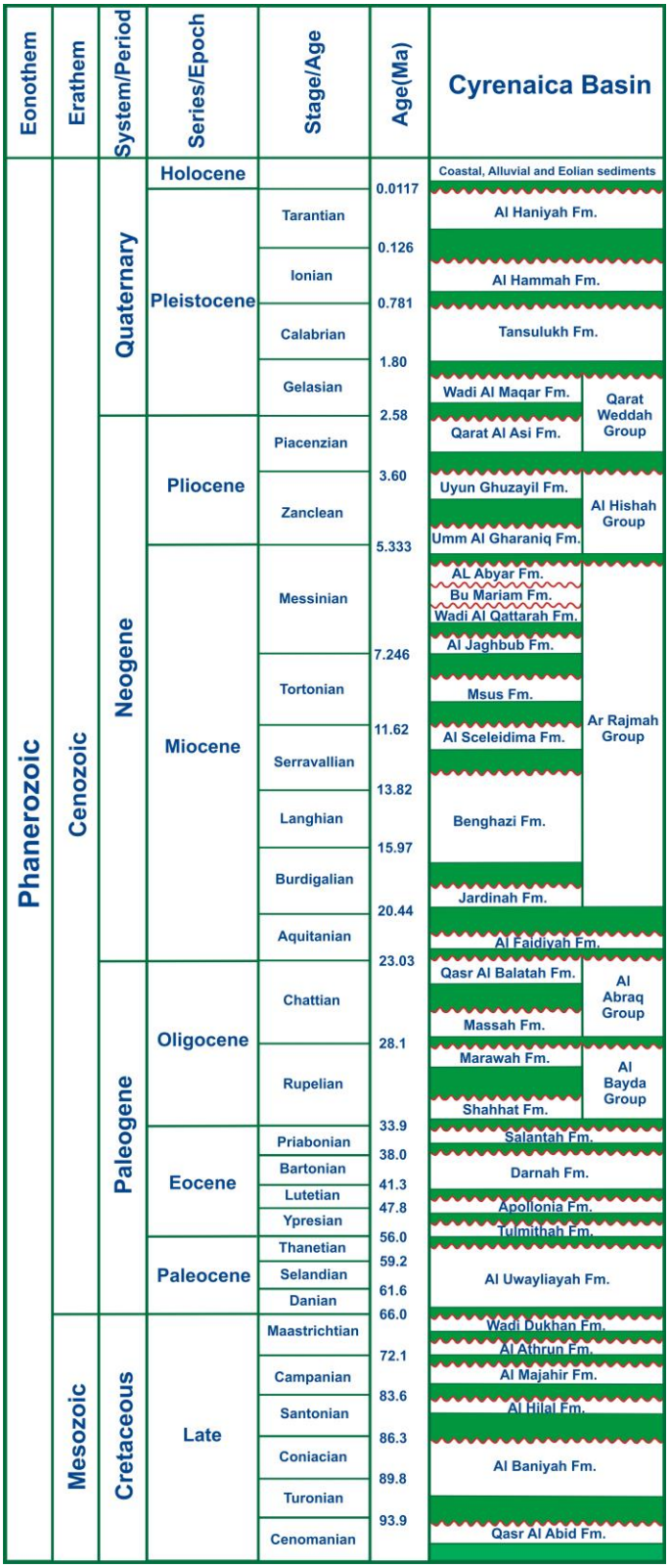

Fig. 1.4: Stratigraphic chart of the exposed rocks in the Cyrenaica Basin (after Shaltami et al., 2018).

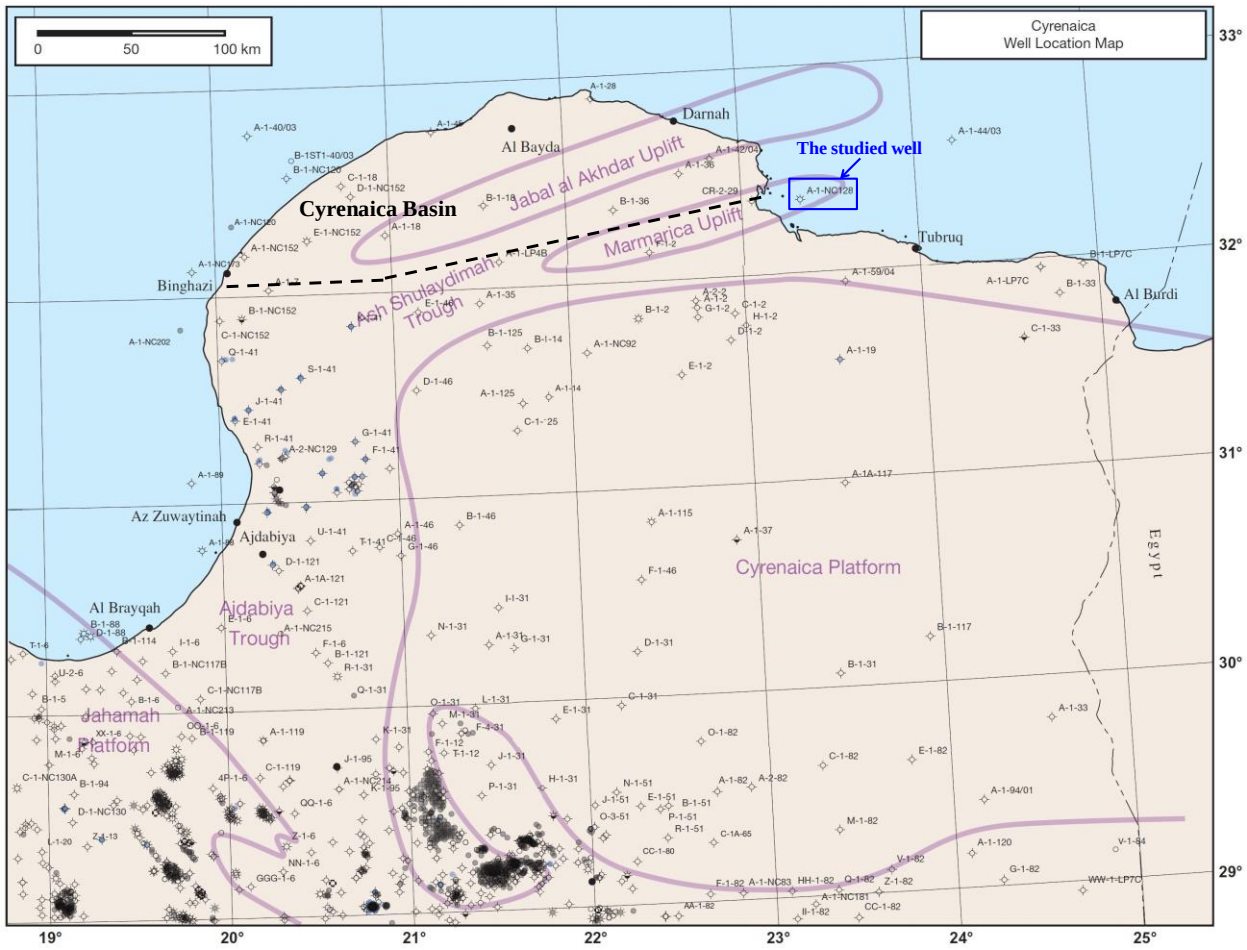

Fig. 1.5: Well location map of the Cyrenaica Basin showing the location of the offshore well Al-NC 128 (modified after Hallett and Clark-Lowes, 2016).

1.5. Previous Work

Despite the existence of source rocks and reservoirs in the sedimentary basins of Libya, the petroleum production is only from the Sirte, Murzuq, Ghadamis and Sabratah basins. However, the source rocks and reservoirs in the Cyrenaica Basin are illustrated in Fig (1.6). There are several studies on the petroleum system of the Cyrenaica Basin and I will present a summary of these studies.

Buitrago *et al.,* (2011) suggested that there are three reservoirs in the Cyrenaica Basin, namely the Early Cretaceous carbonates (Daryanah Formation), the Late Cretaceous carbonates (Al Baniyah Formation) and the Middle-Late Eocene carbonates (Darnah Formation). They added that the Qasr Al Abid and Al Hilal formations (Late Cretaceous shales) are considered as source rocks.

Hallett and Clark-Lowes (2016) suggested that the three main source rocks of Libya (Tanezzuft, Frasnian and Sirte shales) are present in the Cyrenaica Basin, but these rocks are not in a facies capable of generating significant hydrocarbons. The naming of the Middle-Late Jurassic formations of the Cyrenaica basin remains controversial (Hallett, 2016). In some wells these sediments are called Sirual Formation while in other wells they are divided into two rock units: a basal Ghurab Formation and an overlying Mallegh Formation. Hallett and Clark-Lowes (2016) added that the source rocks in the Cyrenaica Basin also include the Middle-Late Jurassic sediments (Sirual Formation) and the Early Cretaceous shales (Qahash and Daryanah formations). There is controversy about the type of kerogen in the Qahash Shale, for example Buitrago *et al.,* (2011) believed that type IV kerogen is prevailing, while Hallett (2016) suggested that the Qahash Shale is dominated by gas-prone type III kerogen.

Shaltami *et al.,* (2018), in two different studies, introduced three new source rocks in the Cyrenaica Basin, namely the Early-Middle Eocene marls (Apollonia Formation) and the Late Oligocene marls (Massah and Qasr Al Balatah formations). Shaltami *et al.,* (2018), in another study, re-evaluated the Qahash and Daryanah formations in the offshore well Al-NC 120. They found the following: 1) The Qahash and Daryanah shales are fair source rocks, while the Qahash Coal has a poor quality, 2) The Qahash and Daryanah shales are characterized by the

predominance of type II/III and III kerogen, whereas the Qahash Coal behaves as type IV kerogen, 3) All organic matter is thermally immature, 4) The Qahash and Daryanah shales are characterized by mixed organic matter formed in suboxic to anoxic conditions, while the Qahash Coal contains terrigenous organic matter formed in oxidizing conditions, 5) The Daryanah Reservoir (limestone and dolostone units) contains immature oils, 6) The petroleum inclusions show indications of oil-water interactions, 7) The oils of the Daryanah Reservoir were sourced from the Qahash and Daryanah shales, and 8) There are two episodes of oil charging occurred in the Daryanah Reservoir.

Shaltami *et al.,* (2019), in eight different studies, evaluated the petroleum system of all exposed rocks in the Cyrenaica Basin. The conclusions of these studies are as follows:

1) The hydrocarbon gases especially C_1 are dominant in the Daryanah Reservoir inclusions, while the inclusions of the Al Baniyah and Darnah reservoirs contain lesser amounts of these gases.

2) The inclusions of the Al Baniyah and Darnah reservoirs contain more non-hydrocarbon gases such as H_2, H_2S, CO_2 and N_2 than those of the Daryanah Reservoir.

3) The upper part of Shahhat Formation is a good source rock, while the rest of the formation has a poor quality.

4) The upper part of Shahhat Formation contains type II/III kerogen (mature organic matter), whereas type III kerogen is dominant in the other parts (immature organic matter).

5) The Shahhat Formation is characterized by mixed organic matter formed in suboxic conditions.

5) The Marawah Formation is one of the reservoirs in the Cyrenaica Basin.

6) C_1 is the main constituent of the Marawah Reservoir.

7) The petroleum inclusions of the Al Baniyah Reservoir contain two oil families.

8) The characteristics of the Family I oils indicate that these oils were sourced from the Late Santonian shale (Al Hilal Formation), while the Late Cenomanian marl (Qasr Al Abid Formation) is the probable source for the Family II oils.

9) The Al Baniyah Reservoir oils are thermally immature.

10) Two episodes of oil charging took place in the Al Baniyah Reservoir.

11) The Miocene shales and marls of the Cyrenaica Basin display three grades of organic richness, namely good (Al Faidiyah and Benghazi shales), fair (Al Faidiyah Marl and Al Sceleidima Shale) and poor (Benghazi Marl, Sceleidima Marl, Msus Shale, Msus Marl and Al Jaghbub Marl).

12) The Al Faidiyah and Benghazi shales are characterized by kerogen of type II.

13) The Al Faidiyah and Benghazi shales contain mature organic matter.

14) Migrated hydrocarbons are dominant in the Al Faidiyah and Benghazi shales.

15) The Al Sceleidima and Al Jaghbub samples are characterized by terrigenous organic matter, whereas mixed organic matter is prevailing in the Al Faidiyah and Benghazi shales.

16) The Benghazi Formation is the only Miocene reservoir in the Cyrenaica Basin.

17) There are two genetically distinct oil families in the Benghazi Reservoir inclusions. 18) All oil families of the Benghazi Reservoir are thermally mature.

19) The Benghazi Reservoir oils are classified as medium to heavy oils.

20) The Middle Aquitanian shale (Al Faidiyah Formation) and the Late Burdigalian-Early Serravallian shale (Benghazi Formation) are the main sources of the Benghazi Reservoir.

21) There are two different charging times took place in the Benghazi Reservoir.

22) The compositions of organic matter repeatedly changed in the Al Uwayliayah Formation, varying from kerogen type-III in the limestones, to type-II in the marls.

23) The Al Uwayliayah Marl can be considered a good source rock (TOC>1%), while the quality of the Al Uwayliayah Limestone ranges from poor to fair (TOC<1%).

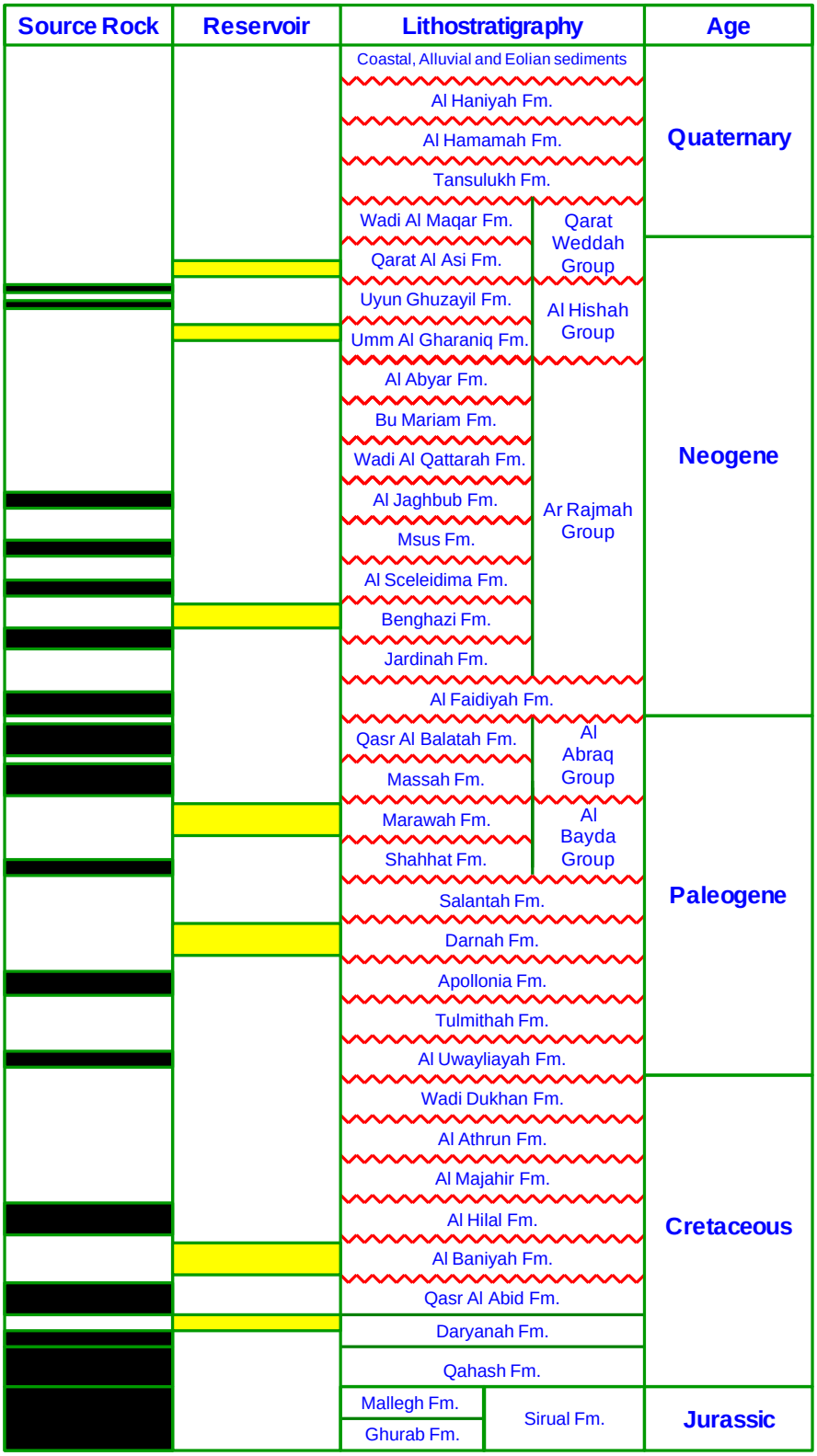

Fig. 1.6: Lithostratigraphic column of the sedimentary infill of the Cyrenaica Basin showing the source rocks and reservoirs (after Shaltami et al., 2019).

24) The Al Uwayliayah Formation contains immature to early mature organic matter.

25) The presence of rearranged diasterenes in the Al Uwayliayah Formation suggests enhanced clay catalysis rather than thermal catalysis.

26) The Al Uwayliayah Marl was deposited under the influence of episodic photic zone anoxia. On the other hand, a fully oxidized photic zone was present during the deposition of the Al Uwayliayah Limestone.

27) The quality of the Apollonia Marl (source rock) ranges from good to excellent

28) The Apollonia Marl contains type-II kerogen.

29) There is one oil family in the petroleum inclusions of the Darnah Reservoir; this oil is of medium type.

30) The Darnah Reservoir oils were derived from the Apollonia Marl.

31) The Darnah Reservoir oils and the Apollonia Marl have entered in the oil generation window.

32) The Uyun Ghuzayil Shale is a fair source rock, while the Uyun Ghuzayil Diatomite has a good quality.

33) The source rocks of the Uyun Ghuzayil Formation have diverse potential ranging from gas-prone to oil-prone.

34) The organic matter in the source rocks of the Uyun Ghuzayil Formation is thermally immature and characterized by the sovereignty of type II/III and III kerogens.

35) Land-plant derived organic matter is dominant in the diatomite and shale of the Uyun Ghuzayil Formation with a small contribution of marine organic matter.

36) The Uyun Ghuzayil Diatomite is the main source rock of the Umm Al Gharaniq Reservoir oils, whereas the Qarat Al Asi Reservoir oils were derived from the Uyun Ghuzayil Shale.

37) The Umm Al Gharaniq and Qarat Al Asi reservoirs contain medium and heavy oils, respectively. These oils are thermally immature.

38) The most abundant gas in the Umm Al Gharaniq and Qarat Al Asi reservoirs is C_1 with lesser amounts of C_2, C_3, nC_4, iC_4, N_2, CO_2 and H_2S.

1.6. Stratigraphy

The lithostratigraphic column of the Daryanah Formation in the offshore well Al-NC 128 is shown in Fig (1.7). Clearly, the Daryanah Formation consists of shale, limestone, dolostone and calcareous sandstone. In the studied well, the Qasr Al Abid Formation (Late Cretaceous) overlies the Daryanah Formation, while the lower boundary of the formation is conformable with the underlying Qahash Formation (Early Cretaceous).

1.7. Methodology

The AGIP Company submitted the data used in the current work to my supervisor (Dr. Osama Shaltami). Twenty samples from the Daryanah Formation were selected (8 samples from the shale, 2 samples from the calcareous sandstone, 7 samples from the limestone and 3 samples from the dolostone, Fig. 1.7). Those samples were subjected to supplementary analyses, including organic petrography, scanning electron microscope (SEM), total organic carbon (TOC) content, Rock Eval pyrolysis, gas chromatography-mass spectrometry (GC-MS) and fluorescence spectrophotometry. Preparation and analysis of the samples were carried out in the laboratory of Chemostratigraphy and Organic Geochemistry (LGQM), State University of Rio de Janeiro (UERJ), Brazil.

1.7.1. Organic Petrography

Organic petrography (Fig. 1.8) of the shale samples was done following standard procedure (ICCP System, 1994a,b). The rock chips prepared from the black shale were then mounted in a block of cold-setting resin and ground and polished (50μm) to give a flat surface. Quantification of the macerals was achieved by employing a point counting device fitted to the microscope stage. Counts were made by traversing the block and alternating the light modes on every move. At least 100 counts were made on every block. The relative abundance of each maceral was reported as a percentage of the sum of all the maceral identified in the block. The reflectance at near normal incidence of vitrinite phytoclasts was measured under oil immersion using a photomultiplier. Before measuring the reflectance, the AMDEL microscope was first calibrated using two standards: synthetic spinel with a reflectance of 0.42% and synthetic yttrium aluminum garnet (YAG) with a reflectance of 0.92% at 546-nm wavelength. Calibrations were

repeated after several measurements in order to maintain identical conditions for the standards and the mounted samples. At least 40 readings were taken from every sample depending on the abundance of vitrinite in the block. A mean random value (Ro) was obtained as the arithmetic average of the total number of readings from the samples.

1.7.2. Total Organic Carbon (TOC) and Rock Eval Pyrolysis

TOC, a measure of the total organic carbon in a rock usually expressed as weight percent (wt. %), was done using LECO C230 instrument (Fig. 1.9). TOC analysis requires decarbonation of the shale samples by treatment with hydrochloric acid (HCl). This is done by treating the samples with concentrated HCL for at least two hours. The samples are then rinsed with water and flushed through a filtration apparatus to remove the acid. The filter is then removed, placed into a LECO crucible and dried in a low temperature oven (110^{o}C) for a minimum of four hours. Samples were weighted after this process in order to obtain a percentage carbonate value based on weight loss. The LECO C230 instrument is calibrated with standards having known carbon contents. This is completed by combustion of these standards by heating to 1200^{o}C in the presence of oxygen. Both carbon monoxide and carbon dioxide are generated and the carbon monoxide is converted to carbon dioxide by a catalyst. The carbon dioxide is measured by an IR cell. Combustion of unknowns is then completed and the response of unknowns per mass unit is compared to that of the calibration standard, thereby the TOC is determined. Rock Eval pyrolysis (Fig. 1.10) technique for the shale samples was also done. It enables the bulk chemical composition of kerogen, and hence its hydrocarbon potential, to be determined. Approximately 100 milligrams of washed, ground (60 mesh) whole rock sample was analyzed in the Rock-Eval instrument and the operating condition was as follows:

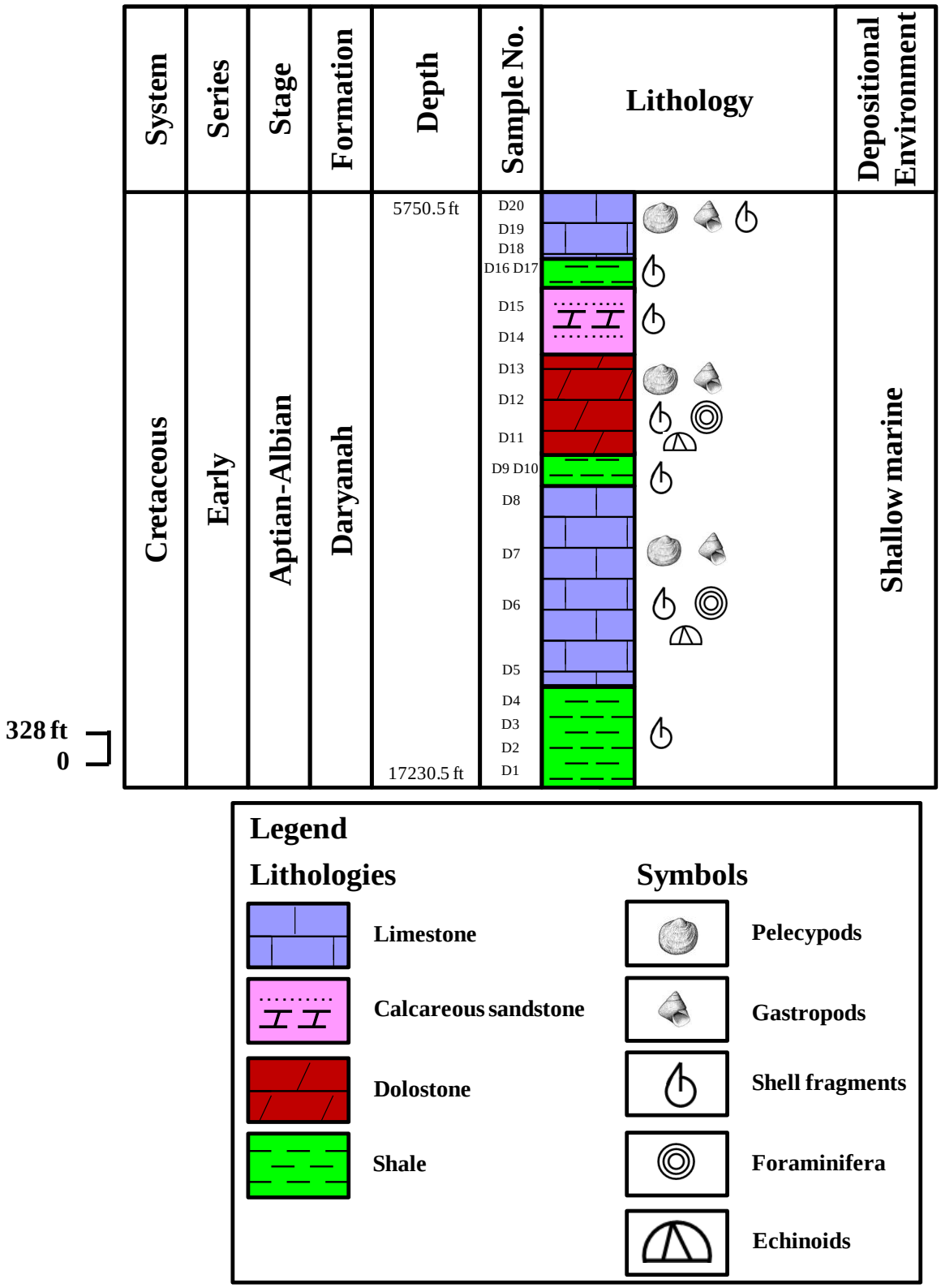

Fig. 1.7: Lithologic column of the Daryanah Formation in the offshore well Al-NC 128.

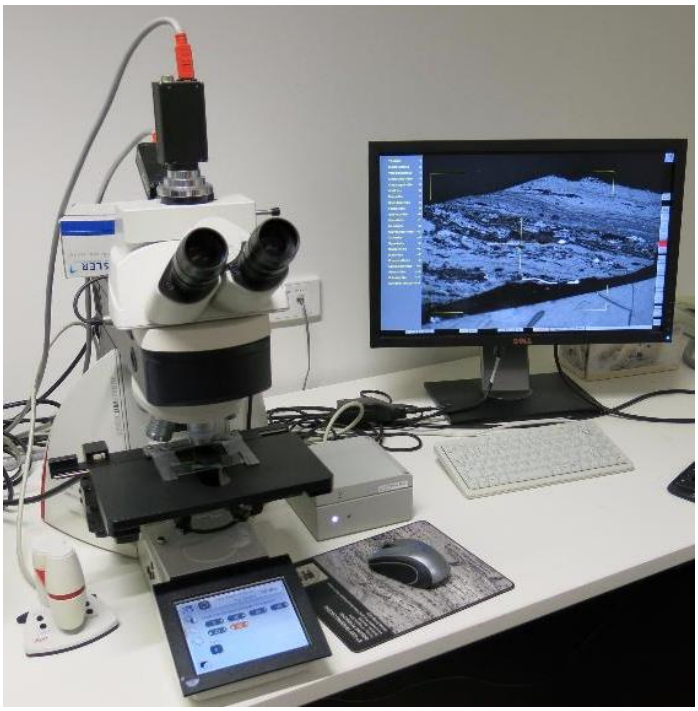

Fig. 1.8: Organic Petrographic Microscope.

S_1: 300^{o}C for 3 minutes

S_2: 300 to 550^{o}C at 25^{o}C/min; hold at 550^{o}C for 1 minute

S_3: trapped between 300 to 390^{o}C

The S_1 signal represents any free hydrocarbons that can be volatilized out of the rock without cracking the kerogen (mg HC/g rock) at 300°C. S_2 measures the amount of hydrocarbons (mg HC/g rock) that are expelled from kerogen cracking at temperature-programmed pyrolysis (300-550°C). The S_2 peak represents the existing potential of a rock to generate petroleum if burial and maturation would continue to completion. S_3 determines the released CO_2 due to pyrolysis break off between 300 and 390°C expressed in milligrams of CO_2 per gram of rock (mg HC/g rock).

1.7.3. Gas Chromatography-Mass Spectrometry (GC-MS)

Gas Chromatography-Mass Spectrometry (Fig. 1.11) analysis of the studied samples were performed using an Agilent 6890N gas chromatograph/5975 MSD mass spectrometer (GC-MS) equipped with a HP-5MS capillary column (30m× 0.25mm×0.25µm film thickness). The GC oven temperature was programmed from 50 to 100°C at the rate of 20°C/min, and then from 100

to 315°C at the rate of 3°C/min with initial and final hold times of 1min and 16min, respectively. Helium was used as a carrier gas. The MS was operated in electron ionization (EI) mode at 70 eV, with the ion source temperature of 230°C. The GC-MS system was operated in the full scan mode and select scan mode.

1.7.4. Fluorescence Spectrophotometry

The samples of limestone, dolostone and calcareous sandstone were prepared as thick doubly polished sections of approximately 100mm thickness for fluid inclusion petrographic analysis and microthermometric measurements. Fluid inclusion petrography and fluid inclusion assemblages were first examined using an Olympus AX 70 microscope equipped with both transmitted white and incident ultraviolet light (UV) sources (λ = 365nm). UV illumination for fluorescence analysis of petroleum inclusions was provided by a mercury lamp with a 400nm barrier epifluorescence filter, so the wavelength of the emission fluorescence is greater than 400nm. The fluorescence spectra of individual petroleum inclusions were measured using an Ocean Optics USB2000 miniature fiber optic spectrometer (Fig. 1.12). CIE-XYZ chromaticity coordinates and Lambda max (λ_{max}) for individual inclusions were calculated from the obtained spectra. Microthermometry of oil, gas and aqueous fluid inclusions was carried out using a calibrated Linkam TH-600 stage. The homogenization temperatures and ice final melting temperatures were obtained by cycling. Homogenization temperature measurements were determined using a heating rate of 10^{o}C/min. The final ice melting temperature measurements, which are dependent on the quantity of salt present in solution, were determined using a heating/cooling rate of 1^{o}C/min. The measured temperature precisions for homogenization and ice melting temperatures are ±1^{o}C and ±0.1^{o}C, respectively. The API gravity was calculated as: API gravity = (141.5/speciflc gravity at 15.6^{o}C)-131.5.

Fig. 1.9: LECO instrument.

Fig. 1.10: Rock-Eval 6 instrument.

Fig. 1.11: Gas Chromatography-Mass Spectrometry (GC-MS) instrument.

Fig. 1.12: Fluorescence spectrophotometer instrument.

1.7.5. Scanning Electron Microscope (SEM)

One technique was applied to characterize the fracture surfaces of the studied samples, namely scanning electron microscopy (SEM, Fig. 1.13). High-resolution electron micrographs were captured using a field-emission SEM (JEOL JSM-7001F) with operating parameters set in the vicinity of 20 kV accelerating voltage and ‘medium’ (11) spot size. The hierarchical nature of the surface was surveyed with magnifications ranging from 1000 × to 15,000 ×. This was carried out at across various representative locations, along the longitudinal centerline of the fracture surface.

Fig. 1.13: Scanning electron microscope instrument.

CHAPTER TWO
ORGANIC PETROGRAPHY AND GEOCHEMISTRY OF SOURCE ROCK

2.1. Introduction

The organic petrography service delivers information about source rock type and associated organic matter, thermal maturity level, and the hydrocarbon generation zone (Chabalala *et al.,* 2011; Hackley and Cardott, 2016; Aviles *et al.,* 2019). Interpretations of thermal maturity level and hydrocarbon generation zone are based on the reflectance measurements and overall observations of organic matter (OM) under the microscope with white and UV light in oil immersion or dry environment (Furmann *et al.,* 2015; Ndip *et al.,* 2019). Understanding of maceral composition of source rocks and interplay between OM and minerals allows for in-depth evaluation of source rock potential in conventional and unconventional exploration and production (Sykes *et al.,* 2014; El Hajj *et al.,* 2019).

Data provided includes both vitrinite reflectance (%VRo) and solid bitumen reflectance (%BRo), which are used as thermal maturity indicators. Reflectance data for solid bitumen are reported in percent vitrinite reflectance equivalent (%VRE) via set of available correlations. Using this information, data are reported with a confidence level that is a function of quantity and quality of OM particles and solid bitumen concentrations in sedimentary rock (Chabalala *et al.,* 2011; Erik *et al.,* 2015 Malachowska *et al.,* 2019).

Maceral analysis offers the detailed composition of OM types (by volume percentage on a mineral matter-free basis) present in source rock as well as oil and gas proneness. Macerals are the components of the source rock describing the origin of a particular organic matter type in coal and organic rich shales (Furmann *et al.,* 2015; Ndip *et al.,* 2019).

Major groups of macerals are liptinite (involved Exinite), vitrinite, and inertinite. The liptinite group is divided into primary (resinite, sporinite, subernite, cutinite and alginite) and secondary (bituminite) liptinites. The vitrinite group is classified into three subgroups, namely gelovitrinite (gelinite and corpohuminite), detrovitrinite (densinite and attrinite) and telovitrinite (collotelinite, ulminite, textinite and telinite). The inertinite group includes seven macerals, namely fusinite, semifusinite, inertodetrinite, micrinite, macrinite funginite and secretinite.

Organic geochemistry can be viewed as forensic science that combines aspects of geology, chemistry and biology and applies them to a colossally long time scale. Molecular and microscopic fossils provide the indicators on which we base our reconstructions of past events and ecosystems. We not only perform basic research, but also work closely with petroleum industrial partners to investigate the processes which lead to the development of fossil fuels (Zongying, 2009; El Atfy *et al.,* 2014; Huo *et al.,* 2019).

2.2. Organic Petrography

In the current study, vitrinite represents the most abundant maceral in the Daryanah Shale. Liptinite is the second common maceral. There is also a small amount of inertinite. The vitrinite group is represented by gelovitrinite (gelinite, Fig. 2.1), detrovitrinite (densinite and attrinite, Figs. 2.2-3) and telovitrinite (collotelinite, telinite ulminite and textinite, Figs. 2.4-7). The observed liptinites are resinite, sporinite, subernite, cutinite, alginite and bituminite (Figs. 2.8-13), while fusinite and inertodetrinite are common inertinites (Figs. 2.14-15). The detected macerals imply that the precursors of the majority of organic matter are higher land plants and aquatic organisms.

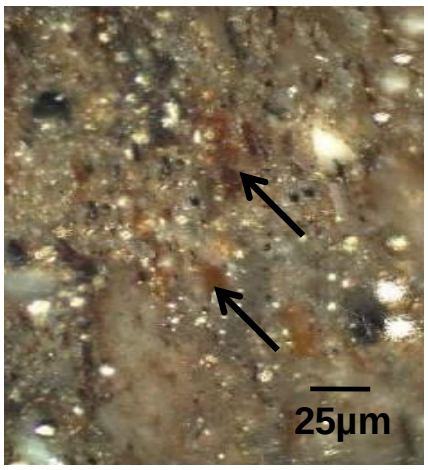

Fig. 2.1: Photomicrograph (oil immersion) showing gelinite (black arrows, sample D3).

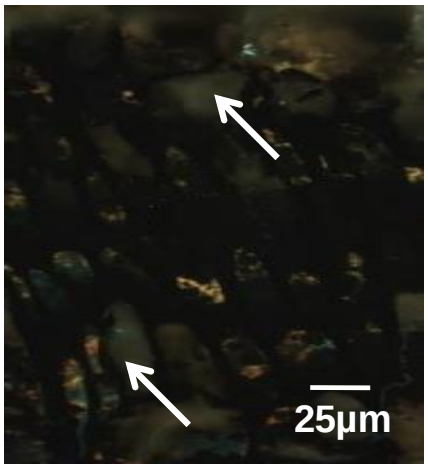

Fig. 2.2: Photomicrograph showing densinite (white arrows, sample D10).

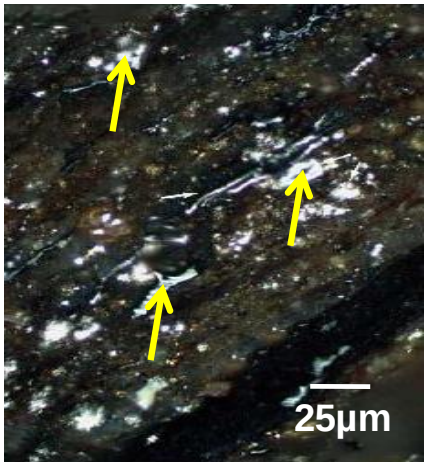

Fig. 2.3: Photomicrograph showing attrinite (yellow arrows, sample D16).

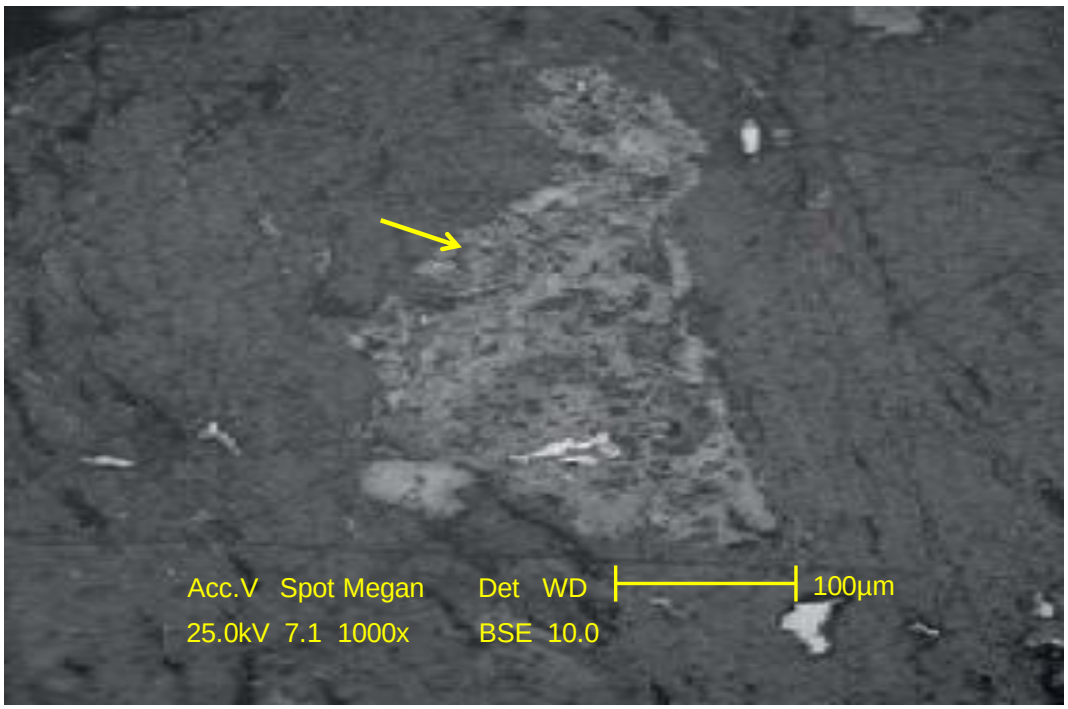

Fig. 2.4: BSE image showing collotelinite (yellow arrow, sample D1).

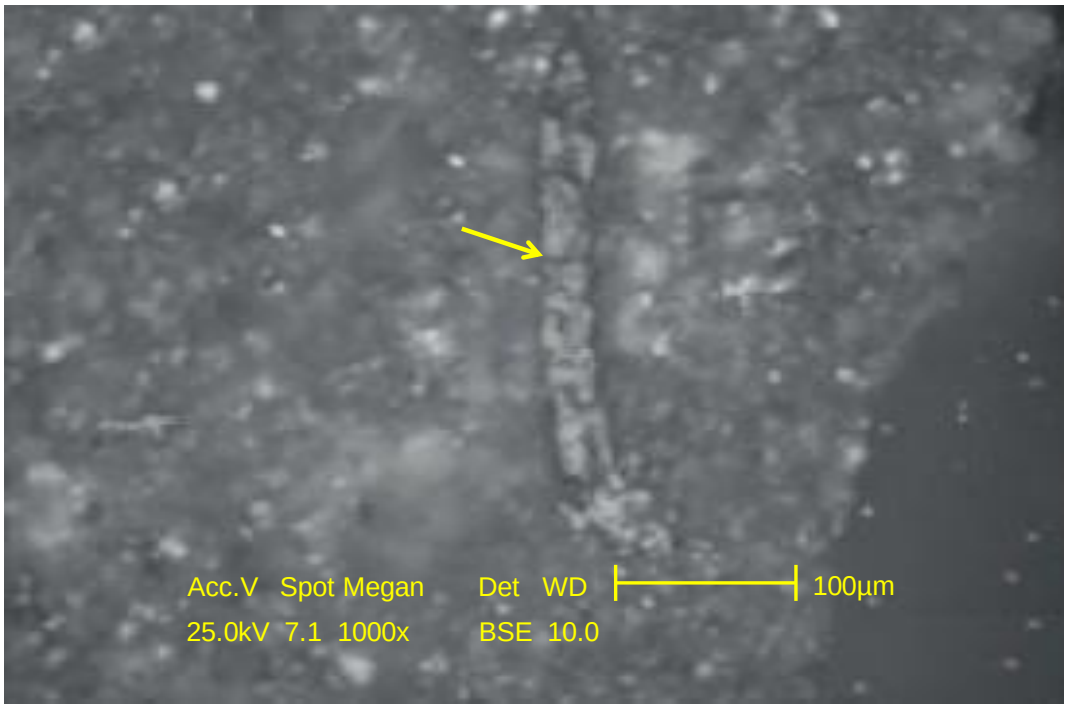

Fig. 2.5: BSE image showing telinite (yellow arrow, sample D1).

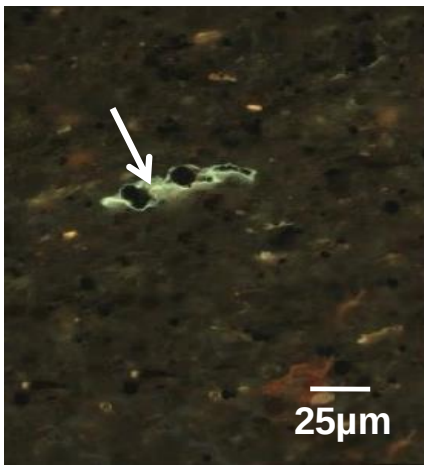

Fig. 2.6: Photomicrograph showing ulminite (white arrow, sample D4).

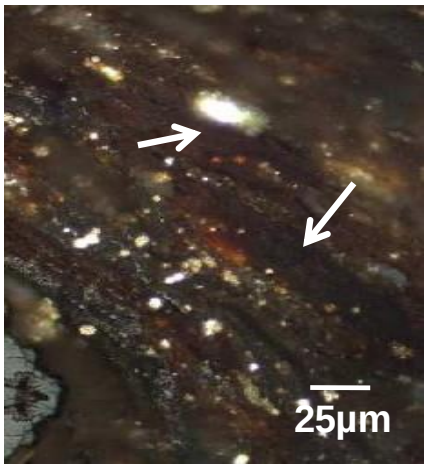

Fig. 2.7: Photomicrograph (oil immersion) showing textinite (white arrows, sample D3).

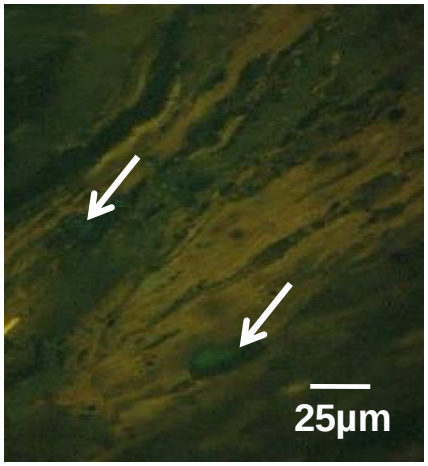

Fig. 2.8: Photomicrograph (oil immersion) showing resinite (white arrows, sample D9).

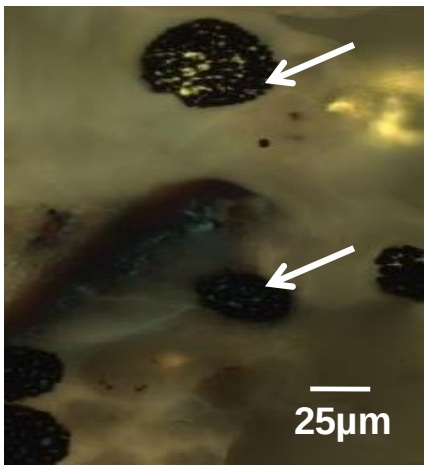

Fig. 2.9: Photomicrograph showing sporinite (white arrows, sample D3).

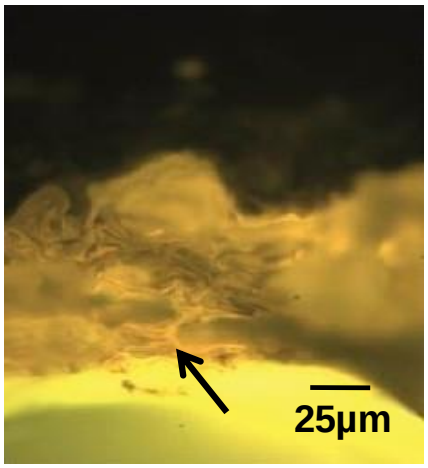

Fig. 2.10: Photomicrograph showing subernite (black arrow, sample D2).

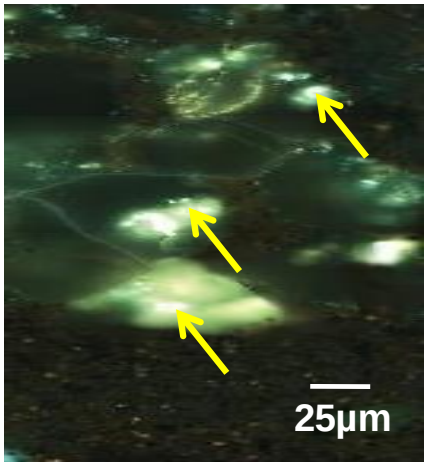

Fig. 2.11: Photomicrograph showing cutinite (yellow arrows, sample D2).

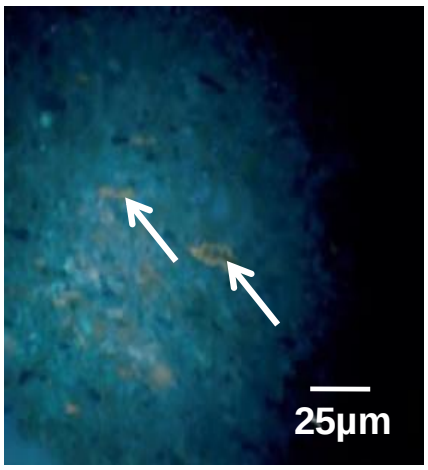

Fig. 2.12: Photomicrograph (oil immersion) showing alginite (white arrows, sample D4).

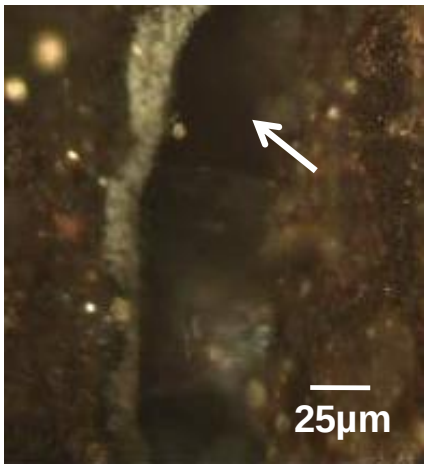

Fig. 2.13: Photomicrograph showing bituminite (white arrow, sample D1).

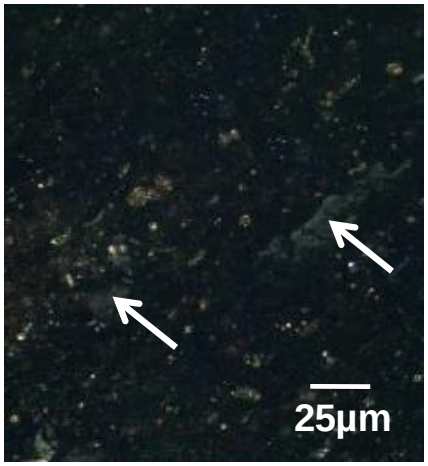

Fig. 2.14: Photomicrograph showing fusinite (white arrows, sample D1).

Fig. 2.15: Photomicrograph showing inertodetrinite (yellow arrows, sample D4).

2.3. Organic Geochemistry

Geochemically, the studied shales were evaluated using LECO, Rock Eval pyrolysis and gas chromatography-mass spectrometry (GC-MS). The results of these analyses are shown in Tables (1-8).

2.3.1. Source Rock Quality

Source rocks are generally organic-rich fine-grained sediments that are naturally capable of generating and releasing hydrocarbons in amounts to form commercial accumulations (Hunt, 1996). Rock-eval pyrolysis is used to determine the petroleum potentiality, thermal maturity of the organic matter and its ability to generate oil and/or gas. The utmost method is widely used for determining the amount and type of the organic matter in the rock and measuring petroleum potential via this method (Espitalie, 1984). The pyrolysis gives rise two parameters; S_1 and S_2, both are expressed as kilograms of hydrocarbons per ton of rock. S_1 measures the amount of free hydrocarbons that can be volatilizing out of the rock without cracking the kerogen (mg HC/g rock) while, S_2 measures the hydrocarbons yield from cracking of kerogen (mg HC/g rock). Generally, the organic richness is divided into five grades (Peters and Cassa, 1994). These grades are excellent (TOC>4%), very good (2%<TOC<4%), good (1%<TOC<2%), fair (0.5%<TOC<1%) and poor (TOC<0.5%).

Table 2.1: LECO and Rock Eval pyrolysis data of the Daryanah Shale

Sample No.	TOC	T_{max}	Ro	S_1	S_2	S_3	HI	OI	GP	PI
D1	0.87	422	0.45	3.33	2.55	1.12	293.10	128.74	5.88	0.57
D2	0.89	428	0.42	3.10	2.31	1.77	259.55	198.88	5.41	0.57
D3	0.80	426	0.49	2.56	2.09	1.10	261.25	137.50	4.65	0.55
D4	0.86	426	0.40	3.00	1.97	0.90	229.07	104.65	4.97	0.60
D9	0.40	419	0.34	2.47	0.92	0.87	230.00	217.50	3.39	0.73
D10	0.37	417	0.38	2.11	0.88	0.76	237.84	205.41	2.98	0.71
D16	0.33	419	0.29	2.05	0.89	0.51	269.70	154.55	2.94	0.70
D17	0.39	420	0.35	2.11	0.79	0.60	202.56	153.85	2.90	0.73

Table 2.2: Gas chromatogram data of normal alkanes and isoprenoids ratios of the Daryanah Shale (calculated on m/z 85)

Sample No.	Pr/Ph	(Pr+n-C_{17})/ (Ph+n-C_{18})	Pr/n-C_{17}	Ph/n-C_{18}	$\sum$(n-C_{12}-n-C_{20})/ ($\sum$(n-C_{12}-n-C_{20})+ $\sum$(n-C_{12}-n-C_{29}))	CPI	WI
D1	1.41	0.90	1.22	0.90	0.71	1.44	0.63
D2	1.58	0.77	1.25	0.81	0.57	1.54	0.70
D3	1.68	0.69	1.39	0.88	0.44	1.50	0.65
D4	1.62	0.81	1.31	0.93	0.62	1.32	0.56
D9	1.55	0.76	1.44	0.80	0.67	1.36	0.54
D10	1.64	0.55	1.29	0.82	0.52	1.33	0.57
D16	1.61	0.42	1.21	0.85	0.46	1.33	0.72
D17	1.50	0.39	1.21	0.77	0.48	1.40	0.77

Table 2.3: Gas chromatogram data of steranes and diasteranes of the Daryanah Shale (calculated on m/z 217)

Sample No.	C_{27}	C_{28}	C_{29}	C_{29} (ββ/ββ+αα)	C_{29} βα(S+R)-dia/ (C_{28} βα(S+R)-dia+ C_{27} βα(S+R)-dia)
D1	46.18	4.45	49.37	0.23	1.00
D2	46.44	3.97	49.59	0.27	0.88
D3	35.28	24.35	40.37	0.22	0.93
D4	35.00	27.29	37.71	0.24	1.05
D9	33.50	31.50	35.00	0.24	0.65
D10	32.08	34.25	33.67	0.16	0.54
D16	44.65	8.87	46.48	0.19	0.44
D17	44.23	10.21	45.56	0.19	0.56

Table 2.4: Continued

Sample No.	C_{29} steranes: ββ/(αα+ββ)	C_{29} steranes: 20S/(20S+20R)	C_{30} sterane index
D1	0.33	0.16	0.09
D2	0.30	0.17	0.08
D3	0.25	0.11	0.07
D4	0.29	0.09	0.09
D9	0.11	0.24	0.14
D10	0.15	0.26	0.13
D16	0.13	0.27	0.13
D17	0.11	0.27	0.15

Table 2.5: Gas chromatogram data of terpanes, hopanes and TPP ratios of the Daryanah Shale (calculated on m/z 217)

Sample No.	$C_{31}R/C_{30}H$	C_{32} 22S/(22S+22R)	G/C_{30}	C_{31} 22R/H	C_{35}/C_{34} homohopanes	Hopanes/(Hopanes+ ∑20R steranes)	TPP
D1	0.47	0.39	0.58	0.28	0.59	0.48	0.19
D2	0.50	0.43	0.64	0.26	0.66	0.52	0.16
D3	0.46	0.33	0.70	0.32	0.88	0.59	0.22
D4	0.45	0.33	0.56	0.39	0.65	0.56	0.21
D9	0.51	0.45	0.82	0.55	0.33	0.33	0.24
D10	0.48	0.41	0.88	0.57	0.29	0.31	0.16
D16	0.49	0.41	0.73	0.59	0.43	0.31	0.17
D17	0.49	0.29	0.70	0.48	0.39	0.44	0.19

Table 2.6: Continued

Sample No.	Ts/(Ts+Tm)	29Ts/(29Ts+30NH)	$(C_{19}+C_{20})/(C_{23}+C_{24})$ TT	C_{24} TeT/C_{26} TT	$(C_{19}+C_{20})/C_{23}$ TT
D1	0.18	0.07	1.11	2.10	1.40
D2	0.19	0.05	0.69	1.82	0.94
D3	0.19	0.05	0.89	1.77	1.15
D4	0.13	0.05	0.78	1.96	1.33
D9	0.05	0.16	0.33	0.82	0.76
D10	0.09	0.18	0.37	0.88	0.69
D16	0.09	0.19	0.41	0.91	0.67
D17	0.08	0.19	0.32	0.90	0.67

Table 2.7: Continued

Sample No.	C_{23}/ C_{21} TT	C_{29} TT/ C_{30} hopane	C_{28} TT/ C_{30} hopane	C_{25} TT/ C_{24} TeT	C_{24} TeT/ (C_{24} TeT+ C_{26} TT)
D1	0.88	0.05	0.09	0.31	0.52
D2	0.72	0.07	0.04	0.84	0.59
D3	0.43	0.04	0.07	0.25	0.50
D4	0.35	0.02	0.05	0.62	0.61
D9	1.14	0.10	0.19	0.17	0.23
D10	1.09	0.12	0.19	0.15	0.25
D16	1.00	0.12	0.17	0.19	0.28
D17	1.05	0.11	0.16	0.18	0.28

Table 2.8: Continued

Sample No.	C_{30} diahopane/ C_{30} hopane	C_{29} diahopane/ C_{29} hopane
D1	0.21	0.41
D2	0.29	0.22
D3	0.35	0.29
D4	0.41	0.33
D9	0.10	0.16
D10	0.10	0.17
D16	0.09	0.17
D17	0.10	0.13

Where:

TOC = total organic carbon (wt. %)

S_1 = amount of free hydrocarbons in sample (mg/g)

S_2 = amount of hydrocarbons generated through thermal cracking (mg/g) – provides the quantity of hydrocarbons that the rock has the potential to produce through diagenesis

S_3 = amount of CO_2 (mg of CO_2/g of rock) - reflects the amount of oxygen in the oxidation step

T_{max} = the temperature at which maximum rate of generation of hydrocarbons occurs

Hydrogen index: HI = 100 * S_2/TOC

Oxygen index: OI = 100 * S_3/TOC

Production index: PI = S_1 / (S_1+S_2)

Semi-quantitative index: GP = S_1/S_2

Ro = vitrinite reflectance (wt. %)

Pr/Ph = Pristane/Phytane

Carbon preference index: CPI = 2(C_{23}+C_{25}+ C_{27}+C_{29})/(C_{22}+2[C_{24}+C_{26}+C_{28}]+C_{30})

Waxiness index: WI = Σ(n-C_{21}-n-C_{31})/Σ(n-C_{15}-n-C_{20})

TPP = tetracyclic polyprenoid

Ts = C_{27} 18α(H)-22,29,30-trisnorneohopane

Tm = C_{27} 17α(H)-22,29,30-trisnorhopane

The lower shale samples contain TOC >0.5% and are fair source rocks according to the standard given by Peters and Cassa (1994). There is no significant difference in the TOC content (<0.5%) in the middle and upper shales, which suggests that these shales have poor quality. To confirm the assumptions mentioned above, the plots of TOC vs. S_2 and TOC vs. GP were used in this chapter (Figs. 2.16-17).

2.3.2. Organic Matter Type

Kerogen includes all solid organic matter in all sedimentary rocks. Most classification of kerogen are based on the chemical properties of kerogen, usually isolated by demineralization techniques, and belong to one of the following types: (i) elemental analysis; (ii) “bitumen” or soluble fraction extraction; (iii) chemical degradation (including oxidation, hydrogenolysis, and pyrolysis); (iv) functional analysis; (v) electron spin resonance studies; and (vi) nuclear magnetic resonance studies (Hutton *et al.*, 1994). Many authors (e.g., Hutton *et al.*, 1994; Xianming *et al.*, 2000; Werner-Zwanziger *et al.*, 2005; Mao *et al.*, 2010; Liao *et al.*, 2015; Burnham, 2019) clearly mean maceral when using the term kerogen.

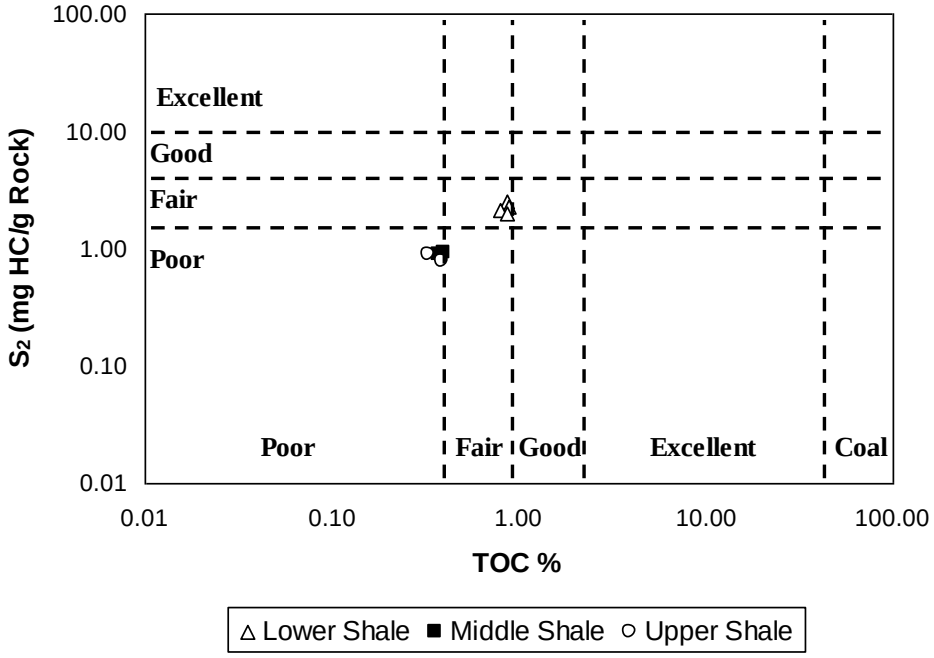

Fig. 2.16: Plot of TOC vs. S_2 showing the hydrocarbon potentialities for the studied shales (fields after Dembicki, 2009).

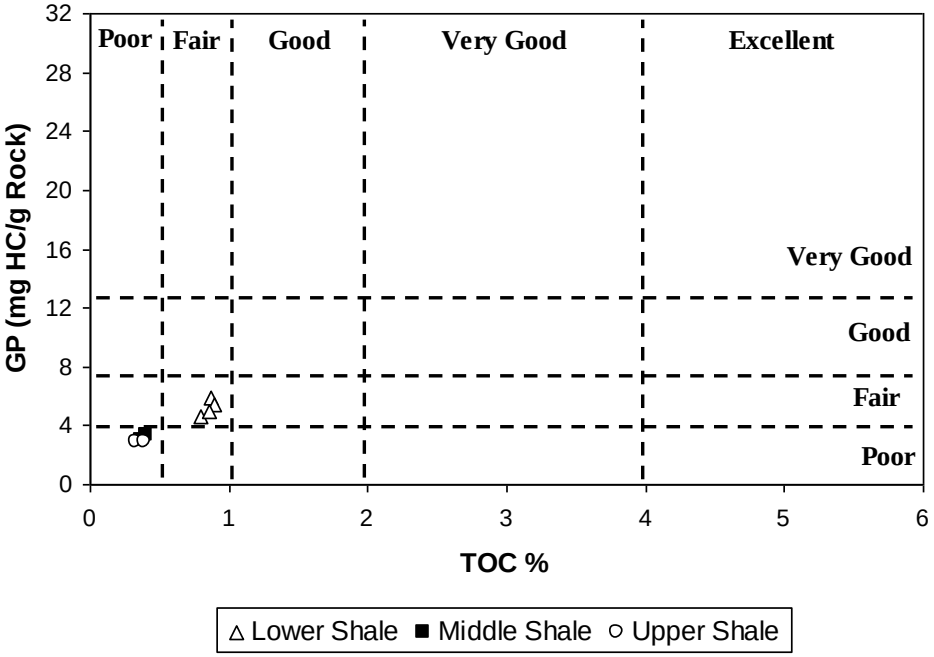

Fig. 2.17: Plot of TOC vs. GP showing the hydrocarbon potentialities for the studied shales (fields after Ghori, 2002).

The TOC, S_2, T_{max}, HI and OI values of the Daryanah Shale range from 0.33 to 0.89%, 0.79 to 2.55mg HC/g Rock, 417 to 428°C, 202.56 to 293.1mg HC/g TOC and 104.65 to 217.5mg CO_2/g TOC, respectively. This finding suggests that the organic matter contains predominantly kerogens of type II/III and III. Confirmation of this hypothesis was done using the plots of T_{max} versus HI, OI versus HI and TOC versus S_2 (Figs. 2.18-20). The dominance of vitrinite and liptinite macerals, and the small contribution of inertinite indicate a mixed origin for the kerogen. However, the significant content of liptinite and vitrinite could influence the measured values of TOC and HI. Additionally, nonindigenous (migrated) hydrocarbons are dominant in the studied shales (Fig. 2.21).

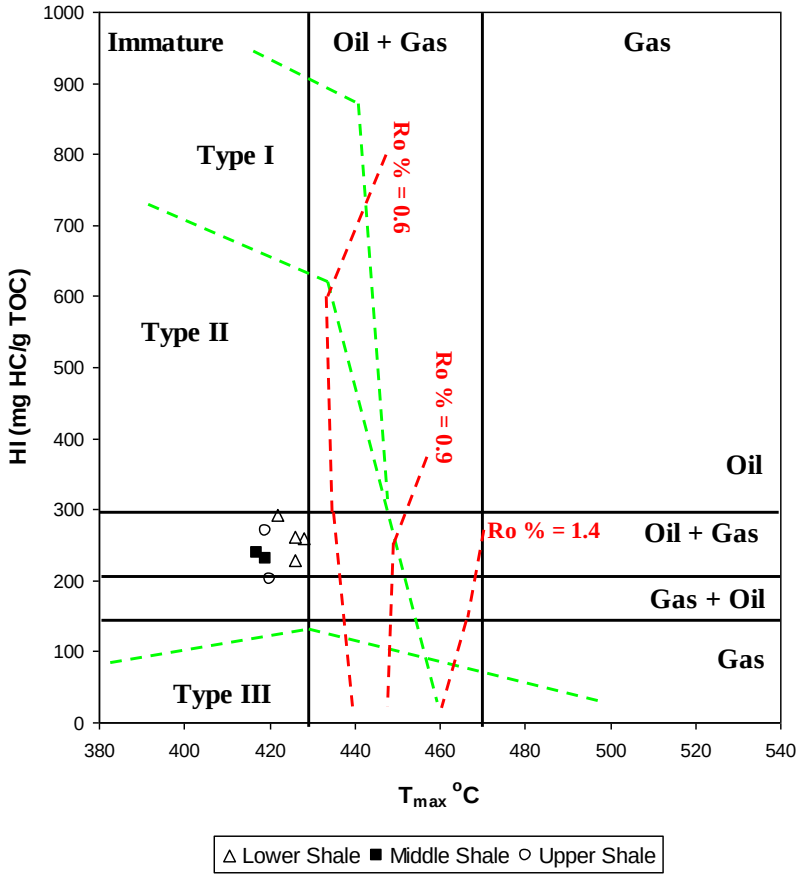

Fig. 2.18: Plot of T_{max} vs. HI showing the thermal maturity for the studied shales (fields after Hall et al., 2016).

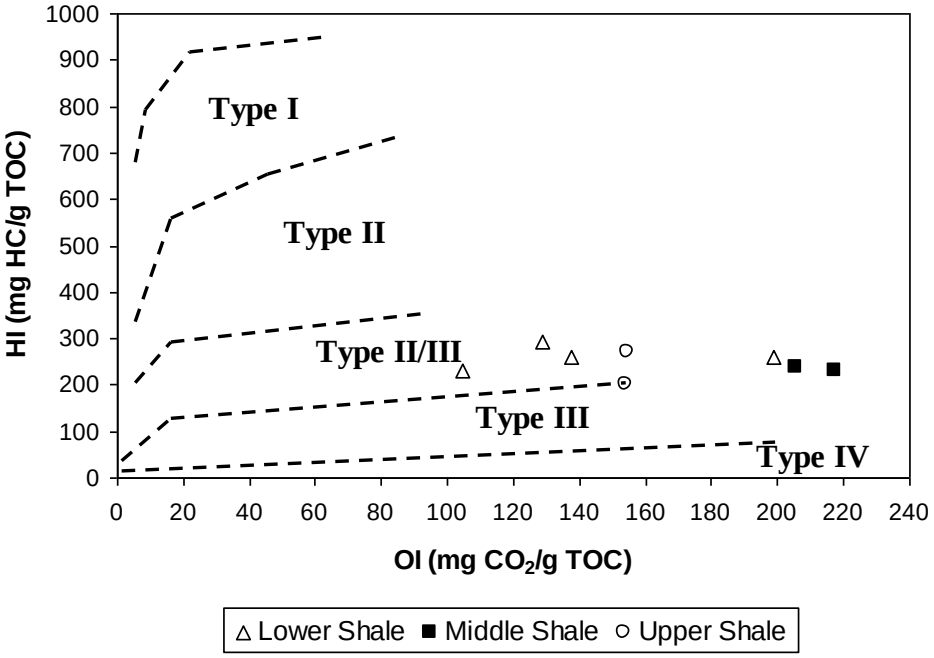

Fig. 2.19: Plot of OI vs. HI showing the kerogen type for the studied shales (fields after Van Krevelen, 1961).

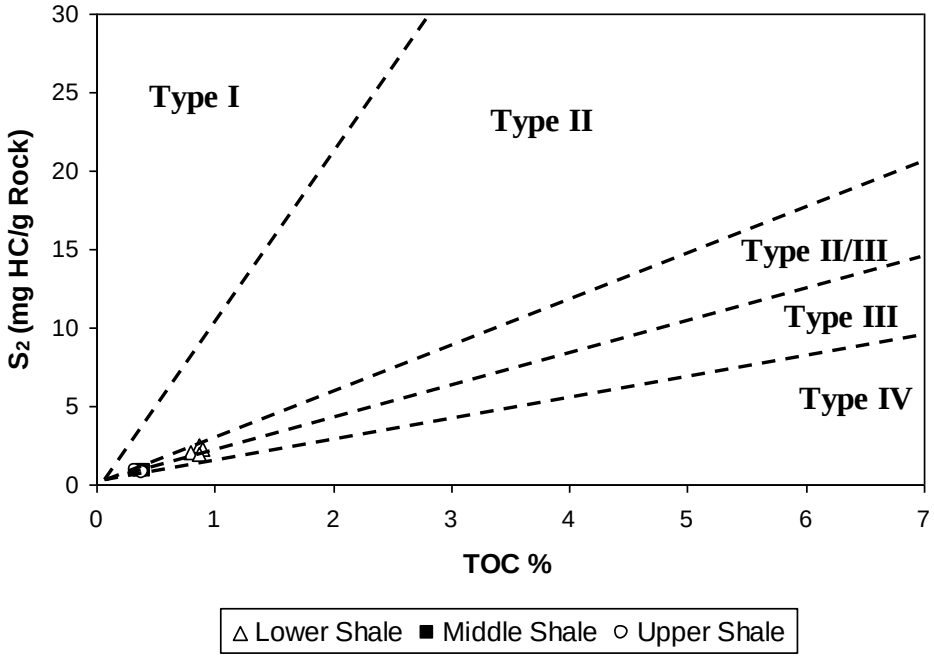

Fig. 2.20: Plot of TOC vs. S_2 showing the kerogen type for the studied shales (fields after Longford and Blanc-Valleron, 1990).

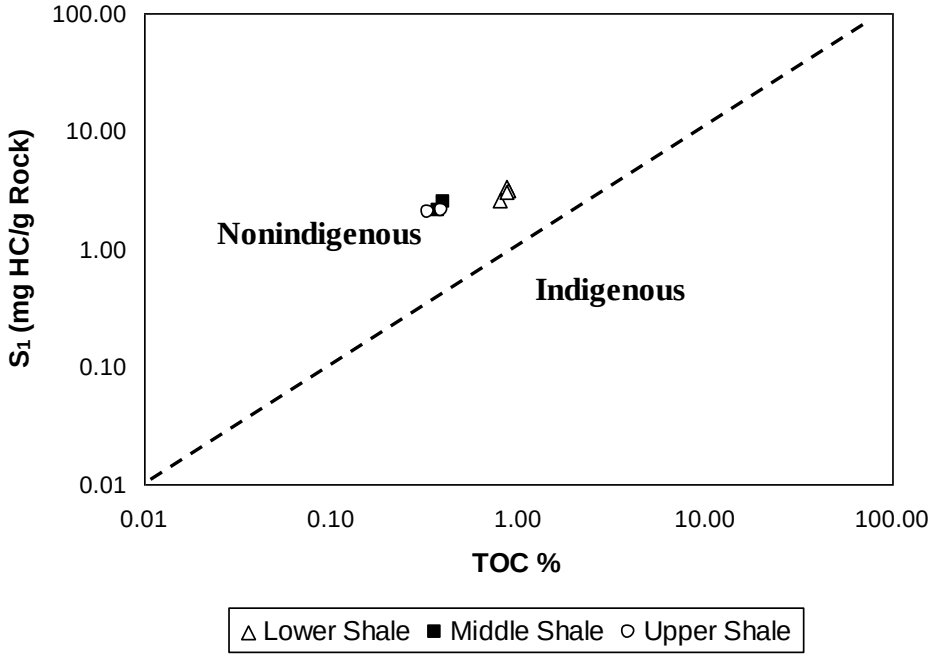

Fig. 2.21: Plot of TOC vs. S_1 showing the status of hydrocarbons for the studied shales (fields after Hunt, 1996).

2.3.3. Thermal Maturity

As a general rule, T_{max} increases linearly with the degree of maturation of the organic matter (Espitalie, 1984), thus giving a rapid estimate of the thermal maturity of sedimentary basins. T_{max} is dependent on the cracking kinetics of the organic matter and is correlated with the type of organic matter: lacustrine (type I), marine (type II) and continental (type III). The relationship between T_{max} and different stages of oil and gas formation zones varies with the type of organic matter; however type III is the most reliable in estimating the degree of maturation (Espitalie, 1984). The variation of T_{max} with the organic matter maturity has been compared to the change in vitrinite reflectance (Ro) and, for the kerogen of type III, the beginning of the oil formation is characterized by Ro of 0.5% and T_{max} in the range 430-435ºC, whereas the transition oil-gas zone is fixed at Ro of 1.35% and T_{max} ~465ºC (Espitalie, 1984). Fig (2.18) and Figs (2.22-23) show the immaturity of organic matter in the studied shales.

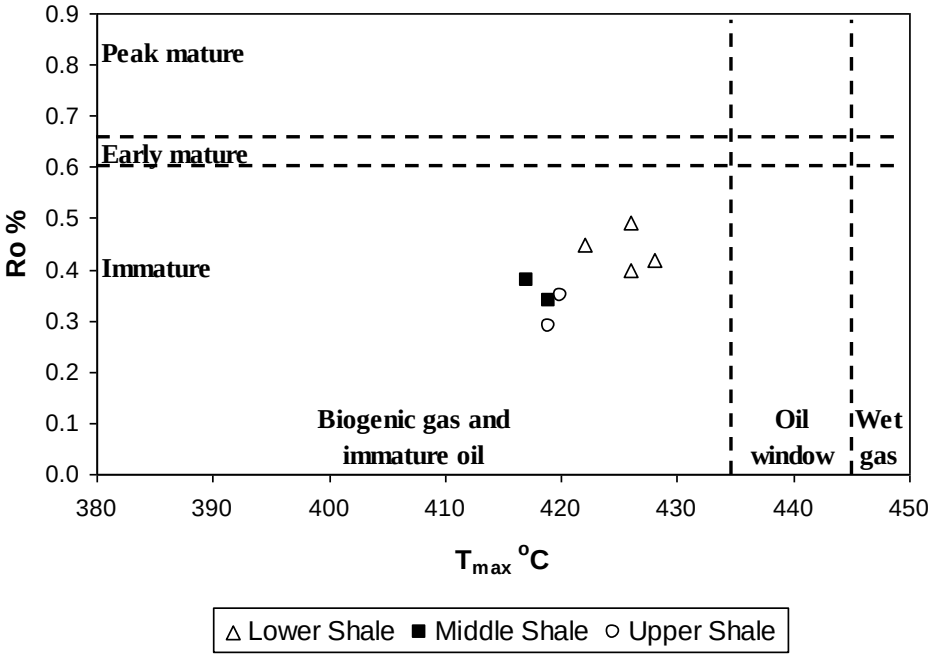

Fig. 2.22: Plot of T_{max} vs. Ro showing the thermal maturity for the studied shales (fields after Atta-Peters and Garrey, 2014).

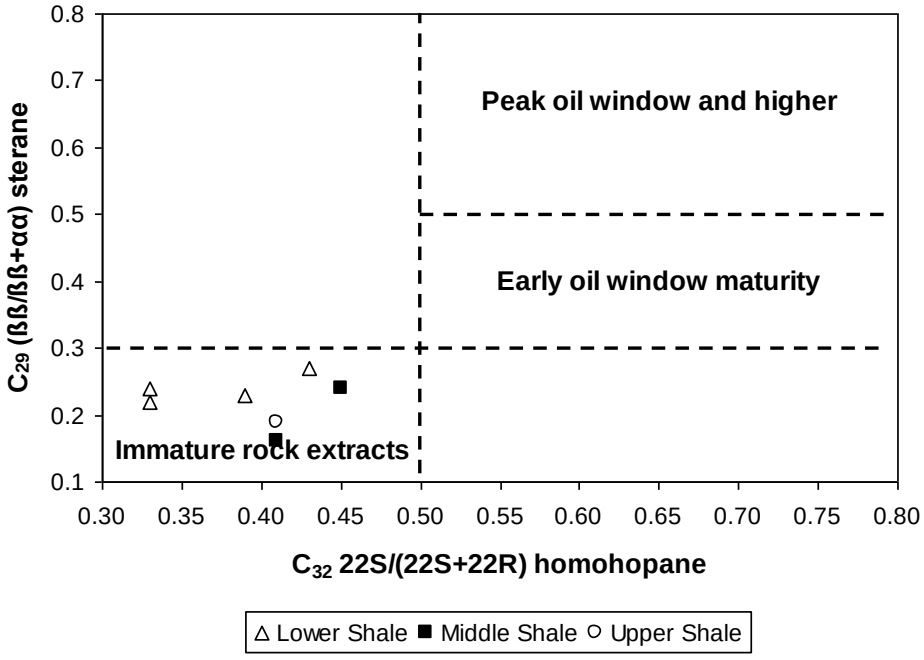

Fig. 2.23: Plot of C_{32} 22S/(22S+22R) homohopane vs. C_{29} (ßß/ßß+αα) sterane showing the thermal maturity for the studied shales (fields after Peters and Moldowan, 1993).

2.3.4. Organic Matter Input, Redox Condition and Depositional Environment

Biomarkers are natural products that can be assigned as particular biosynthetic origin (Cai *et al.,* 2009; Song *et al.,* 2013; El-Sabagh *et al.,* 2018). These compounds are useful in geological and environmental studies, where, they are recalcitrant against geochemical changes and easily analyzable in environmental samples (Cai *et al.,* 2009; Song *et al.,* 2013; Cheng *et al.,* 2019). Accordingly, biomarkers can be regarded as a chemical fossil, meaning that these compounds originated from formerly living organisms (Mello *et al.,* 1988; Simoneit, 2004). Occurrences and distributions of biological markers patterns of crude oils are commonly used for oil/oil and oil/source rock correlations and to assess such source rock attributes as lithology, depositional environment, kerogen type and maturity (Peters *et al.,* 2005). The exploration applications of biomarkers rely on the premise that the biomarker pattern of oil is imprinted by the source rock. However, the source-related biomarker pattern may have been altered by a number of processes after generation and expulsion from the source rock. One of the most important processes which affect crude oils in reservoirs, especially shallow reservoirs, is biodegradation. Most researchers consider aerobic bacteria to be the principal agents in the subsurface degradation of petroleum (Peters *et al.,* 2005). To determine the organic matter input, redox condition and depositional environment, several plots were used in this study. The triplot of C_{27}-C_{28}-C_{29} regular steranes (Fig. 2.24) and the biplots of Pr/Ph versus CPI, Pr/Ph versus WI, Pr/Ph versus C_{29}/C_{27} regular steranes, Ph/n-C_{18} versus Pr/n-C_{17}, Pr/Ph versus $\sum$(n-C_{12}-n-C_{20})/($\sum$(n-C_{12}-n-C_{20})+$\sum$(n-C_{12}-n-C_{29})) and Pr/Ph versus C_{29} ßα(S+R)-dia/(C_{28} ßα(S+R)-dia+C_{27} ßα(S+R)-dia) (Figs. 2.25-30) refer to the dominance of mixed organic matter formed under suboxic conditions. Furthermore, the biplots of Pr/Ph versus C_{31}22R/C_{30}- Hopane, Pr/Ph versus (Pr+n-C_{17})/(Ph+n-C_{18}), Hopanes/(Hopanes+$\sum$20R steranes) versus TPP and Pr/Ph versus G/C_{30} (Figs. 2.31-34) suggest deposition in a high salinity marine environment.

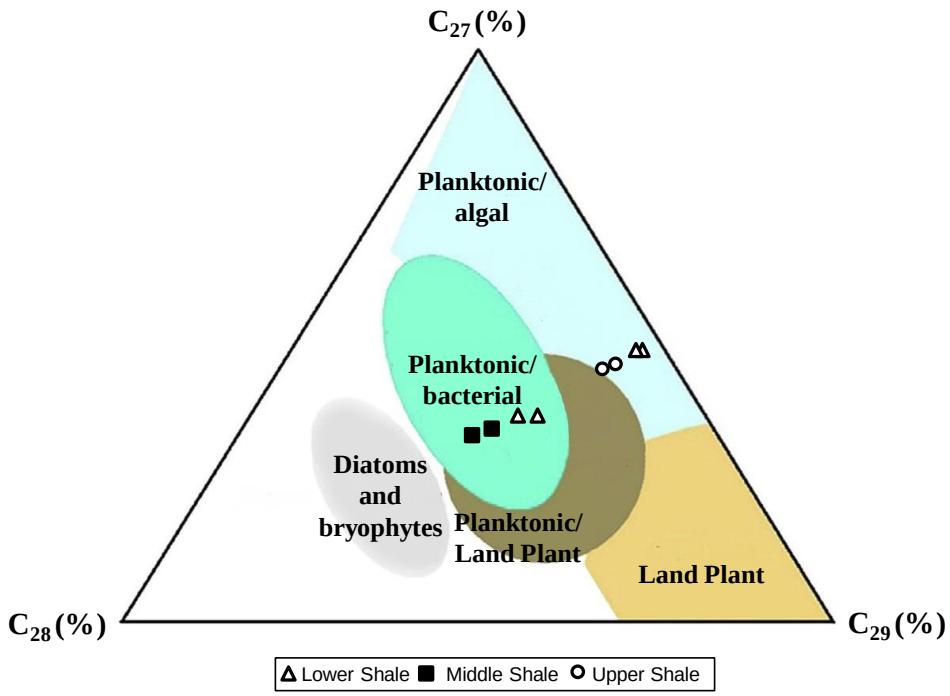

Fig. 2.24: Ternary diagram of C_{27}-C_{28}-C_{29} regular steranes showing the organic matter origin for the studied shales (fields after Huang and Meinschein, 1979).

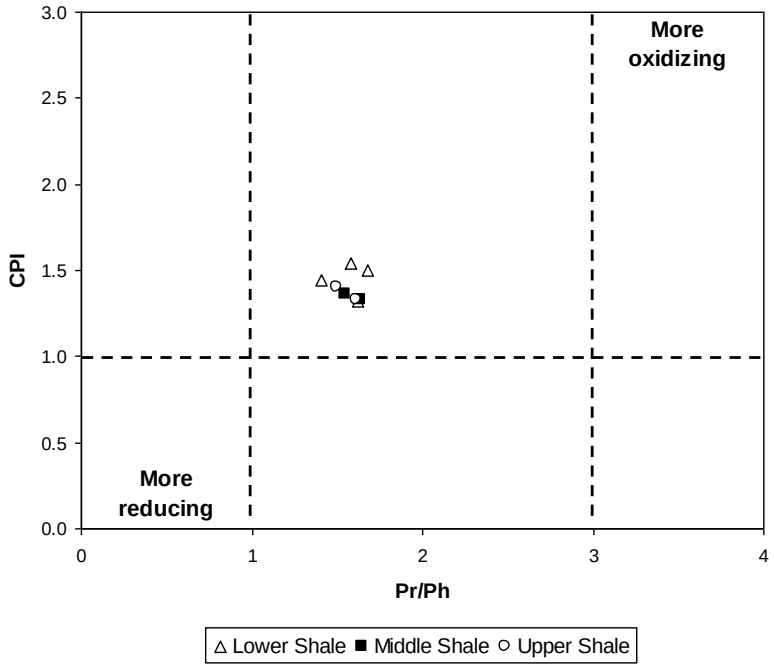

Fig. 2.25: Plot of Pr/Ph vs. CPI showing the organic matter origin and redox conditions for the studied shales (fields after Akinlua et al., 2007).

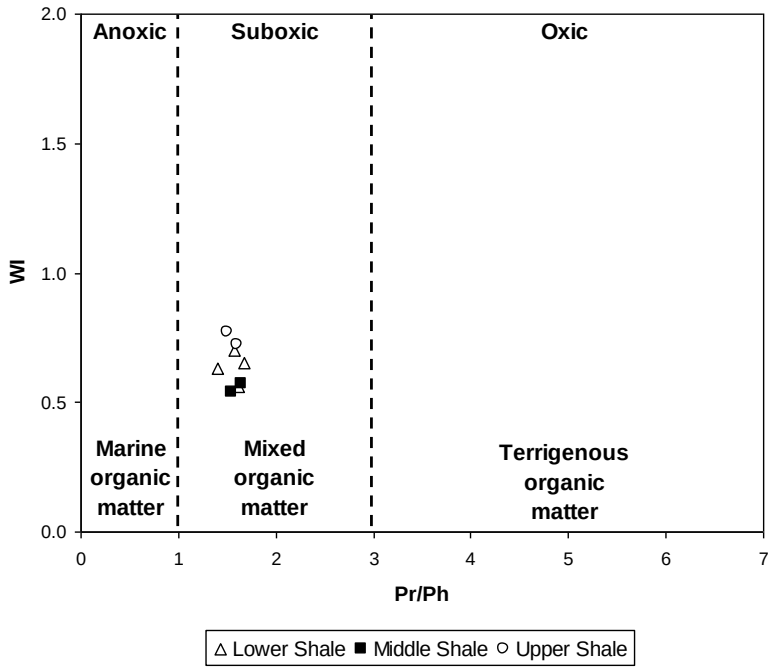

Fig. 2.26: Plot of Pr/Ph vs. WI showing the organic matter origin and redox conditions for the studied shales (fields after El Diasty and Moldowan, 2012).

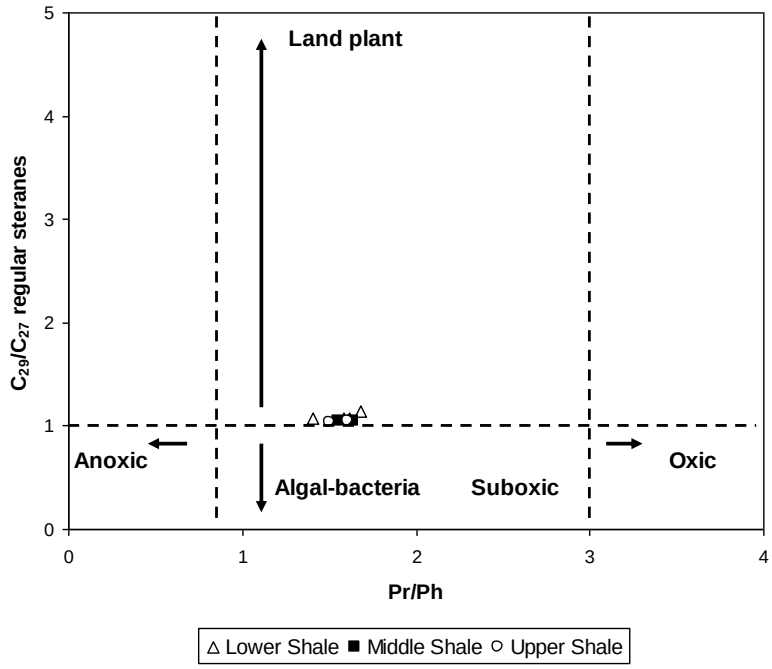

Fig. 2.27: Plot of Pr/Ph vs. C_{29}/C_{27} regular steranes showing the organic matter origin and redox conditions for the studied shales (fields after Yandoka et al., 2015).

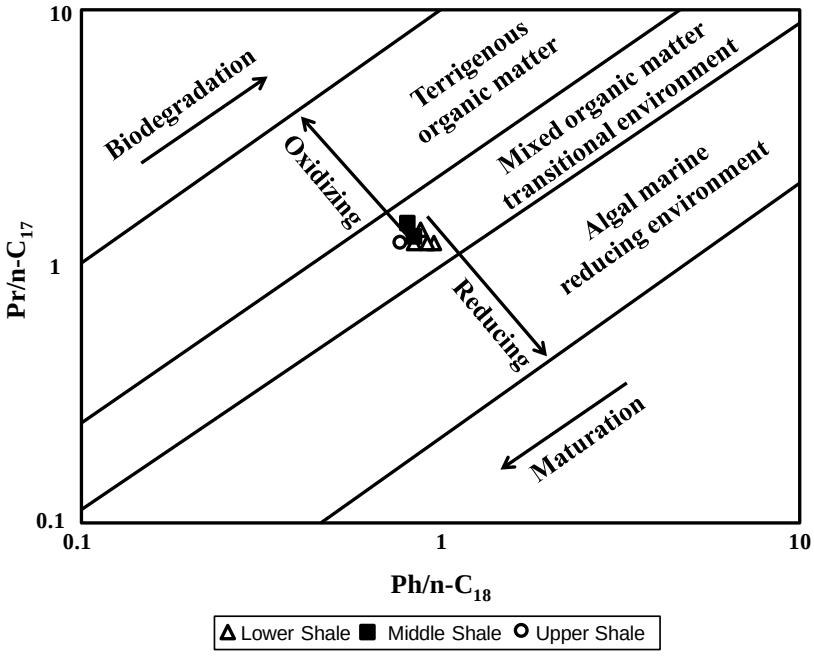

Fig. 2.28: Plot of Ph/n-C_{18} vs. Pr/n-C_{17} showing the organic matter origin and redox conditions for the studied shales (fields after Shanmugam, 1985).

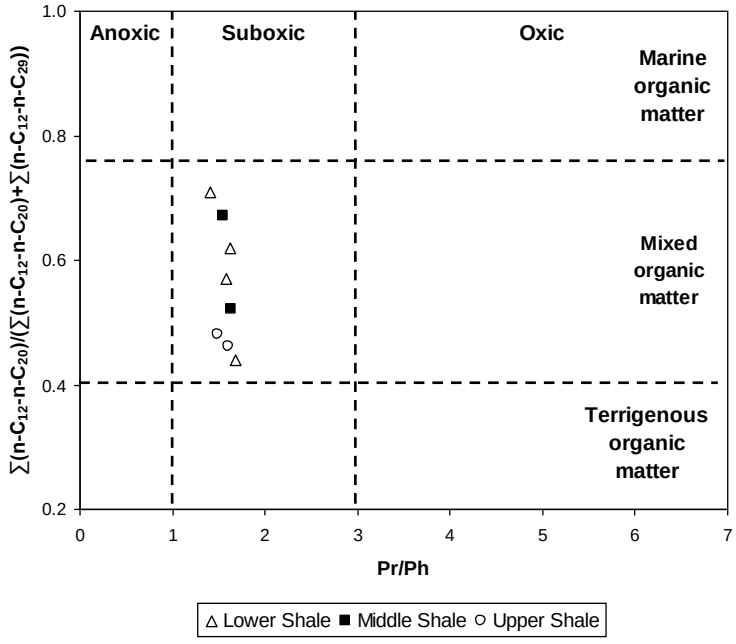

Fig. 2.29: Plot of Pr/Ph vs. n-alkane SLR (Σn-C_{12-20})/(Σn-C_{12-29}) showing the organic matter origin and redox conditions for the studied shales (fields after Shaltami et al., 2019).

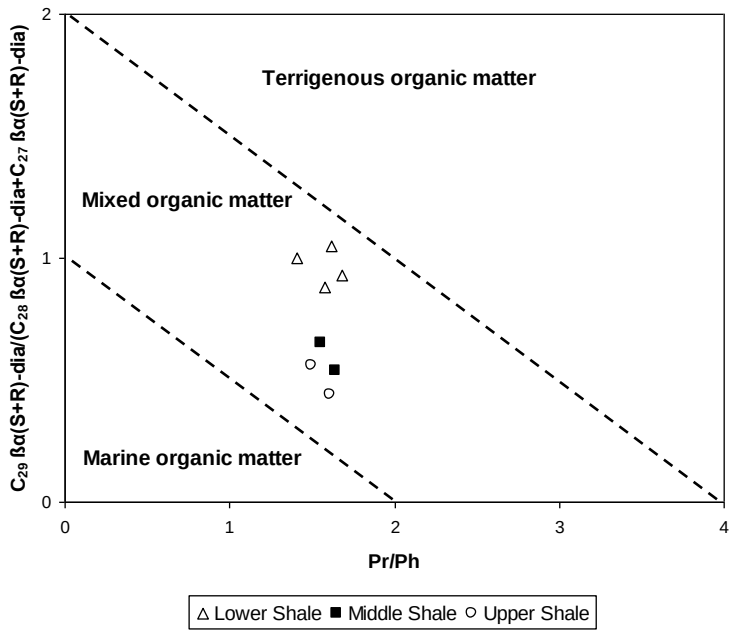

Fig. 2.30: Plot of Pr/Ph vs. predominance of C_{29} -components amongst diasteranes showing the organic matter origin for the studied shales (fields after Shaltami et al., 2019).

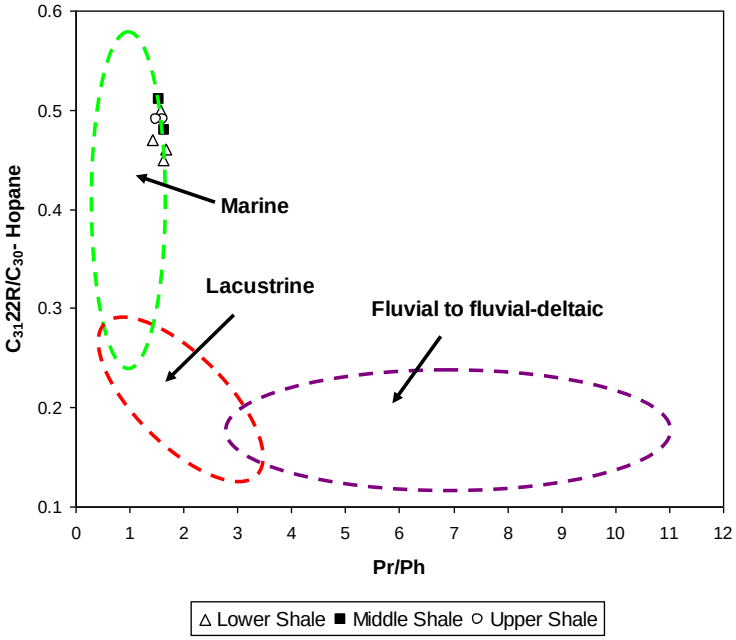

Fig. 2.31: Plot of Pr/Ph vs. $C_{31}R/C_{30}$ hopane showing the depositional environment of the studied shales (fields after Peters et al., 2005).

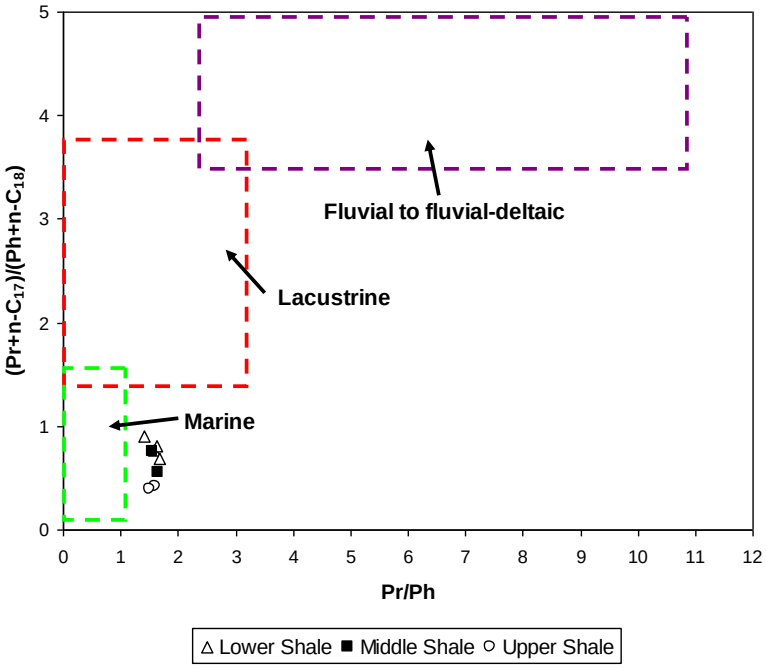

Fig. 2.32: Plot of Pr/Ph vs. (Pr+n-C_{17})/(Ph+n-C_{18}) showing the depositional environment of the studied shales (fields after Shaltami et al., 2019).

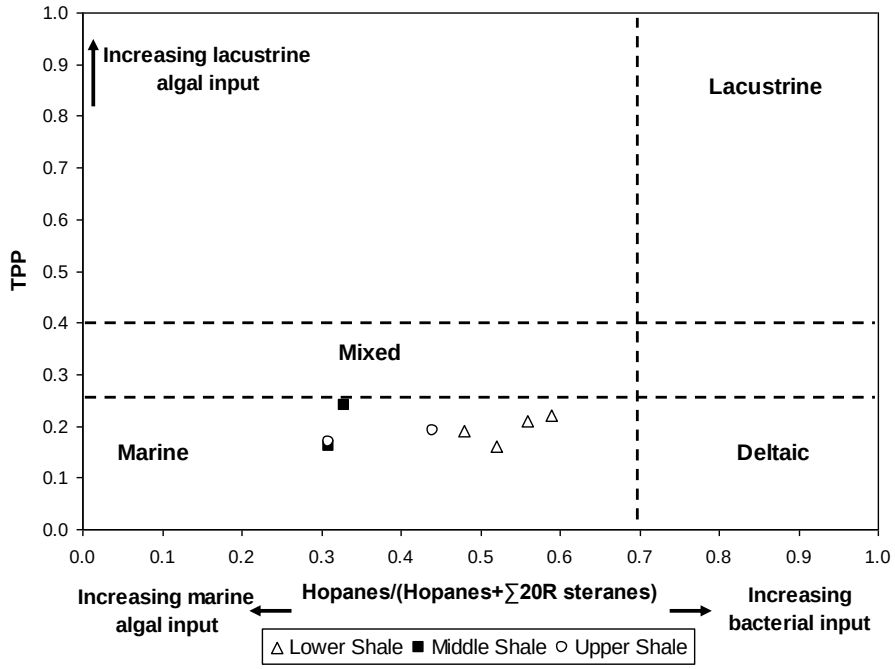

Fig. 2.33: Plot of TPP vs. hopane/(hopanes+Σ20R steranes) showing the depositional environment of the studied shales (fields after Holba et al., 2003).

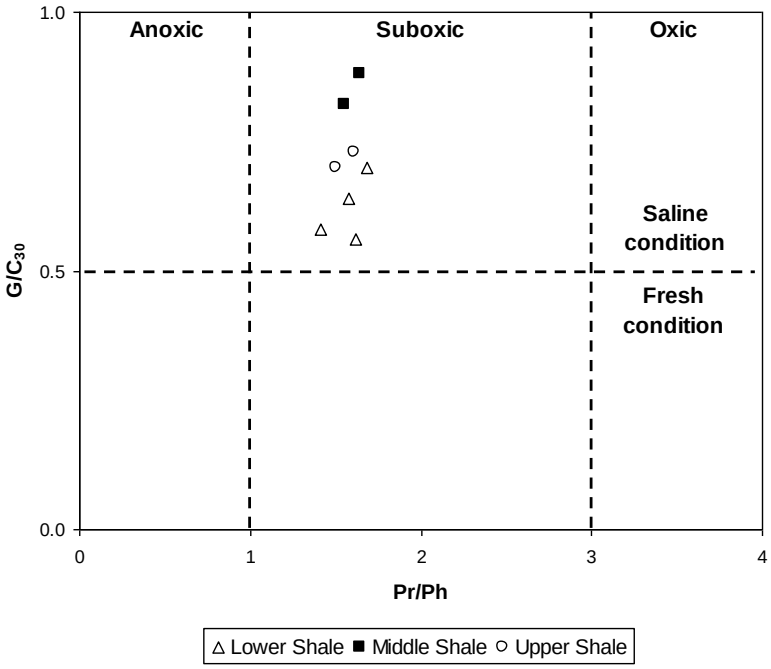

Fig. 2.34: Plot of Pr/Ph vs. G/C_{30} showing the paleosalinity and redox conditions for the studied shales (fields after Zhou and Huang, 2008).

CHAPTER THREE
RESERVOIR GEOCHEMISTRY

3.1. Introduction

Traditionally, fluid geochemistry has played little role in reservoir engineering practice, with some notable exceptions (Larter *et al.,* 1997). Since 1985, however, the focus of geochemistry in the petroleum industry has shifted away from exploration toward reservoir appraisal and production (Larter *et al.,* 1997; England, 2007; Li *et al.,* 2018). This new focus has been termed "reservoir geochemistry" and has been recently reviewed by many authors (e.g., Carpentier *et al.,* 2007; Zhu *et al.,* 2015; Yang *et al.,* 2019). Because geochemists deal with both reservoir rocks and their contained fluids, reservoir geochemistry provides a natural, but underexploited, link between reservoir geologists and reservoir/petroleum engineers (Carpentier *et al.,* 2007; Kolchugin *et al.,* 2016; Li *et al.,* 2019).

Petroleum-bearing fluid inclusions (petroleum inclusions) are small aliquots of pore fluids trapped within the framework of rock-forming minerals. These fluid inclusions typically range in size from <1µm to ~20µm and are present in a wide variety of different minerals (e.g., Burruss, 1981; Pironon *et al.,* 1995; Munz, 2001; Arouri *et al.*, 2009; Liu *et al.,* 2014; Shaltami *et al.,* 2018). They offer direct evidence about the nature of pore-filling petroleum at different times in the geological past. This makes them the witness of paleo-fluid compositions during petroleum migration and accumulation, offering an opportunity to map petroleum presence and composition through time and space (Volk and George, 2019). The presence of petroleum inclusions indicates that petroleum was present in the pore space at the time that the host mineral phase formed or when a fracture was propagated through an existing mineral (Burruss, 1981; Munz, 2001; Liu *et al.,* 2014; Shaltami *et al.,* 2019).

Shaltami *et al.,* (2018) are the first to apply the technology of petroleum inclusions to evaluate reservoirs in Libya. This study was a geochemical evaluation of the crude oil found in the petroleum inclusions of the Achabiyat and Hawaz reservoirs in the Dur Al Qussah area,

Murzuq Basin, SW Libya. This chapter is a geochemical evaluation of the natural gas and crude oil in the petroleum inclusions of the Daryanah Reservoir.

3.2. Petroleum Inclusions

The SEM shows that the lower limestone is rich in petroleum inclusions, while the inclusions are very rare or not found in the dolostone, calcareous sandstone and upper limestone. Accordingly, the lower limestone can be considered a reservoir (Daryanah Limestone) and therefore the study was focused on it. The detected petroleum inclusions are of two-phase (Figs. 3.1-4). The two phases are mainly crude oil and natural gas in most inclusions. These inclusions have irregular patterns and different shapes. Clearly, the inclusions have a different chemical composition.

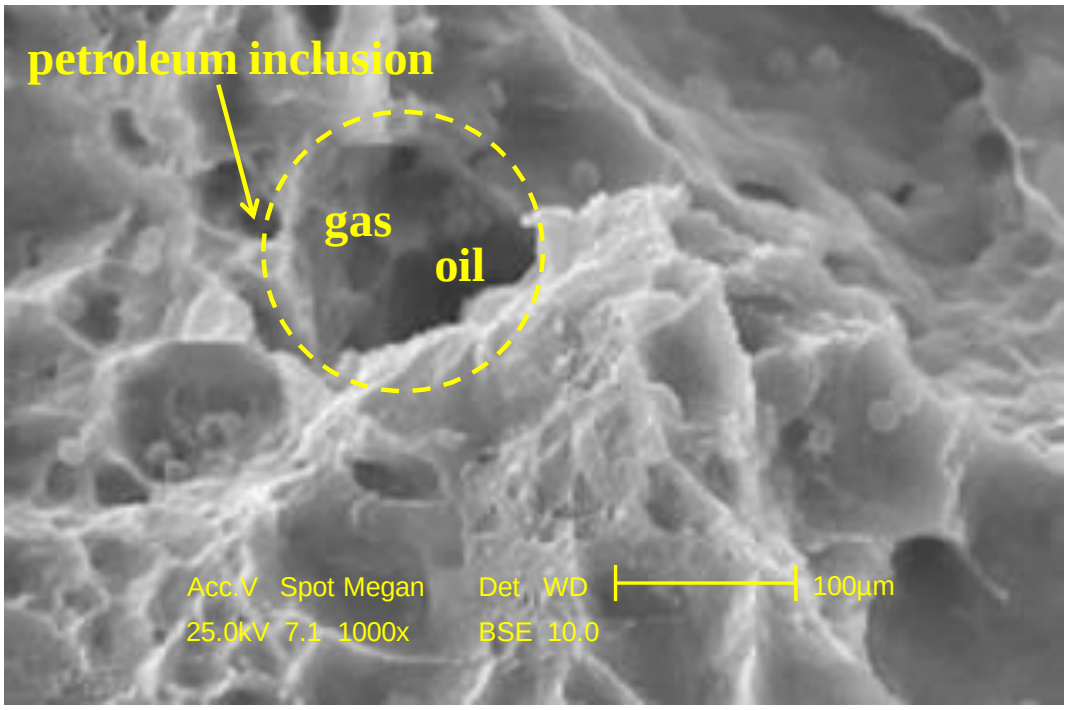

Fig. 3.1: BSE image of irregular petroleum inclusions (Sample D5).

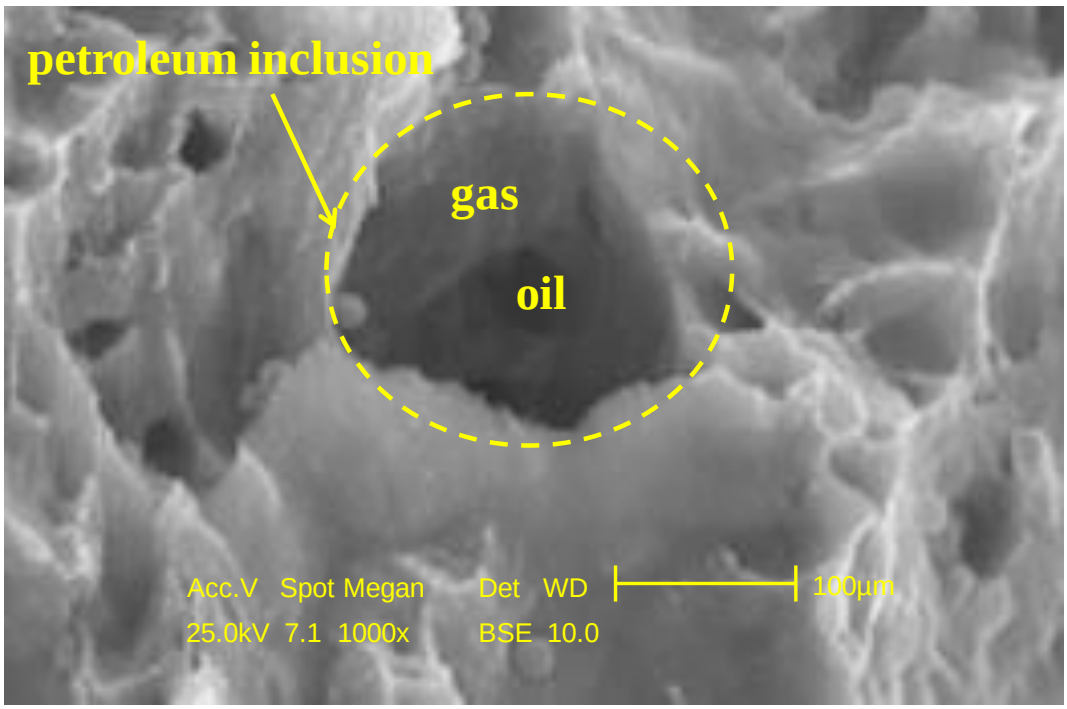

Fig. 3.2: BSE image of irregular petroleum inclusions (Sample D6).

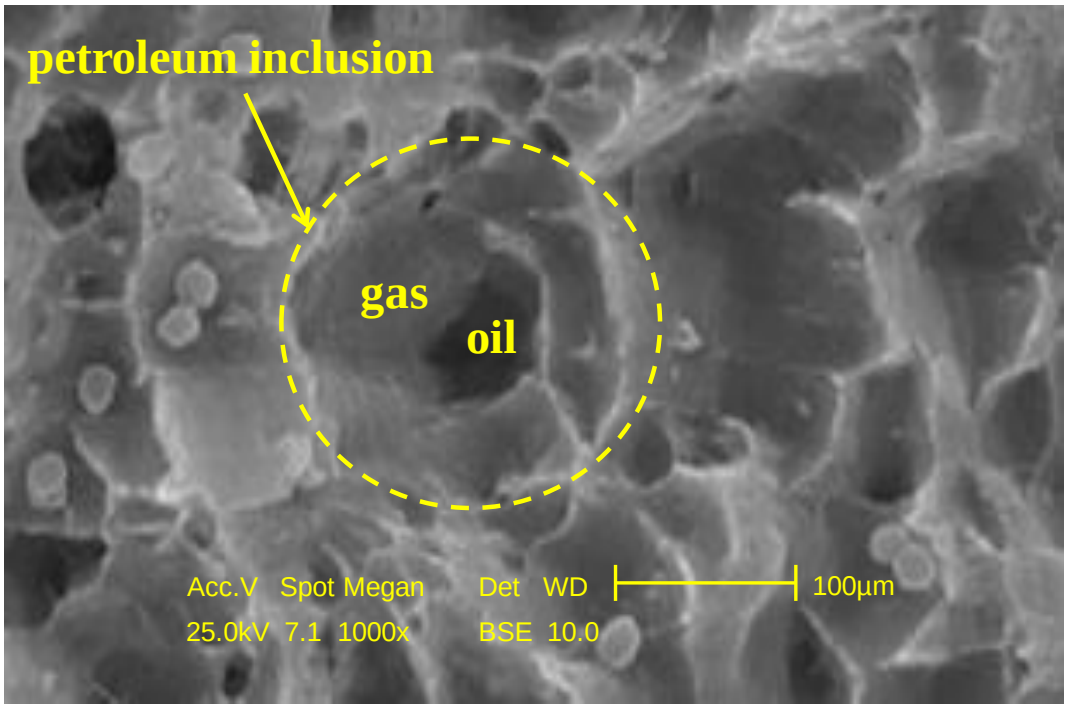

Fig. 3.3: BSE image of irregular petroleum inclusions (Sample D7).

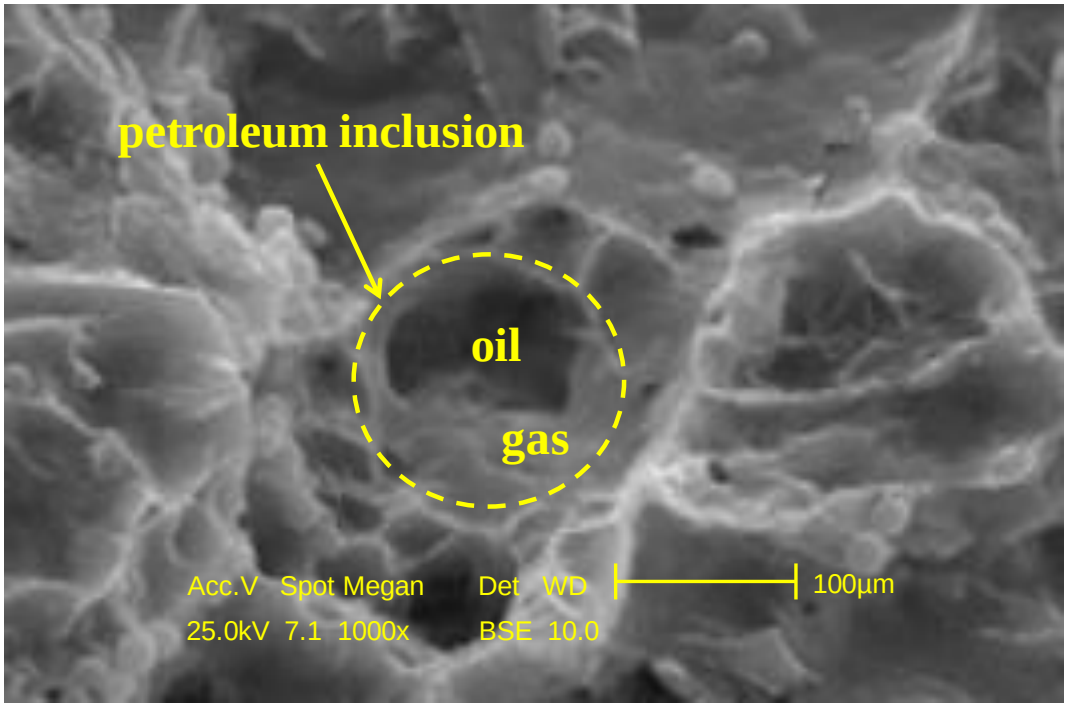

Fig. 3.4: BSE image of irregular petroleum inclusions (Sample D8).

3.3. Types of Natural Gas

Hydrocarbon gases are common in marine sediments (Claypool and Kvenvolden, 1983; Prinzhofer *et al.*, 2000; Alsaab *et al.*, 2008; Liao *et al.*, 2015; Zhao *et al.*, 2019). Such gases originate from decomposition of organic matter by biochemical and chemical processes. These gases are shown in Table (3.1). In addition, inorganic gases such as N_2 and Ar are present, but usually as minor or trace components in natural gas (Claypool and Kvenvolden, 1983). There are also gases of mixed origin, such as CO_2 and H_2S, but they are also found in small quantities in marine sediments. According to Claypool and Kvenvolden (1983) there are three main stages of natural gas formation. The earliest stage is biological C_1 formation, which occurs at low temperatures (<50^{o}C) under certain environmental conditions. The next stage is early thermogenic (nonbiological) gas formation, in which the whole series of gaseous and liquid hydrocarbons are formed at rates that become geologically significant when burial temperatures are in the range of 80-120^{o}C. Late thermogenic C_1-rich gas is produced during the last stage of gas formation, at temperatures higher than about 150^{o}C at which previously formed heavier

hydrocarbons are converted to C_1. Natural gas formed during each of these stages has a characteristic chemical and isotopic composition.

The types of natural gas in the petroleum inclusions are listed in Table (3.2). In general, the Daryanah Reservoir inclusions contain high concentration of hydrocarbon gases (especially C_1, Fig. 3.5) with lesser content of nonhydrocarbon gases (H_2, H_2S, CO_2 and N_2).

Table 3.1: Hydrocarbon gases in marine sediments (after Claypool and Kvenvolden, 1983)

Name	Symbol	Molecular formula
Methane	C_1	CH_4
Ethane	C_2	C_2H_6
Ethene (Ethylene)	$C_{2=}$	C_2H_4
Propane	C_3	C_3H_8
Propene	$C_{3=}$	C_3H_6
Isobutane	iC_4	C_4H_{10}
n-Butane	nC_4	C_4H_{10}

Table 3.2: Components of gases (%) in the Daryanah Reservoir inclusions

Sample No.	C_1	C_2	$C_{2=}$	C_3	$C_{3=}$	iC_4	nC_4	H_2	H_2S	CO_2	N_2
D5(1)	79.00	9.20	0.04	6.11	0.02	1.57	1.50	0.77	0.11	2.00	0.09
D5(2)	77.77	11.05	0.04	6.17	0.02	1.60	1.63	0.81	0.09	1.85	0.12
D5(3)	81.09	8.67	0.06	5.55	0.03	1.46	1.41	0.69	0.10	1.74	0.17
D6(1)	74.63	13.00	0.04	7.07	0.04	1.71	1.66	0.92	0.22	1.36	0.26
D6(2)	56.21	22.21	0.08	10.23	0.04	3.32	2.92	3.34	2.79	3.00	0.98
D6(3)	57.00	21.88	0.08	10.00	0.04	3.56	3.50	3.06	2.83	2.77	1.05
D7(1)	56.09	23.10	0.08	10.19	0.04	3.41	3.44	2.71	3.05	2.59	0.84
D7(2)	90.13	2.31	0.02	2.17	0.01	1.12	1.12	0.34	0.08	1.68	0.08
D7(3)	89.89	2.54	0.02	2.20	0.01	1.20	1.22	0.40	0.08	1.59	0.08
D8(1)	94.70	1.34	0.02	1.41	0.02	1.00	1.00	0.23	0.05	1.81	0.09
D8(2)	95.19	1.21	0.02	1.33	0.02	1.00	1.00	0.27	0.05	1.67	0.07
D8(3)	95.54	1.18	0.02	1.39	0.02	0.94	0.96	0.19	0.09	1.90	0.07

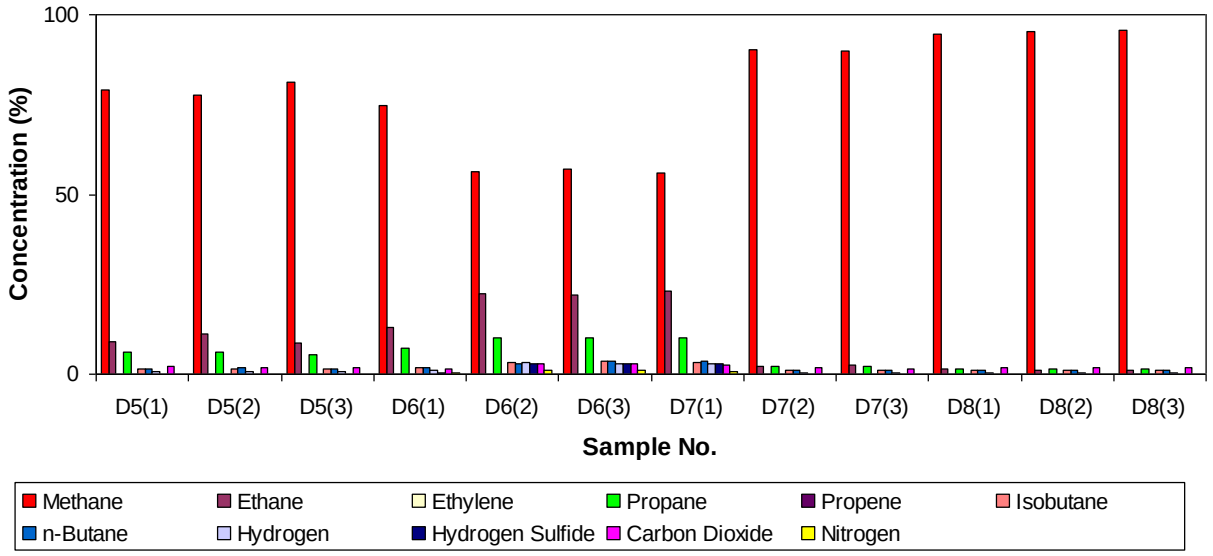

Fig. 3.5: Concentration of natural gas in the Daryanah Reservoir inclusions.

3.4. Crude Oil Type

There are two different classifications for crude oil. The first classification was introduced by Martinez *et al.*, (1984). They divided crude oils into three types, namely light oils (API gravity>31.1°), medium oils (API gravity ranges from 27.3° to 31.1°) and heavy oils (API gravity<27.3°). The second classification was established by Waples (1985). He divided crude oils into two types, namely biodegraded oils (API gravity<20°), and condensate oils (API gravity>45°). Biodegradation occurs when bacteria, fungi, or other organism or biological process chemically dissolves materials. The process can be beneficial or detrimental within the industry depending on the circumstances. For instance, biodegradation via bacteria can aid in the cleanup of oil spills.

The chemical analysis data of the studied crude oil are illustrated in Tables (3.3-8). The API gravity values of the crude oil range from 27.93° to 29.17°, which suggests that the Daryanah Reservoir inclusions contain medium crude oil (Fig. 3.6). Moreover, the crude oil samples fall in the field between biodegraded oil and condensate oil (Fig. 3.7).

Table 3.3: API gravity and SARA values of crude oil of the Daryanah Reservoir inclusions

Sample No.	API (°)	SAT (%)	ARO (%)	NSO (%)
D5a	29.11	12.81	31.25	55.94
D5b	28.00	11.42	31.77	56.81
D5c	27.93	19.96	31.11	48.93
D6a	29.09	20.59	32.13	47.28
D6b	29.00	19.47	35.96	44.57
D6c	28.28	18.59	35.55	45.86
D7a	29.17	21.34	35.29	43.37
D7b	27.98	20.23	37.05	42.72
D7c	28.91	15.50	30.61	53.89
D8a	28.88	15.81	30.38	53.81
D8b	29.05	12.18	30.96	56.86
D8c	28.00	12.48	31.15	56.37

Table 3.4: Peak wavelength (λ_{max}), Q_{F535} and $Q_{650/500}$ values of the micro-beam fluorescence spectra of crude oil of the Daryanah Reservoir inclusions

Sample No.	λ_{max} (nm)	$Q_{650/500}$	Q_{F535}
D5a	500.00	0.30	0.69
D5b	504.00	0.38	0.88
D5c	503.00	0.41	1.00
D6a	500.00	0.38	0.79
D6b	500.00	0.31	0.77
D6c	504.00	0.45	1.22
D7a	546.00	0.44	1.39
D7b	551.00	0.49	1.52
D7c	548.00	0.69	1.43
D8a	550.00	0.75	1.52
D8b	550.00	0.66	1.57
D8c	552.00	0.75	1.40

Table 3.5: Biomarker analysis of crude oil of the Daryanah Reservoir inclusions (calculated on m/z 217)

Sample No.	C_{29} steranes: ßß/(αα+ßß)	C_{29} steranes: 20S/(20S+20R)	C_{30} sterane index	C_{35}/C_{34} homohopanes	C_{31} 22R/H
D5a	0.22	0.19	0.07	0.67	0.30
D5b	0.21	0.17	0.07	0.81	0.30
D5c	0.29	0.17	0.09	0.76	0.39
D6a	0.22	0.14	0.09	0.70	0.32
D6b	0.19	0.13	0.08	0.92	0.33
D6c	0.21	0.19	0.08	0.90	0.33
D7a	0.22	0.11	0.08	0.90	0.36
D7b	0.18	0.15	0.09	0.77	0.39
D7c	0.18	0.18	0.09	0.86	0.31
D8a	0.20	0.13	0.07	0.85	0.31
D8b	0.17	0.17	0.07	0.85	0.35
D8c	0.17	0.16	0.07	0.90	0.35

Table 3.6: Continued

Sample No.	Ts/ (Ts+Tm)	29Ts/ (29Ts+30NH)	Pr/Ph	C_6H_6/C_6H_{12}	C_7H_8/C_7H_{14}
D5a	0.09	0.09	0.90	0.22	0.30
D5b	0.10	0.07	0.88	0.21	0.32
D5c	0.35	0.16	3.13	0.40	0.45
D6a	0.33	0.17	3.42	0.39	0.43
D6b	0.13	0.10	1.23	0.34	0.29
D6c	0.17	0.10	1.30	0.34	0.31
D7a	0.16	0.11	2.22	0.33	0.35
D7b	0.12	0.10	0.92	0.29	0.29
D7c	0.12	0.09	0.95	0.32	0.28
D8a	0.09	0.11	1.11	0.29	0.33
D8b	0.13	0.11	1.10	0.28	0.33
D8c	0.13	0.09	1.00	0.31	0.31

Table 3.7: Continued

Sample No.	$(C_{19}+C_{20})/(C_{23}+C_{24})$ TT	C_{24} TeT/ C_{26} TT	$(C_{19}+C_{20})/C_{23}$ TT	C_{23}/C_{21} TT	C_{29} TT/ C_{30} hopane
D5a	0.89	1.55	0.95	0.44	0.03
D5b	1.00	2.17	0.90	0.78	0.03
D5c	1.12	1.89	1.37	0.82	0.06
D6a	0.93	1.76	1.51	0.39	0.05
D6b	0.68	2.33	1.17	0.77	0.04
D6c	0.77	1.91	1.28	0.69	0.02
D7a	0.83	1.95	1.22	0.54	0.07
D7b	1.08	1.67	1.47	0.47	0.06
D7c	0.76	1.78	0.97	0.59	0.02
D8a	0.66	2.00	0.70	0.83	0.03
D8b	1.10	1.90	1.42	0.87	0.05
D8c	0.80	1.73	1.26	0.80	0.05

Table 3.8: Continued

Sample No.	C_{28} TT/ C_{30} hopane	C_{25} TT/ C_{24} TeT	C_{24} TeT/ (C_{24} TeT+ C_{26} TT)	C_{30} diahopane/ C_{30} hopane	C_{29} diahopane/ C_{29} hopane	DMDI-1	DMDI-2
D5a	0.10	0.89	0.51	0.45	0.24	66.61	0.55
D5b	0.08	0.33	0.55	0.20	0.28	70.00	0.41
D5c	0.08	0.56	0.72	0.27	0.44	73.09	0.38
D6a	0.04	0.49	0.67	0.33	0.39	69.69	0.39
D6b	0.06	0.80	0.63	0.39	0.31	63.18	0.38
D6c	0.07	0.80	0.61	0.24	0.30	70.16	0.55
D7a	0.07	0.37	0.59	0.27	0.30	67.80	0.50
D7b	0.05	0.21	0.54	0.40	0.42	71.19	0.50
D7c	0.10	0.54	0.71	0.37	0.28	72.21	0.43
D8a	0.10	0.50	0.66	0.21	0.22	66.23	0.52
D8b	0.04	0.50	0.53	0.23	0.20	65.41	0.43
D8c	0.08	0.61	0.70	0.43	0.20	70.34	0.41

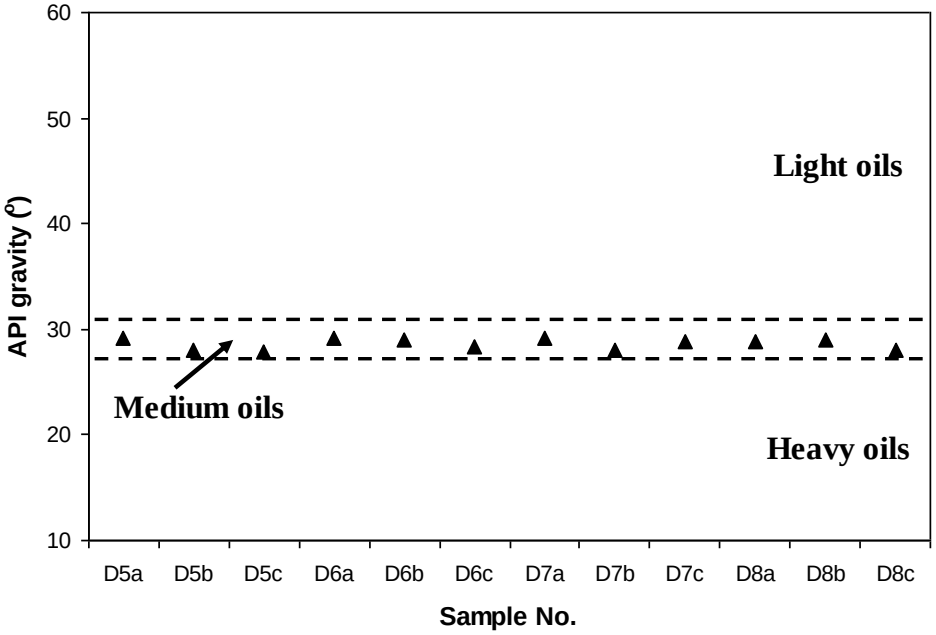

Fig. 3.6: API gravity values of the studied crude oil (fields after Martinez et al., 1984).

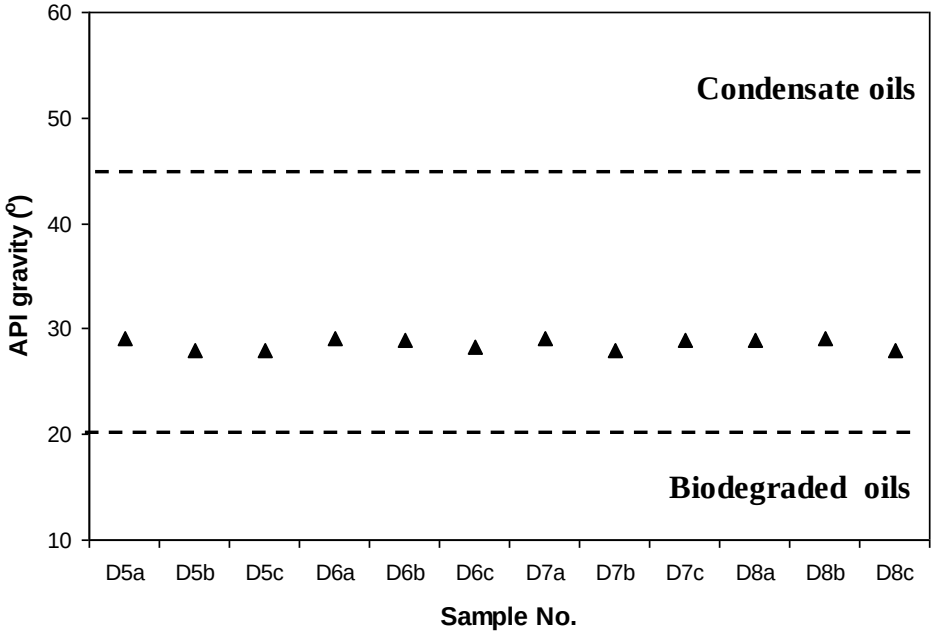

Fig. 3.7: API gravity values of the studied crude oil (fields after Waples, 1985).

3.5. Oil-Source rock Correlation

Correlation of a crude oil to one or more source rocks is a common industrial application of petroleum geochemistry (Curiale, 2008; Korkmaz *et al.,* 2013; Xiao *et al.,* 2019). Confirmation that oil has been generated in the target sedimentary basin is the most critical piece of knowledge a petroleum explorationist can derive; second in importance is the determination of the source(s) of that oil (Curiale, 2008; Korkmaz *et al.,* 2013; Xiao *et al.,* 2019). For this reason, an extensive arsenal of analytical methods is utilized to collect primary data on the organic matter in crude oils and possible source rocks, and various components of these data are used to relate oils causally to their prospective sources (Curiale, 2008; Korkmaz *et al.,* 2013; Xiao *et al.,* 2019). Oil–source rock correlations at various confidence levels have been established for the petroleum systems of all major sedimentary basins. Any successful oil–source rock correlation must include three attributes: 1) requirement of causality, 2) comparable chemical data for all samples, and 2) geological support (Curiale, 2008).

Aquino Neto *et al.,* (1983) systematically investigated the distribution of tricyclic terpanes in oils and source rock extracts in a variety of depositional environments and pointed out that C_{23}TT is often the dominant homologue in marine oils and saline lacustrine oils. Generally, C_{19}TT and C_{20}TT are more abundant in terrestrial oils (Zhu, 1997; Chen *et al.,* 2013; Xiao *et al.,* 2019). Based on this, we can infer that these variations in C_{19}/C_{23}TT, C_{20}/C_{23}TT, $(C_{19}+C_{20})$TT/C_{23}TT and $(C_{19}+C_{20})$TT/ $(C_{23}$TT+C_{24}TT) ratios may in some way reflect a relative distribution of terrigenous versus marine organic matter (Zumberge, 1987; Zhang and Huang, 2005; Tao *et al.,* 2015). In addition, a higher abundance of long-chain tricyclic terpanes (C_{28}TT and C_{29}TT) are often found in brackish to saline water sedimentary environments and are mainly derived from aquatic algal plankton (Tuo *et al.,* 1999; Hao *et al.,* 2009). More importantly, the proportion of C_{24}TeT relative to tricyclic terpanes may also be facies dependent wherein relatively higher C_{24}TeT abundances in source rocks and related oils are found to be associated with terrigenous organic matter input (Philp and Gilbert, 1986; Zhang and Huang, 2005). Therefore, C_{19}-C_{24} tricyclic and C_{24} tetracyclic terpanes could be useful indicators for providing a variety of geological and geochemical information. C_{19}-C_{24} tricyclic and C_{24} tetracyclic

terpanes related parameters have been extensively used in oil-oil and oil-source rock correlations studies (e.g., Xiao *et al.,* 2019).

In the present study, the plots of Pr/Ph versus C_{35}/C_{34} homohopanes, C_{31} 22R/H versus C_{30} sterane index, $(C_{19}+C_{20})/(C_{23}+C_{24})$ TT versus C_{24} TeT/C_{26} TT, $(C_{19}+C_{20})/C_{23}$ TT versus C_{23}/C_{21} TT, C_{29} TT/C_{30} hopane versus C_{28} TT/C_{30} hopane, C_{25} TT/C_{24} TeT versus C_{24} TeT/(C_{24} TeT+C_{26} TT) and C_{30} diahopane/C_{30} hopane versus C_{29} diahopane/C_{29} hopane (Figs. 3.8-14) indicate that there is one oil family in the Daryanah Reservoir inclusions. These plots also illustrate that the majority of the crude oils and the source rock (Daryanah Shale) fall into the same zone, which suggests that the Daryanah Shale is the main source rock of the Darnah Reservoir. This assumption is further supported by the diamondoid diagram (Fig. 3.15).

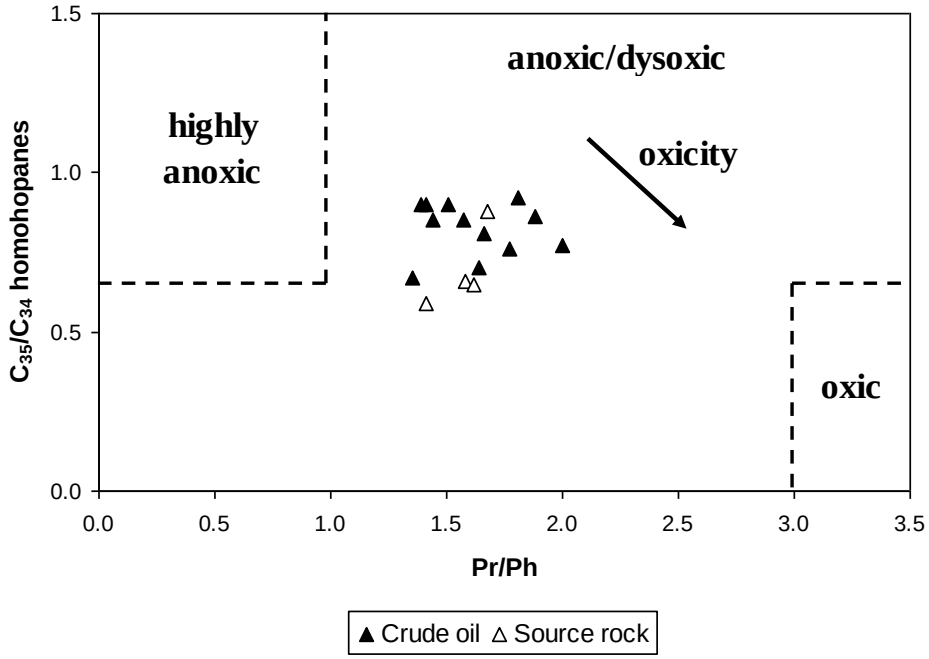

Fig. 3.8: Plot of C_{31} 22R/H vs. C_{30} sterane index showing the source rock for the studied crude oil (fields after Ziegs et al., 2018).

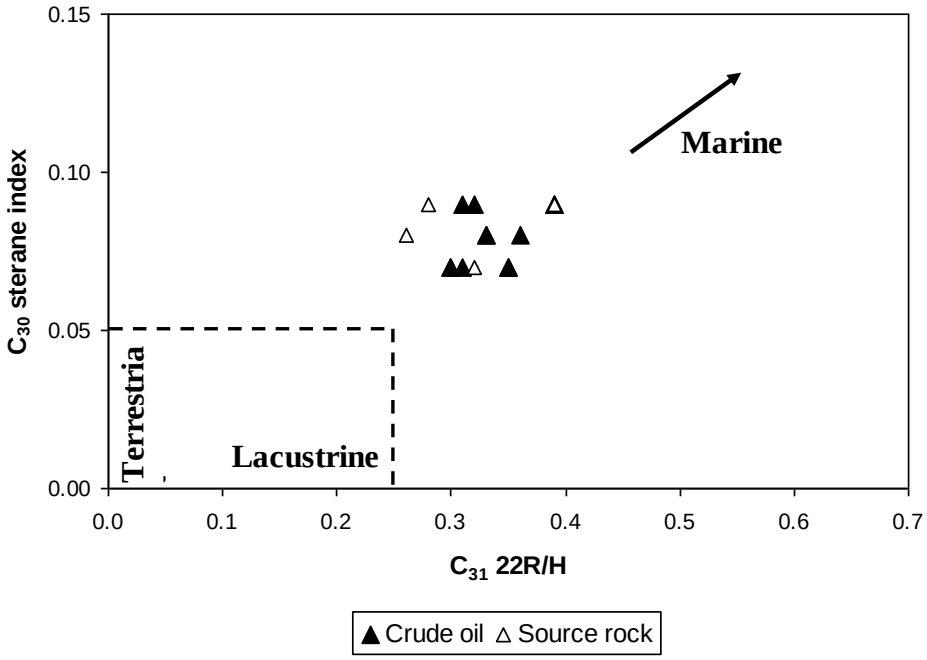

Fig. 3.9: Plot of C_{31} 22R/H vs. C_{30} sterane index showing the source rock for the studied crude oil (fields after Ziegs et al., 2018).

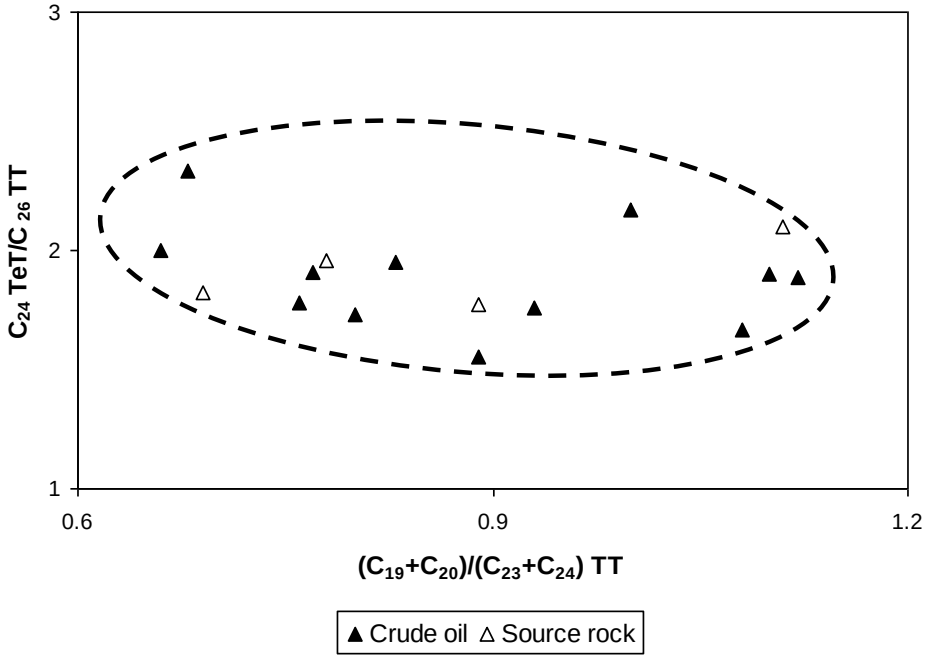

Fig. 3.10: Plot of $(C_{19}+C_{20})/(C_{23}+C_{24})$ TT vs. C_{24} TeT/C_{26} TT showing the source rock for the studied crude oil.

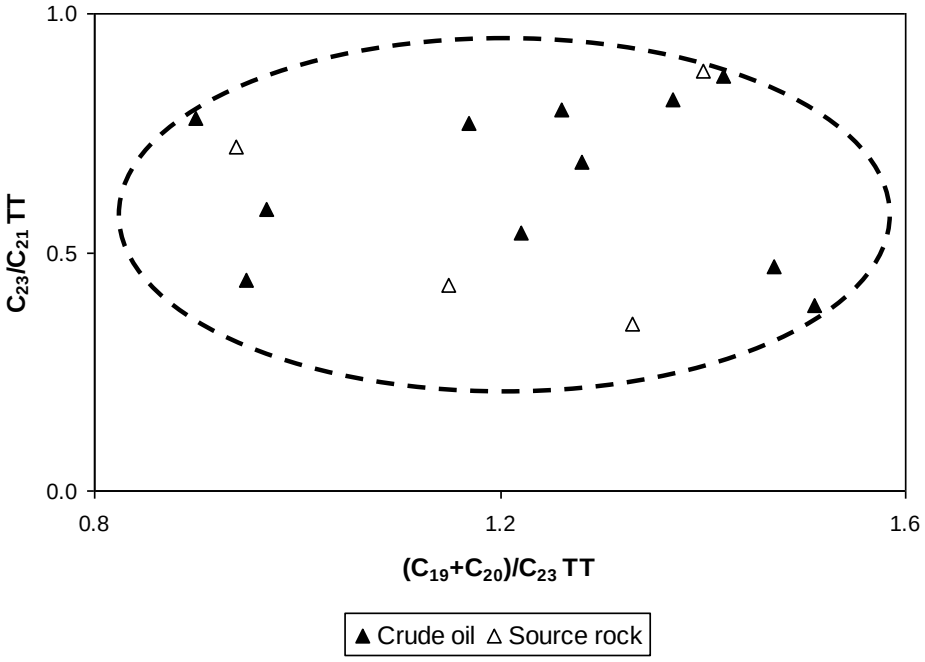

Fig. 3.11: Plot of $(C_{19}+C_{20})/C_{23}$ TT vs. C_{23}/C_{21} TT showing the source rock for the studied crude oil.

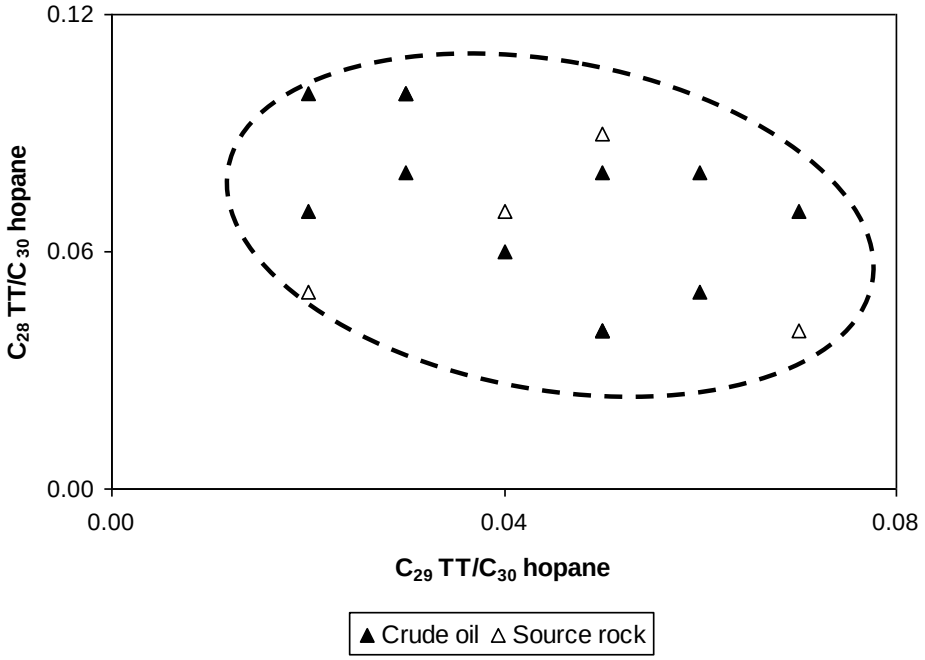

Fig. 3.12: Plot of C_{29} TT/C_{30} hopane vs. C_{28} TT/C_{30} hopane showing the source rock for the studied crude oil.

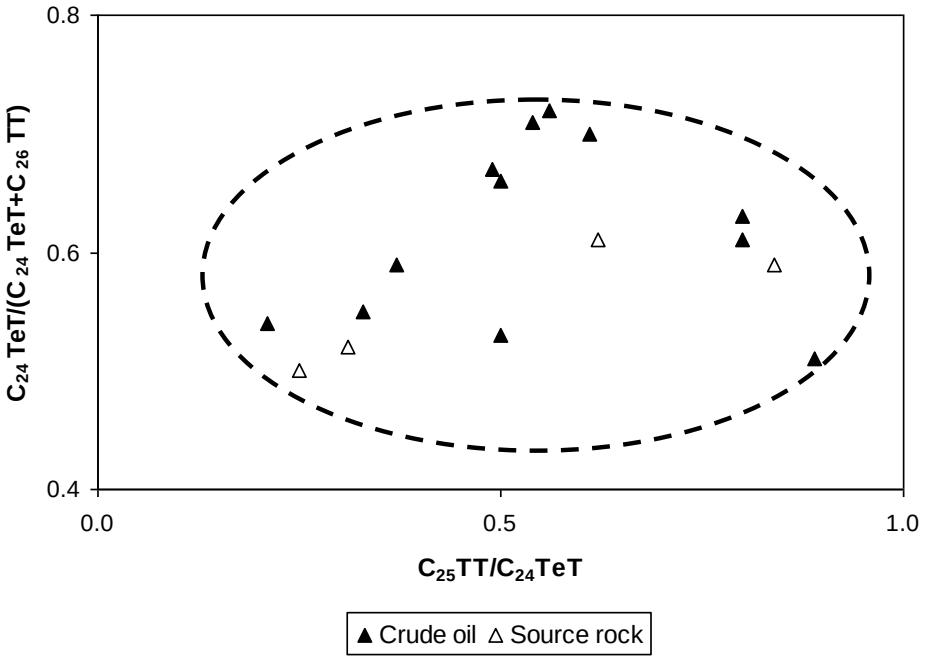

Fig. 3.13: Plot of C_{25} TT/C_{24} TeT vs. C_{24} TeT/(C_{24} TeT+C_{26} TT) showing the source rock for the studied crude oil.

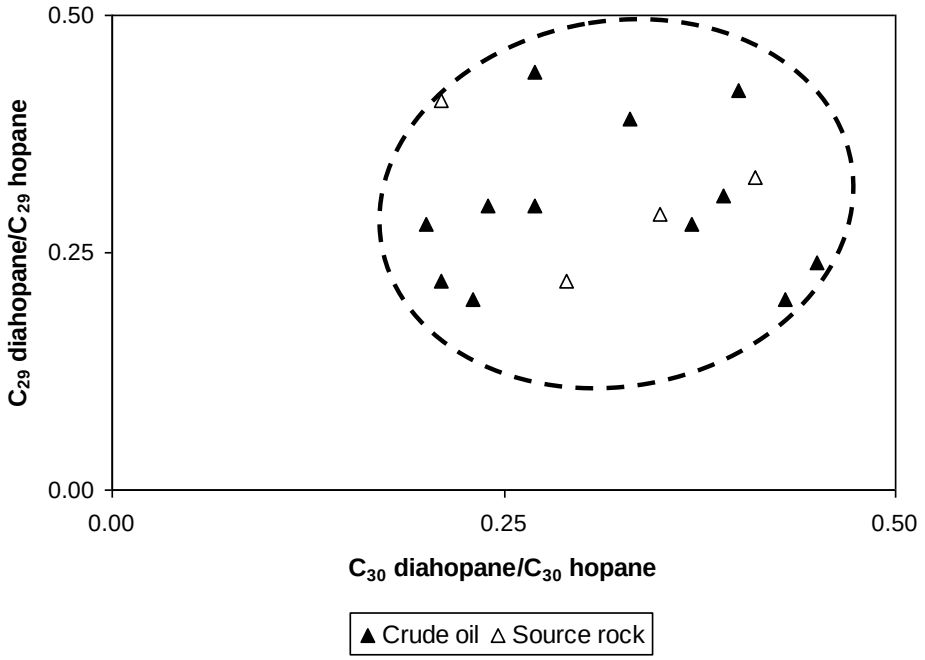

Fig. 3.14: Plot of C_{30} diahopane/C_{30} hopane vs. C_{29} diahopane/C_{29} hopane showing the source rock for the studied crude oil.

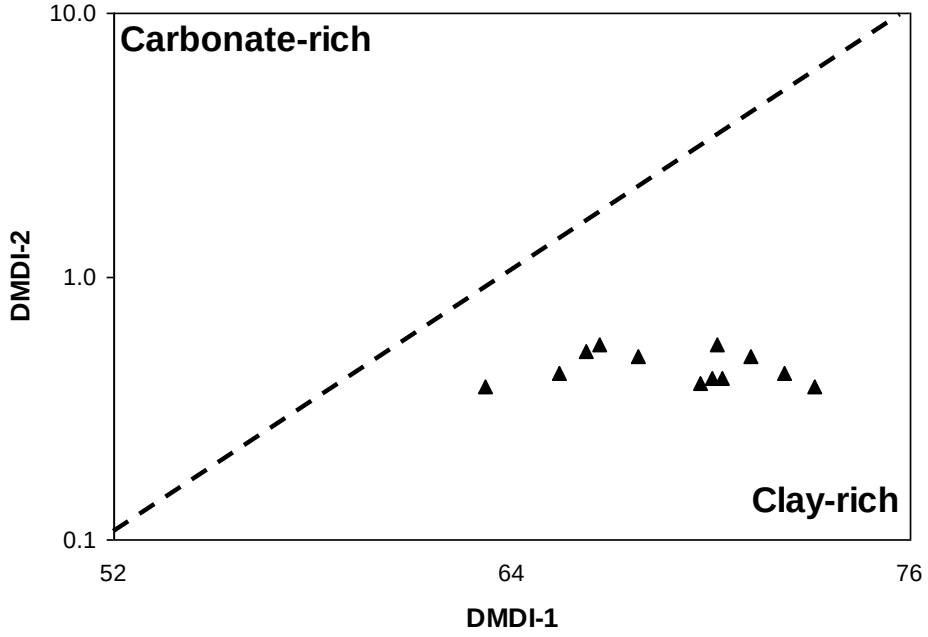

Fig. 3.15: Plot of DMDI-1 vs. DMDI-2 showing the source rock lithology for the studied crude oil (fields after Aldahik et al., 2017).

3.6. Thermal Maturity and Oil-Water Interactions

Many detailed chemical parameters have been proposed as indicators of thermal maturity of crude oil (Obermajer *et al.,* 2010; Jiang *et al.,* 2019). Among these parameters, the molecular distributions of metalloporphyrins, cyclic hydrocarbons and low molecular-weight hydrocarbons are most commonly used (Jiang *et al.*, 2019).

In this chapter, several binary plots have been used to determine the maturity of crude oil and the oil-water Interactions such as Ts/(Ts+Tm) versus 29Ts/(29Ts+30NH), C_{29} steranes:ßß/(αα+ßß) versus C_{29} steranes:20S/(20S+20R), C_6H_6/C_6H_{12} (benzene/ cyclohexane) versus C_7H_8/C_7H_{14} (toluene/methyl cyclohexane) as well as the ternary plot of SARA (saturated hydrocarbons, aromatic hydrocarbons and resins plus asphaltenes) (Figs. 3.16-19). The samples of crude oil and source rock have entered in the immature window. Furthermore, there are indications of oil-water interactions.

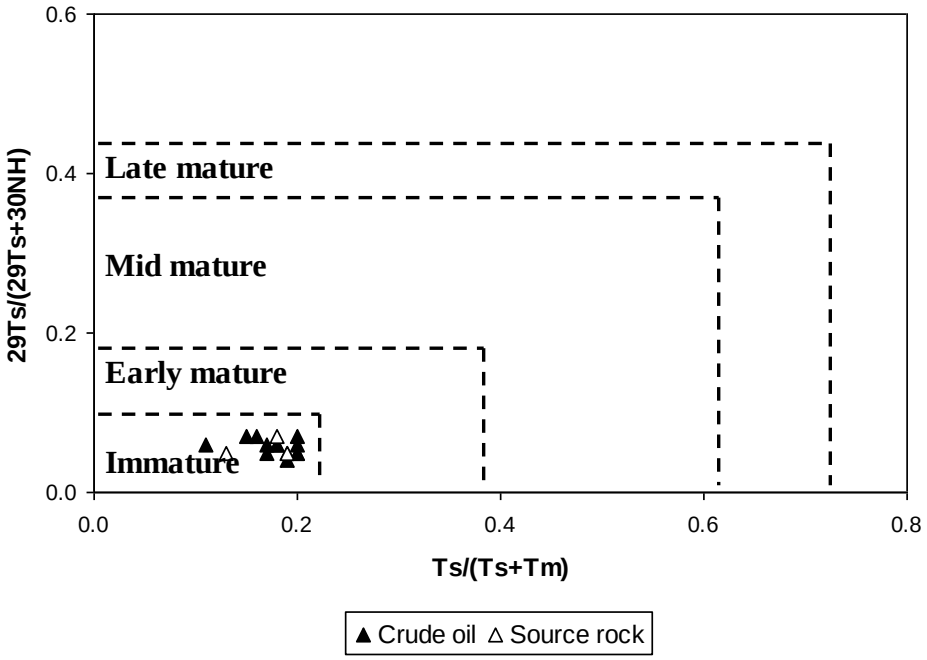

Fig. 3.16: Plot of Ts/(Ts+Tm) vs. 29Ts/(29Ts+30NH) showing the maturity for the studied crude oil (fields after Peters et al., 2005).

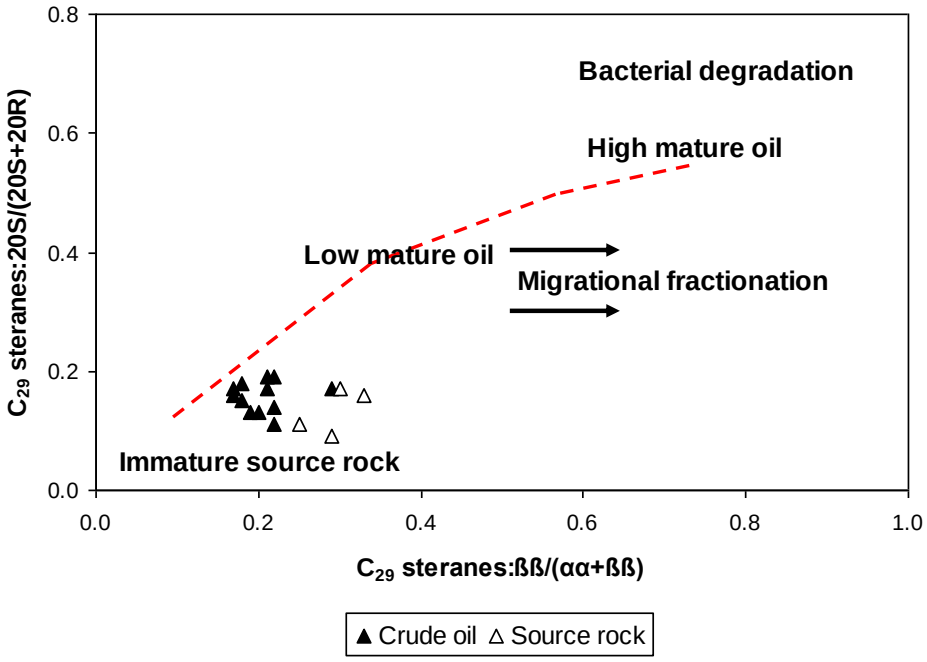

Fig. 3.17: Plot of C_{29} steranes:ββ/(αα+ββ) vs. C_{29} steranes:20S/(20S+20R) showing the maturity for the studied crude oil (fields after Waples and Machihara, 1990).

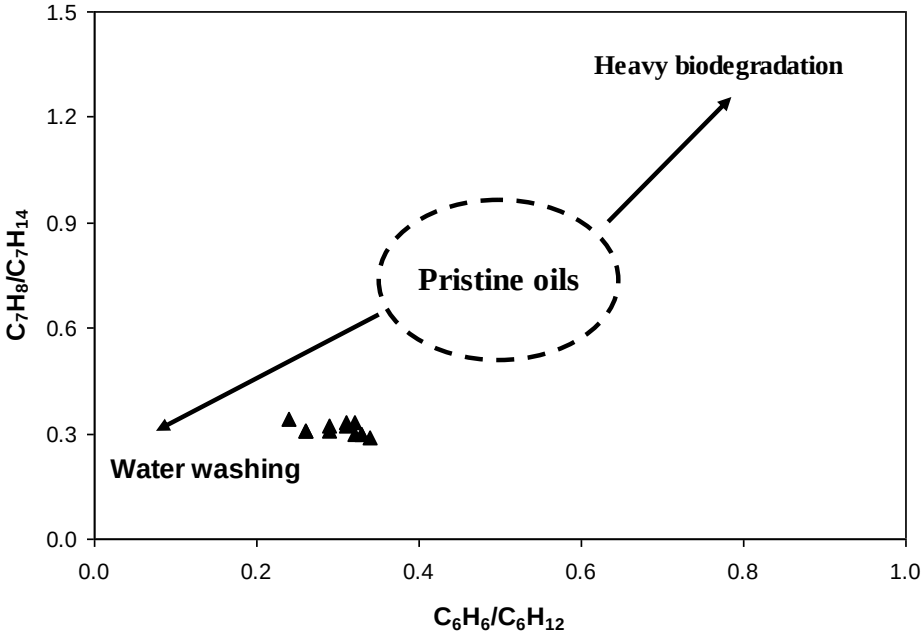

Fig. 3.18: Plot of C_6H_6/C_6H_{12} vs. C_7H_8/C_7H_{14} showing the oil-water interactions in the Daryanah Reservoir inclusions (fields after Ziegs et al., 2018).

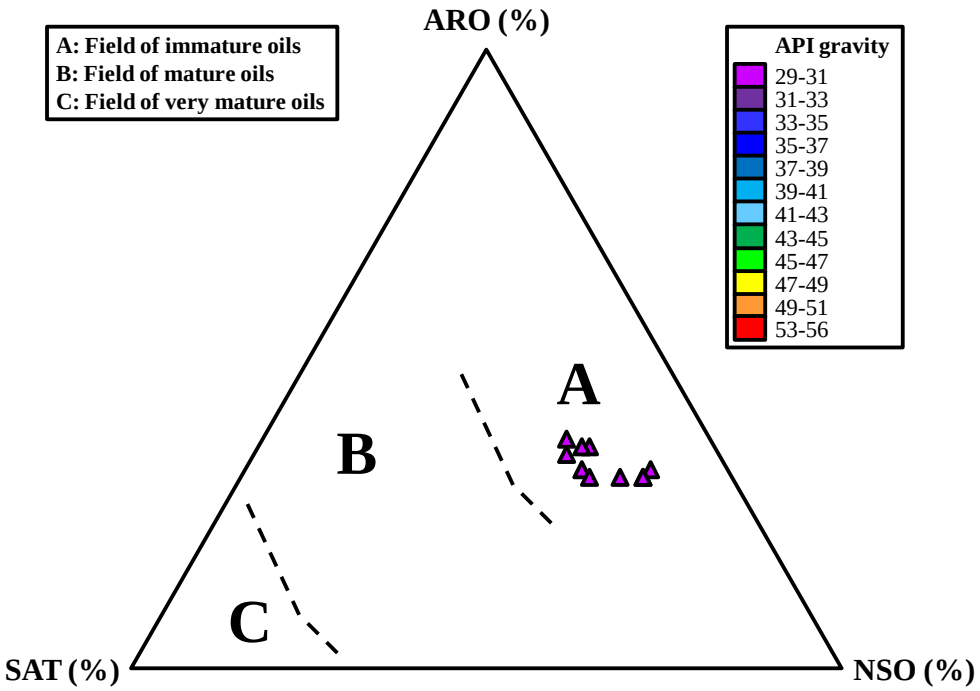

Fig. 3.19: Ternary plot of SARA showing the maturity for the studied crude oil (fields after Peters et al., 2005).

3.7. Charging Episodes

Petroleum reservoirs are often charged by oil that has been expelled from different source rocks over a considerable maturity range. Over geological time, different oils in a petroleum reservoir tend to form a homogeneous mixture (England *et al.,* 1987). In addition, early oil charges may be displaced by subsequent gas charges or mixed with subsequent oil charges, or may be altered by biodegradation or water-washing prior to later oil charge (Baba *et al.,* 2019). All these processes blur geochemical differences and often make it difficult to reconstruct the detailed charge history of a petroleum reservoir based on the analysis of recovered oils alone. The geochemical analysis of petroleum inclusions offers an opportunity to obtain information on the composition of petroleum during an earlier stage of the fill history (Shaltami *et al.,* 2019). Petroleum inclusions are encapsulations of paleo-oil that are commonly formed in diagenetic cements and in healed fractures cross-cutting detrital grains and cements in petroleum reservoirs (Zhang *et al.,* 2012).

In the current study, the charging episodes of hydrocarbons are determined based on the peak wavelength (λ_{max}) values and intensities of the micro-beam fluorescence spectra parameters ($Q_{650/500}$ and Q_{F535}). There are two peak wavelength values, namely 500nm, and 545nm (Figs. 3.20-21). These peaks indicate that two episodes of crude oil charging occurred in the Daryanah Reservoir.

Briefly, the petroleum system of the Daryanah Formation is as follows:

1) The lower shale (Daryanah Shale) represents the source rock.
2) The lower limestone (Daryanah Limestone) represents the reservoir.
3) The middle shale represents the cap rock (seal).

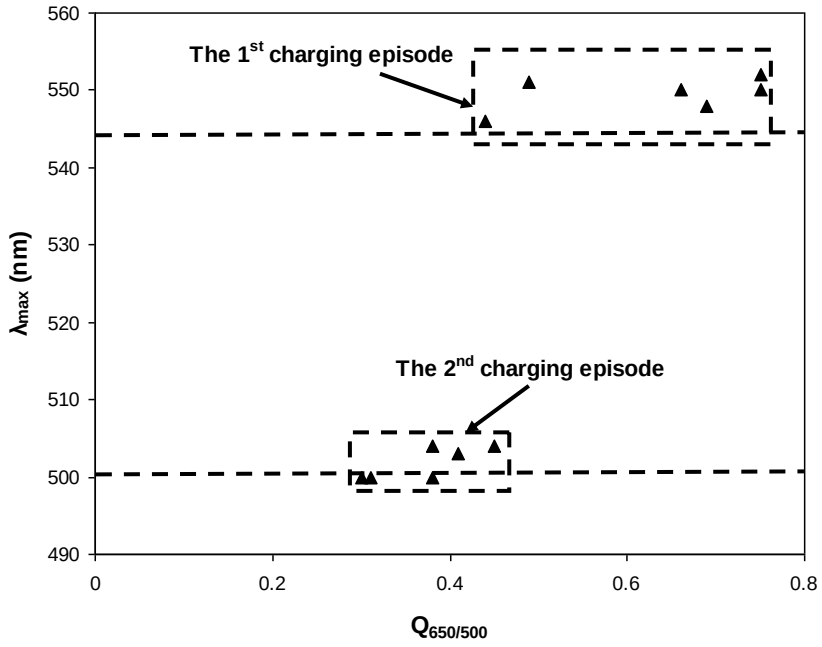

Fig. 3.20: Plot of $Q_{650/500}$ vs. λ_{max} showing the charging episodes for the Daryanah Reservoir.

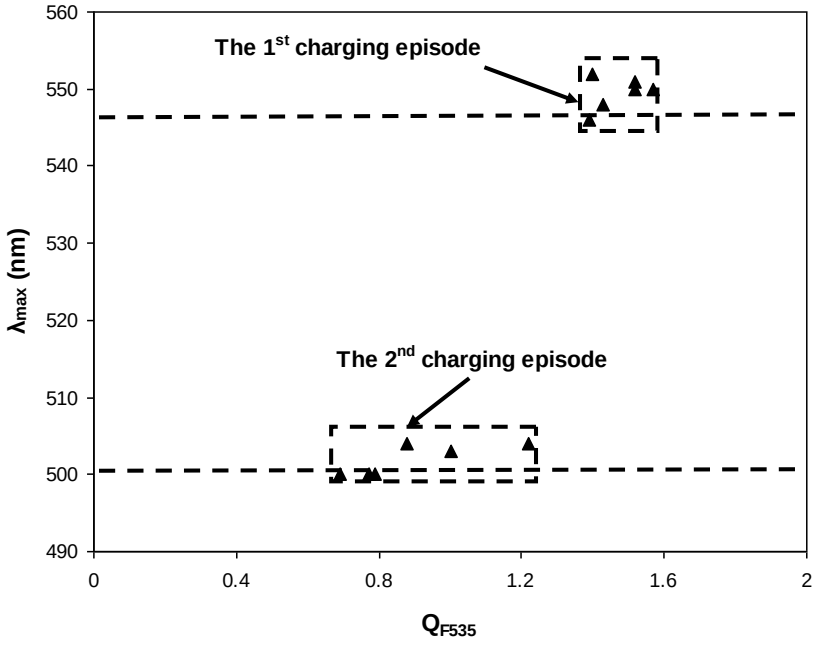

Fig. 3.21: Plot of Q_{F535} vs. λ_{max} showing the charging episodes for the Daryanah Reservoir.

CHAPTER FOUR
CONCLUSIONS

The evaluation of the Daryanah Formation in the offshore well Al-NC 128, Cyrenaica Basin, NE Libya, is the objective of the current study. Six techniques have been used to achieve this purpose, namely organic petrography, scanning electron microscope (SEM), LECO C230, Rock Eval pyrolysis, gas chromatography-mass spectrometry (GC-MS) and fluorescence spectrophotometry. Moreover, natural gas and crude oil were assessed using petroleum inclusions. The conclusions of this study are as follows:

1) Vitrinite (gelinite, densinite, attrinite, collotelinite, telinite ulminite and textinite) represents the most abundant maceral in the shales. Liptinite (resinite, sporinite, subernite, cutinite, alginite and bituminite) is the second common maceral. There is also a small amount of inertinite (fusinite and inertodetrinite).

2) The lower shale samples contain TOC >0.5% (fair source rock) while the middle and upper shales have TOC <0.5% (poor source rock).

3) All shales contain kerogens of type II/III and III.

4) Organic matter in the shales is immature thermally.

5) All shales contain mixed organic matter formed under suboxic conditions.

6) The highly saline marine environment is the proved origin of the Daryanah Formation.

7) The petroleum inclusions in the Daryanah Reservoir (lower limestone) contain two phases, namely crude oil and natural gas.

8) The Daryanah Reservoir inclusions contain high concentration of hydrocarbon gases (especially C_1) with lesser content of nonhydrocarbon gases.

9) Medium crude oil is dominant in the petroleum inclusions.

10) The Daryanah Shale is the main source rock of the Darnah Reservoir. Furthermore, the cap rock is the middle shale.

11) The crude oil and source rock have entered in the immature window.

12) There two episodes of crude oil charging occurred in the Daryanah Reservoir.

REFERENCES

Akinlua, A., Ajayi, T.R. and Adeleke, B.B. (2007): Organic and inorganic geochemistry of northwestern Niger Delta oils. Geochemical Journal; 41: 271-281.

Aldahik, A., Schulz, H.M., Horsfield, B., Wilkes, H., Dominik, W. and Nederlof, P. (2017): Crude oil families in the Euphrates Graben (Syria). Marine and Petroleum Geology; 86: 325-342.

Alsaab, D., Elie, M., Izart, A., Sachsenhofer, R.F., Privalov, V.A., Suarez-Ruiz, I. and Martinez, L. (2008): Comparison of hydrocarbon gases (C1-C5) production from Carboniferous Donets (Ukraine) and Cretaceous Sabinas (Mexico) coals. International Journal of Coal Geology; 74: 154-162.

Aquino Neto, F.R., Trendel, J.M., Restle, A., Connan, J. and Albrecht, P. (1983): Occurrence and formation of tricyclic terpanes in sediments and petroleums. In: Bjoroy, M., Albrecht, P., Cornford, C., de Groot, K., Eglinton, G., Galimov, E., Leythaeuser, D., Pelet, R., Rullkötter, J., Speers, G. (Eds.), Advances in Organic Geochemistry 1981. Wiley, Chichester; pp. 659-667.

Arouri, K.R., Al-Saleh, S.H. and Al-Hilal, Z.M. (2009): Residual oil as a tool in migration and filling history analysis of petroleum reservoirs, Ghazal Field, Saudi Arabia. Organic Geochemistry; 40(5): 617-627.

Atta-Peters, D. and Garrey, P. (2014): Source rock evaluation and hydrocarbon potential in the Tano basin, South Western Ghana, West Africa. International Journal of Oil, Gas and Coal Engineering; 2(5): 66-77.

Aviles, M.A., Ardakani, O.H., Cheadle, B.A. and Sanei, H. (2019): Organic petrography and geochemical characterization of the Upper Cretaceous Second White Specks and Upper Belle Fourche alloformations, west-central Alberta: Analysis of local maturity anomalies. International Journal of Coal Geology; 203: 60-73.

Baba, M., Parnell, J., Muirhead, D. and Bowden, S. (2019): Oil charge and biodegradation history in an exhumed fractured reservoir, Devonian, UK. Marine and Petroleum Geology; 101: 281-289.

Burruss, R.C. (1981): Hydrocarbon fluid inclusions in studies of sedimentary diagenesis. In: Hollister, L.S., Crawford, M.L. (Eds.), Fluid Inclusions: Applications to Petrology; pp. 138-156.

Buitrago, J., Diaz, C., Gruenwald, R., Suarez, J. and Tawengi, K.S. (2011): New insights into the stratigraphy and petroleum geology of western Cyrenaica, NE Libya. 5th North African Mediterranean Petroleum and Geosciences Conference and Exhibition, Tripoli, Libya.

Burnham, A.K. (2019): Kinetic models of vitrinite, kerogen, and bitumen reflectance. Organic Geochemistry; 131: 50-59.

Cai, C., Li, K., Anlai, M., Zhang, C., Xu, Z., Worden, R.H., Wu, G., Zhang, B. and Chen, L. (2009): Distinguishing Cambrian from Upper Ordovician source rocks: Evidence from sulfur isotopes and biomarkers in the Tarim Basin. Organic Geochemistry; 40(7): 755-768.

Carmignani, L. (1984): Geological map of Libya, 1:250000, Sheet: Wadi Al Hamim, NH 34-7, Explanatory Booklet, Industrial Research Center (IRC), Tripoli, 98p.

Carpentier, B., Wilhelms, A. and Mansoori, G.A. (2007): Reservoir organic geochemistry: Processes and applications. Journal of Petroleum Science and Engineering; 58(3-4): 341-343.

Chabalala, V.P., Wagner, N. and Potgieter-Vermaak, S. (2011): Investigation into the evolution of char structure using Raman spectroscopy in conjunction with coal petrography; Part 1. Fuel Processing Technology; 92(4): 750-756.

Chen, A., Zhao, J., Qi, J. and Shao, M. (2013): Distribution of tricyclic terpane and sterane with application to oil-source correlation in southern Turgay Basin. Xinjiang Petroleum Geology; 34: 602-606.

Cheng, B., Chen, Z., Chen, T., Yang, C. and Wang, T.G. (2019): Biomarker signatures of the Ediacaran-Early Cambrian origin petroleum from the central Sichuan Basin, South China: Implications for source rock characteristics. Marine and Petroleum Geology; 96: 577-590.

Claypool, G.E. and Kvenvolden, K.A. (1983): Methane and other hydrocarbon gases in marine sediment. Annual Review of Earth and Planetary Sciences; 11: 299-327.

Curiale, J.A. (2008): Oil-source rock correlations – Limitations and recommendations. Organic Geochemistry; 39: 1150-1161.

Dembicki, H.J. (2009): Three common source rock evaluation errors made by geologists during prospect or play appraisals. AAPG Bulletin; 93(3): 341-356.

Di Cesare, F., Franchino, A. and Sommaruga, C. (1963): The Pliocene-Quaternary of Giarabub Erg region. Rev. l'Inst. Fr. Petrol.; 18(10): 1344-1362.

Duronio, P., Dakshe, A. and Bellini, E. (1991): Stratigraphy of the offshore Cyrenaica (Libya). Third Symposium on the Geology of Libya, vol. 4 (eds. M.J. Salem, O.S. Hammuda and B.A. Eliagoubi), Elsevier, Amsterdam, pp. 1589-1620.

El Diasty, W.S. and Moldowan, J.M. (2012): Application of biological markers in the recognition of the geochemical characteristics of some crude oils from Abu Gharadig Basin, north Western Desert–Egypt. Marine and Petroleum Geology; 35:28-40.

El Atfy, H., Brocke, R., Uhl, D., Ghassal, B., Stock, A.T. and Littke, R. (2014): Source rock potential and paleoenvironment of the Miocene Rudeis and Kareem formations, Gulf of Suez, Egypt: An integrated palynofacies and organic geochemical approach. International Journal of Coal Geology; 131: 326-343.

El Hajj, L., Baudin, F., Littke, R., Nader, F.H., Geze, R., Maksoud, S. and Azar, D. (2019): Geochemical and petrographic analyses of new petroleum source rocks from the onshore Upper Jurassic and Lower Cretaceous of Lebanon. International Journal of Coal Geology; 204: 70-84.

El Hawat, A.S. and Abdulsamad, E.O. (2004): The Geology of Cyrenaica: A Field Seminar. Geology of East Libya, Field Trip, ESSL, Tripoli, Libya; 130p.

El Hawat, A.S. and Shelmani, M.A. (1993): Short notes and guidebook on the geology of Al Jabal Al Akhdar, Cyrenaica, NE Libya. Interprint Limited Malta; 70p.

El-Sabagh, S.M., El-Naggar, A.Y., El Nady, M.M., Ebiad, M.A., Rashad, A.M. and Abdullah, E.S. (2018): Distribution of triterpanes and steranes biomarkers as indication of organic matters

input and depositional environments of crude oils of oilfields in Gulf of Suez, Egypt. Egyptian Journal of Petroleum; 27: 969-977.

England, W.A. (2007): Reservoir geochemistry–A reservoir engineering perspective. Journal of Petroleum Science and Engineering; 58: 344-354.

England, W.A., Mackenzie, A.S., Mann, D.M. and Quigley, T.M. (1987): The movement and entrapment of petroleum fluids in the subsurface, Journal of the Geological Society, London; 144: 327-347.

Erik, N.Y., Aydemir, A. and Buyuksarac, A. (2015): Investigation of the organic matter properties and hydrocarbon potential of the Sivas Basin, Central Eastern Anatolia, Turkey, using Rock-Eval data and organic petrography. Journal of Petroleum Science and Engineering; 127: 148-168.

Espitalie, J. (1984): Geochemical logging. In: Voorhees, K.J. (Ed.), Analytical Pyrolysis-Techniques and Applications. Boston Butterworth, pp. 276-304.

Francis, M. and Issawi, B. (1977): Geological Map of Libya, 1:250000, Sheet: Soluq, NI 34-2, Explanatory Booklet, Industrial Research Center (IRC), Tripoli, 86p.

Furmann, A., Mastalerz, M., Brassell, S.C., Pedersen, P.K., Zajac, N.A. and Schimmelmann, A. (2015): Organic matter geochemistry and petrography of Late Cretaceous (Cenomanian-Turonian) organic-rich shales from the Belle Fourche and Second White Specks formations, west-central Alberta, Canada. Organic Geochemistry; 85: 102-120.

Ghori, K.A.R. (2002): Modeling the hydrocarbon generative history of the Officer Basin, Western Australia. Journal of Philosophy of Education Society of Australasia (PESA); 29: 29-42.

Giammarino, S. (1984): Geological Map of Libya, 1:250000, Sheet: Wadi Al Khali, NI 34-8, Explanatory Booklet, Industrial Research Center (IRC), Tripoli, 73p.

Hackley, P.C. and Cardott, B.J. (2016): Application of organic petrography in North American shale petroleum systems: A review. International Journal of Coal Geology; 163: 8-51.

Hall, L.S., Boreham, C.J., Edwards, D.S., Palu, T.J., Buckler, T., Hill, A.J. and Troup, A. (2016): Cooper Basin source rock geochemistry: Regional hydrocarbon prospectivity of the Cooper Basin. Geoscience Australia, Part2; 62p.

Hallett, D. (2002): Petroleum geology of Libya. Amsterdam, Elsevier Inc., 503p.

Hallett, D. and Clark-Lowes, D. (2016): Petroleum geology of Libya. 2nd edition, Amsterdam, Elsevier Inc., 404p.

Hao, F., Zhou, X., Zhu, Y. and Yang, Y. (2009): Mechanisms for oil depletion and enrichment on the Shijiutuo uplift, Bohai Bay Basin, China. AAPG Bulletin; 93: 1015-1037.

Holba, A.G., Dzoub, L.I., Wood, G.D., Ellisd, L., Adame, P., Schaeffere, P., Albrechte, P., Greenef, T. and Hughes, W.B. (2003): Application of tetracyclic polyprenoids as indicators of input from fresh-brackish water environments. Organic Geochemistry; 34: 441-469.

Huang, W.Y. and Meinschein, W.G. (1979): Sterols as ecological indicators. Geochimica et Cosmochimica Acta; 43: 739-745.

Hunt, J.M. (1996): Petroleum geochemistry and geology, 2nd edition, vol. 743. New York: Freeman and Company.

Huo, Z., Pang, X., Chen, J., Zhang, J., Song, M., Guo, K., Li, P., Li, W. and Liang, Y. (2019): Carbonate source rock with low total organic carbon content and high maturity as effective source rock in China: A review. Journal of Asian Earth Sciences; 176: 8-26.

Hutton, A., Bharati, S. and Robl, T. (1994): Chemical and petrographic classification of kerogen/macerals. Energy and Fuels: 8: 1478-1488.

ICCP System (1994a): Methods for the petrographic analysis of bituminous coal and anthracite-part 3: method of determining maceral group composition-ISO 7404-33:1994. ISO, Geneva.

ICCP System (1994b): Methods for the petrographic analysis of bituminous coal and anthracite-part 5: method of determining Microscopically the reflectance of vitrinite-ISO 7404-53: 1994. ISO, Geneva.

Jiang, W., Li, Y. and Xiong, Y. (2019): Source and thermal maturity of crude oils in the Junggar Basin in northwest China determined from the concentration and distribution of diamondoids. Organic Geochemistry; 128: 148-160.

Klen, L. (1974): Geological map of Libya, 1:250000, Sheet: Benghazi, NI 34-14, Explanatory Booklet, Industrial Research Center (IRC), Tripoli, 56p.

Kolchugin, A.N., Immenhauser, A., Walter, B.F. and Morozov, V.P. (2016): Diagenesis of the palaeo-oil-water transition zone in a Lower Pennsylvanian carbonate reservoir: Constraints from cathodoluminescence microscopy, microthermometry, and isotope geochemistry. Marine and Petroleum Geology; 72: 45-61.

Korkmaz, S., Kara-Gulbay, R. and Iztan, Y.H. (2013): Organic geochemistry of the Lower Cretaceous black shales and oil seep in the Sinop Basin, Northern Turkey: An oil-source rock correlationstudy. Marine and Petroleum Geology; 43: 272-283.

Larter, S.R., Aplin, A.C., Corbett, P.W.M., Ementon, N., Chen, M. and Taylor, P.N. (1997): Reservoir geochemistry: A link between reservoir geology and engineering? SPE Reservoir Engineering; 12(1):12-17.

Li, J., Sagoe, G., Yang, G., Liu, D. and Li, Y. (2019): The application of geochemistry to bicarbonate thermal springs with high reservoir temperature: A case study of the Batang geothermal field, western Sichuan Province, China. Journal of Volcanology and Geothermal Research; 371: 20-31.

Li, M., Liu, X., Wang, T.G., Jiang, W., Fang, R., Yang, L. and Tang, Y. (2018): Fractionation of dibenzofurans during subsurface petroleum migration: Based on molecular dynamics simulation and reservoir geochemistry. Organic Geochemistry; 115: 220-232.

Liao, Y., Zheng, Y., Pan, Y., Sun, Y. and Geng, A. (2015): A method to quantify C_1–C_5 hydrocarbon gases by kerogen primary cracking using pyrolysis gas chromatography. Organic Geochemistry; 79: 49-55.

Liu, K., George, S.C., Lu, X., Gong, S., Tian, H. and Gui, L. (2014): Innovative fluorescence spectroscopic techniques for rapidly characterising oil inclusions. Organic Geochemistry; 72: 34-45.

Longford, F.F. and Blanc-Valleron, M.M. (1990): Interpreting Rock–Eval pyrolysis data using graphs of pyrolyzable hydrocarbons vs. total organic carbon, AAPG Bulletin; 74: 799-804.

Malachowska, A., Mastalerz, M., Hampton, L.B., Hupka, J. AND Drobniak, A. (2019): Origin of bitumen fractions in the Jurassic-early Cretaceous Vaca Muerta Formation in Argentina: insights from organic petrography and geochemical techniques. International Journal of Coal Geology; 205: 155-165.

Mao, J., Fang, X., Lan, Y., Schimmelmann, A., Mastalerz, M., Xu, L. and Schmidt-Rohr, K. (2010): Chemical and nanometer-scale structure of kerogen and its change during thermal maturation investigated by advanced solid-state C NMR spectroscopy. Geochimica et Cosmochimica Acta; 74(7): 2110-2127.

Martinez, A.R., Ion, D.C., Desorcy, G.J. and Dekker, H. (1984): Classification and nomenclature systems for petroleum and petroleum reserves. 11th World Petroleum Congress, London, Wiley, Chichester; 2: 325-343.

Mazhar, A. and Issawi, B. (1977): Geological Map of Libya, 1:250000, Sheet: Zt. Msus, NI 34-3, Explanatory Booklet, Industrial Research Center (IRC), Tripoli, 80p.

Mello, M.R., Gaglianone, P.C., Brassell, S.C. and Maxwell, J.R. (1988): Geochemical and biological marker assessment of depositional environments using Brazilian offshore oils. Marine and Petroleum Geology; 5: 205-223.

Mijalkovic, N. (1977): Geological Map of Libya, 1:250000, Sheet: Al Qaddahiyah, NH 33-3, Explanatory Booklet, Industrial Research Center (IRC), Tripoli, 66p.

Munz, I.A. (2001): Petroleum inclusions in sedimentary basins: systematics, analytical methods and applications. Lithos; 55(1-4): 195-212.

Ndip, E.A., Agyingi, C.M., Nton, M.E., Hower, J.C. and Oladunjoye, M.A. (2019): Organic petrography and petroleum source rock evaluation of the Cretaceous Mamfe Formation, Mamfe basin, southwest Cameroon. International Journal of Coal Geology; 202: 27-37.

Obermajer, M., Dewing, K. and Fowler, M.G. (2010): Geochemistry of crude oil from Bent Horn field (Canadian Arctic Archipelago) and its possible Paleozoic origin. Organic Geochemistry; 41(9): 986-996.

Peters, K.E. and Cassa, M.R. (1994): Applied source rock geochemistry. In: Magoon, L.B., Dow, W.G. (Eds.): The petroleum system from source to trap, AAPG, Mem.; 60: 93-117.

Peters, K.E. and Moldowan, J.M. (1993): The biomarker guide: Interpreting molecular fossils in petroleum and ancient sediments. Prentice-Hall, Inc, Englewood Cliffs, New Jersey.

Peters, K.E., Walters, C.C. and Moldowan, J.M. (2005): The biomarker guide: Biomarkers and isotopes in petroleum exploration and Earth history. 2nd edition, vol. 2. Cambridge University Press, Cambridge.

Philp, R.P. and Gilbert, T.D. (1986): Biomarker distributions in Australian oils predominantly derived from terrigenous source material. Organic Geochemistry; 10: 73-84.

Pietersz, C.R. (1968): Proposed nomenclature for rock units in Northern Cyrenaica. In: Barr, F.T. (Ed.), Geology and Archaeology of Northern Cyrenaica, Libya. The Petroleum Exploration Society of Libya, 10th Annual Conference, Tripoli, pp. 125-130.

Pironon, J., Pagel, M., Walgenwitz, F. and Barres, O. (1995): Organic inclusions in salt. Part 2: oil, gas and ammonium in inclusions from the Gabon margin. Organic Geochemistry; 23(8): 739-750.

Prinzhofer, A. Vega, M.A.G., Battani, A. and Escudero, M. (2000): Gas geochemistry of the Macuspana Basin (Mexico): thermogenic accumulations in sediments impregnated by bacterial gas. Marine and Petroleum Geology; 17(9): 1029-1040.

Rohlich, P. (1974): Geological Map of Libya, 1:250,000, Sheet: Al Bayda, NI 34-15, Explanatory Booklet, Industrial Research Center (IRC), Tripoli, Libya, 70p.

Shaltami, O.R. (2012): Mineral composition and environmental geochemistry of the beach sediments along the Mediterranean Coast from Benghazi to Bin Jawwad, Northeast Libya. Unpublished PhD Thesis, Cairo University, Egypt.

Shaltami, O.R., Fares, F.F., EL Oshebi, F.M., and Errishi, H. (2017): Isotope age of the Early Oligocene shallow marine carbonates, Al Jabal Al Akhdar, NE Libya. The 12th International Symposium on Applied Isotope Geochemistry (AIG-12), Copper Mountain, Colorado, USA, Proceeding Book; pp. 23-34.

Shaltami, O.R., Fares, F.F., EL Oshebi, F.M., Errishi, H. and Bustany, I. (2018): High-resolution strontium isotope stratigraphy of the Eocene deposits in the Al Jabal Al Akhdar, NE Libya. 20th International Sedimentological Congress (ISC), Québec, Canada, Proceeding Book; pp. 33-42.

Shaltami, O.R., Fares, F.F., EL Oshebi, F.M., Errishi, H. and Bustany, I. (2018): Strontium isotopes as paleo-indicators of unconformities: A case of the Late Cretaceous-Paleocene deposits in the Al Jabal Al Akhdar, NE Libya. International Conference on Scientific Research and Innovation (ICSRI), Chennai, India, Proceeding Book; pp. 12-22.

Shaltami, O.R., Fares, H., EL Oshebi, F.F., Errishi, F.M., Bustany, I. and Musa, M.M. (2018): Depositional environment and absolute age of the Pliocene-early Pleistocene sediments in the Cyrenaica Basin, NE Libya. 16th Annual Conference on Isotope Geology (ACIG-16), Department of Geosciences and Natural Resource Management Faculty of Science University of Copenhagen Denmark, Proceeding Book; pp. 67-83.

Shaltami, O.R., Fares, F.F., EL Oshebi, F.M., Errishi, H., Bustany, I., Salloum, F.M., El Shawaihdi, M.H. and Musa, M.M. (2018): Absolute age of the Miocene deposits in the Cyrenaica Basin, NE Libya: Implications for the Messinian Salinity Crisis. IAEG Annual Conference 2018 - Geochemistry, Irish Association for Economic Geology; pp. 62-76.

Shaltami, O.R., Fares, F.F., EL Oshebi, F.M., Errishi, H. and Santos, P. (2018): New high-precision $^{87}Sr/^{86}Sr$ ages on Late Oligocene-Early Miocene rocks in the Al Jabal Al Akhdar, NE

Libya. International Conference on Advances in Chronostratigraphy (ICAC 2018), Bangkok, Thailand, Proceeding Book; pp. 57-66.

Shaltami, O.R., Fares, F.F., EL Oshebi, F.M., Errishi, H. and Santos, P. (2018): Paleoclimate across the Cretaceous/Paleogene boundary event: A case study of the Al Jabal Al Akhdar, NE Libya. Advanced Carbonate Geology, Kuala Lumpur, Malaysia, Proceeding Book; pp. 10-14.

Shaltami, O.R., Fares, F.F., EL Oshebi, F.M., Errishi, H. and Santos, P. (2018): Hydrology of the Mediterranean Sea during the Messinian Salinity Crisis: A case study of the Cyrenaica Basin, NE Libya. 64th Annual Institute on Lake Superior Geology, Iron Mountain, Michigan, USA, Proceeding Book; pp. 16-21.

Shaltami, O.R., Fares, F.F., EL Oshebi, F.M., Errishi, H. and Souza, R. (2018): Isotope geochronology of the Pliocene-Quaternary deposits in the Al Jabal Al Akhdar, NE Libya. International Conference on Applied Science and Engineering (ICASE), Bangkok, Thailand, Proceeding Book; pp. 21-29.

Shaltami, O.R., Fares, F.F., Errishi, H., EL Oshebi, F.M. and Bustany, I. (2017): Rare earth element geochemistry and isotope geochronology of the Quaternary calcarenites in the Al Jabal Al Akhdar, NE Libya. 10th International Conference on Applied Geochemistry (ICG-10), Institute of Geosciences Federal University of Rio Grande do Sul, Porto Alegre, Brazil, Proceeding Book; pp. 50-68.

Shaltami, O.R., Fares, F.F., Errishi, H., EL Oshebi, F.M. and Bustany, I. (2018): Redox conditions and depositional environment of the Tulmithah and Apollonia Formations, Al Jabal Al Akhdar, NE Libya. GeoBaikal 2018, Irkutsk, Russia, Proceeding Book; pp. 77-83.

Shaltami, O.R., Fares, F.F., Errishi, H., EL Oshebi, F.M. and Souza, R. (2018): Chemostratigraphy of the Al Abraq Group, Cyrenaica Basin, NE Libya. 4th International Conference on Applied Science and Engineering (ICASE), Bhubaneswar, Odisha, Proceeding Book; pp. 30-39.

Shaltami, O.R., Jorgensen, L., Elkjaer, C., Fares, F.F., Errishi, H., EL Oshebi, F.M. and Souza, R. (2018): Petroleum geochemistry of the Qahash and Daryanah formations, Cyrenaica Basin, NE Libya. 4th Annual AAPG/EAGE/MGS Myanmar Oil & Gas Conference, Yangon, Myanmar, Proceeding Book; pp. 34-50.

Shaltami, O.R., Liu, Y., Jorgensen, L., Elkjaer, C., Fares, F.F., Errishi, H., EL Oshebi, F.M. and Souza, R. (2019): Chemostratigraphy of the Al Uwayliayah Formation, Cyrenaica Basin, NE Libya. International Conference on Geological and Environmental Sustainability (ICGES-19), Visakhapatnam India, Proceeding Book; pp. 49-57.

Shaltami, O.R., Jorgensen, L., Elkjaer, C., Fares, F.F., Errishi, H., EL Oshebi, F.M. and Souza, R. (2019): Gas geochemistry of reservoirs in the Cyrenaica Basin, NE Libya. International Conference on Geological and Environmental Engineering (ICGEE), New York, USA, Proceeding Book; pp. 13-23.

Shaltami, O.R., Liu, Y., Jorgensen, L., Elkjaer, C., Fares, F.F., Errishi, H., EL Oshebi, F.M. and Souza, R. (2019): Organic geochemistry of shale and marl: A case study of the Miocene deposits in the Cyrenaica Basin, NE Libya. World Chemistry 2019, Philadelphia, USA, Proceeding Book; pp. 70-82.

Shaltami, O.R., Jorgensen, L., Elkjaer, C., Fares, F.F., Errishi, H., EL Oshebi, F.M. and Souza, R. (2019): Petroleum Geochemistry of the Al Baniyah Formation, Cyrenaica Basin, NE Libya. 23th International Conference on Engineering, Technology and Applied Science (ETAS-23) Seoul, South Korea, Proceeding Book; pp. 13-21.

Shaltami, O.R., Jorgensen, L., Elkjaer, C., Fares, F.F., Errishi, H., EL Oshebi, F.M. and Souza, R. (2019): Petroleum geochemistry of the Al Bayda Group, Cyrenaica Basin, NE Libya. 12th International Conference on Applied Science and Engineering (ICASE), Bangkok, Thailand, Proceeding Book; pp. 43-57.

Shaltami, O.R., Liu, Y., Jorgensen, L., Elkjaer, C., Fares, F.F., Errishi, H., EL Oshebi, F.M. and Souza, R. (2019): Petroleum geochemistry of the Benghazi Formation, Cyrenaica Basin, NE Libya. 2019 SME Annual Conference & Expo, Denver, Colorado, USA, Proceeding Book; pp. 22-38.

Shaltami, O.R., Liu, Y., Jorgensen, L., Elkjaer, C., Fares, F.F., Errishi, H., EL Oshebi, F.M. and Souza, R. (2019): Petroleum Geochemistry of the Eocene Deposits, Cyrenaica Basin, NE Libya. 21st International Conference on Engineering, Technology and Applied Science (ETAS-21), Taipei, Taiwan, Proceeding Book; pp. 10-26.

Shaltami, O.R., Liu, Y., Jorgensen, L., Elkjaer, C., Fares, F.F., Errishi, H., EL Oshebi, F.M. and Souza, R. (2019): Petroleum Geochemistry of the Pliocene Deposits, Cyrenaica Basin, NE Libya. Petroleum Istanbul 2019, Turkey, Proceeding Book; pp. 11-29.

Shaltami, O.R., Siasia, G.D., Fares, F.F., Errishi, H. and EL Oshebi, F.M. (2018): Petroleum geochemistry of reservoir: A case study of the Achabiyat and Hawaz formations in the Dur Al Qussah area, SW Libya. Deloitte Oil and Gas Conference, Houston, Texas, USA, Proceeding Book; pp. 22-31.

Shaltami, O.R., Siasia, G.D., Fares, F.F., Errishi, H., EL Oshebi, F.M. and Souza, R. (2018): Petroleum geochemistry of the Akakus Formation in the Dur Al Qussah area, Murzuq Basin, SW Libya. 4th Annual IoT in Oil and Gas Conference, Houston, Texas, USA, Proceeding Book; pp. 11-23.

Shanmugam, G. (1985): Significance of coniferous rain forests and related organic matter in generating commercial quantities of oil, Gippsland Basin, Australia. American Association of Petroleum Geologists Bulletin; 69: 1241-1254.

Simoneit, B.R.T. (2004): Biomarkers (molecular fossils) as geochemical indicators of life. Advances in Space Research; 33(8): 1255-1261.

Song, Z., Qin, Y., George, S.C., Wang, L., Guo, J. and Feng, Z. (2013): A biomarker study of depositional paleoenvironments and source inputs for the massive formation of Upper Cretaceous lacustrine source rocks in the Songliao Basin, China. Palaeogeography, Palaeoclimatology, Palaeoecology; 385: 137-151.

Swedan A. and Issawi, B. (1977): Geological Map of Libya, 1:250,000, Sheet: Bir Hacheim, NI 34-4, Explanatory Booklet, Industrial Research Center (IRC), Tripoli, Libya, 80p.

Sykes, R., Volk, H., George, S.C., Ahmed, M., Higgs, K.E., Johansen, P.E. and Snowdon, L.R. (2014): Marine influence helps preserve the oil potential of coaly source rocks: Eocene Mangahewa Formation, Taranaki Basin, New Zealand. Organic Geochemistry; 66: 140-163.

Tao, S., Wang, C., Du, J., Liu, L. and Chen, Z. (2015): Geochemical application of tricyclic and tetracyclic terpanes biomarkers in crude oils of NW China. Marine and Petroleum Geology; 67: 460-467.

Tuo, J., Wang, X. and Chen, J. (1999): Distribution and evolution of tricyclic terpanes in lacustrine carbonates. Organic Geochemistry; 30: 1429-1435.

Van Krevelen, D.W. (1961): Coal: typology-chemistry-physics-constitution: Elsevier Science, Amsterdam; 514p.

Volk, H. and George, S.C. (2019): Using petroleum inclusions to trace petroleum systems – A review. Organic Geochemistry; 129: 99-123.

Waples, D.W. (1985): Geochemistry in petroleum exploration. Boston, MA: International Human Resources Development Corporation, 232p.

Waples, D.W. and Machihara, T. (1990): Application of sterane and triterpane biomarkers in petroleum exploration. Bulletin of Canadian Petroleum Geology; 38: 357-380.

Werner-Zwanziger, U., Lis, G., Mastalerz, M. and Schimmelmann, A. (2005): Thermal maturity of type II kerogen from the New Albany Shale assessed by ^{13}C CP/MAS NMR. Solid State Nuclear Magnetic Resonance; 27(1-2): 140-148.

Xianming, X., Wilkins, R.W.T., Dehan, L., Zufa, L. and Jiamu, F. (2000): Investigation of thermal maturity of lower Palaeozoic hydrocarbon source rocks by means of vitrinite-like maceral reflectance—a Tarim Basin case study. Organic Geochemistry; 31(10): 1041-1052.

Xiao, H., Li, M., Liu, J., Mao, F., Cheng, D. and Yang, Z. (2019): Oil-oil and oil-source rock correlations in the Muglad Basin, Sudan and South Sudan: New insights from molecular markers analyses. Marine and Petroleum Geology; 103: 351-365.

Yandoka, B.M.S., Abdullah, W.H., Abubakar, M.B., Hakimi, M.H. and Adegoke, A.K. (2015): Geochemical characterisation of Early Cretaceous lacustrine sediments of Bima Formation, Yola Sub-basin, Northern Benue Trough, NE Nigeria: Organic matter input, preservation, paleoenvironment and palaeoclimatic conditions. Marine and Petroleum Geology; 61: 82-94.

Yang, Z., Li, M., Cheng, D., Xiao, H., Lai, H. and Chen, Q. (2019): Geochemistry and possible origins of biodegraded oils in the Cretaceous reservoir of the Muglad Basin and their application in hydrocarbon exploration. Journal of Petroleum Science and Engineering; 173: 889-898.

Zert, B. (1974): Geological map of Libya, 1:250000, Sheet: Darnah, NI 34-16, Explanatory Booklet, Industrial Research Center (IRC), Tripoli, 49p.

Zhang, S. and Huang, H. (2005): Geochemistry of Palaeozoic marine petroleum from the Tarim Basin, NW China: Part 1. Oil family classification. Organic Geochemistry; 36: 1204-1214.

Zhang, Z., Greenwood, P., Zhang, Q., Rao, D. and Shi, W. (2012): Laser ablation GC-MS analysis of oil-bearing fluid inclusions in petroleum reservoir rocks. Organic Geochemistry; 43: 20-25.

Zhao, S., Chen, W., Zhou, L., Zhou, P. and Zhang, J. (2019): Characteristics of fluid inclusions and implications for the timing of hydrocarbon accumulation in the cretaceous reservoirs, Kelasu Thrust Belt, Tarim Basin, China. Marine and Petroleum Geology; 99: 473-487.

Zhou, S. and Huang, H. (2008): Controls on alkylphenol occurrence and distribution in oils from lacustrine rift basins in East China. Science in China Series D: Earth Sciences; 51(7): 976-983.

Zhu, G., Wang, H., Weng, N., Yang, H., Zhang, K., Liao, F. and Neng, Y. (2015): Geochemistry, origin and accumulation of continental condensate in the ultra-deep-buried Cretaceous sandstone reservoir, Kuqa Depression, Tarim Basin, China. Marine and Petroleum Geology; 65: 103-113.

Zhu, Y. (1997): Geochemical characteristics of terrestrial oils of the Tarim Basin. Acta Sedimentologica Sinica; 15: 26-30.

Ziegs, V., Noah, M., Poetz, S., Horsfield, B., Hartwig, A., Rinna, J. and Skeie, J.E. (2018): Unravelling maturity- and migration-related carbazole and phenol distributions in Central Graben crude oils. Marine and Petroleum Geology; 94: 114-130.

Zongying, Z. (2009): Quantitative analysis of variation of organic carbon mass and content in source rock during evolution process. Petroleum Exploration and Development; 36(4): 463-46.

Zumberge, J.E. (1987): Prediction of source rock characteristics based on terpane biomarkers in crude oils: A multivariate statistical approach. Geochimica et Cosmochimica Acta; 51: 1625-1637.

جيوكيمياء النفط لتكوين دريانة في البئر الشاطئ A1-NC128 حوض برقة، شمال شرق ليبيا

من:

أبوبكر عزالدين القماطي

تحت إشراف:

أم .أسامة الشلطامي

الخُلاصة

قد تحققت في هذه الدراسة تقييمات بتروغرافية وجيوكيميائية لصخر المصدر (دريانة الصخر الزيتي)، و لِلمَكمَن (دريانة الحجر الجيري) في البئر البحري Al-NC 128، في حوض برقه. في دريانة الصخر الزيتي، تشير المؤشرات الحيوية إلى مدخلات مختلطة من العوالق المائية، والمواد العضوية القارية، ترسّبت تحت ظروف متوسّطة الأكسدة. الكيروجين من النوع الثاني\الثالث، والنوع الثالث. صخر المصدر يملك جودة شبه الضعيفة. المَكمَن يحتوي نفط خام متوسط الجودة. ينتمي هذا النفط إلى صخر المصدر من دريانة الصخر الزيتي، كما أُثبِت عن طريق العلاقة ما بين النفط – صخر المصدر. الميثان هو الغاز الرئيسي في المَكمَن. كُل مِن النفط الخام، وصخر المصدر يقعان في النافذة الغير ناضجة. المَكمَن دريانة شُحِن بالهيدروكربونات في مرتين مختلفتين. يُمكن اعتِبار الصخر الزيتي الأوسط كصخرة الغطاء في النظام النفطي لِتكوين دريانة.

الكلمات الدليلية: علم الصخور العضوية، الجيوكيمياء العضوية، صخر المصدر، المكمن، تكوين دريانة، حوض برقة، ليبيا

جيوكيمياء النفط لتكوين دريانة في البئر الشاطئ A1-NC128 حوض برقة شمال شرق ليبيا

قدمت من قبل:

أبوبكر عزالدين عمر القماطي

تحت إشراف:

د. أسامة رحيل الشلطامي

قدمت هذه الرسالة استكمالا لمتطلبات الحصول على درجة الماجستير في العلوم الأرض

جامعة بنغازي

كلية العلوم

ديسمبر 2019